Icarus 339 (2020) 113526

Contents lists available at ScienceDirect

Icarus

journal homepage: www.elsevier.com/locate/icarus

The mineral diversity of Jezero crater: Evidence for possible lacustrine carbonates on Mars

Briony H.N. Horgan [a,*], Ryan B. Anderson [b], Gilles Dromart [c], Elena S. Amador [d], Melissa S. Rice [e]

[a] Department of Earth, Atmospheric, and Planetary Sciences, Purdue University, West Lafayette, IN, USA
[b] U.S. Geological Survey, Astrogeology Center, Flagstaff, AZ, USA
[c] Laboratoire de Géologie de Lyon, Université de Lyon, Lyon, France
[d] Division of Geological & Planetary Sciences, California Institute of Technology, Pasadena, CA, USA
[e] Department of Physics & Department of Geology, Western Washington University, Bellingham, WA, USA

A B S T R A C T

Noachian-aged Jezero crater is the only known location on Mars where clear orbital detections of carbonates are found in close proximity to clear fluvio-lacustrine features indicating the past presence of a paleolake; however, it is unclear whether or not the carbonates in Jezero are related to the lacustrine activity. This distinction is critical for evaluating the astrobiological potential of the site, as lacustrine carbonates on Earth are capable of preserving biosignatures at scales that may be detectable by a landed mission like the Mars 2020 rover, which is planned to land in Jezero in February 2021. In this study, we conduct a detailed investigation of the mineralogical and morphological properties of geological units within Jezero crater in order to better constrain the origin of carbonates in the basin and their timing relative to fluvio-lacustrine activity. Using orbital visible/near-infrared hyperspectral images from the Compact Reconnaissance Imaging Spectrometer for Mars (CRISM) along with high resolution imagery and digital elevation models, we identify a distinct carbonate-bearing unit, the "Marginal Carbonates," located along the inner margin of the crater, near the largest inlet valley and the western delta. Based on their strong carbonate signatures, topographic properties, and location in the crater, we propose that this unit may preserve authigenic lacustrine carbonates, precipitated in the near-shore environment of the Jezero paleolake. Comparison to carbonate deposits from terrestrial closed basin lakes suggests that if the Marginal Carbonates are lacustrine in origin, they could preserve macro- and microscopic biosignatures in microbialite rocks like stromatolites, some of which would likely be detectable by Mars 2020. The Marginal Carbonates may represent just one phase of a complex fluvio-lacustrine history in Jezero crater, as we find that the spectral diversity of the fluvio-lacustrine deposits in the crater is consistent with a long-lived lake system cataloging the deposition and erosion of regional geologic units. Thus, Jezero crater may contain a unique record of the evolution of surface environments, climates, and habitability on early Mars.

1. Introduction

Carbonates are a common product of the interaction between CO_2, water, and rocks on the Earth, and thus should have been produced on Mars under the potentially thick CO_2-rich atmosphere and relatively wet climate predicted for the Noachian epoch (~3.8–4 Gy; e.g., Kahn, 1985; Pollack et al., 1987; Ramirez and Craddock, 2018). While the vast carbonate deposits associated with the carbon cycle on Earth have not yet been identified on Mars, carbonates have been detected in ancient martian terrains from orbital remote sensing (Ehlmann et al., 2008a; Wray et al., 2016), with landed assets (Morris et al., 2010), and in high latitude sediments altered under modern climate conditions (Boynton et al., 2009). Carbonates may also be present as a component of the ubiquitous martian dust (Bandfield et al., 2003). Ancient carbonates on Mars are a major target for future landed investigations and eventual Mars sample return both because their isotopic composition could serve as a record of atmospheric loss on Mars (e.g., Hu et al., 2015) and because carbonate precipitation in aqueous environments is an excellent mechanism for biosignature preservation (e.g., Farmer and Des Marais, 1999).

In this study we investigate carbonates and related deposits in Jezero crater (18.9°N, 77.5°E; Fig. 1), a 45 km diameter Noachian-aged crater located on the NW rim of the Isidis basin. Jezero is located within one of the largest continuous carbonate-bearing geologic units identified on Mars, which extends across the NW rim of the Isidis basin and also exhibits strong olivine spectral signatures (Ehlmann et al., 2009; Mustard et al., 2009). The regional carbonate-bearing unit has been inferred to mantle the rim and portions of the interior of Jezero crater (Goudge et al., 2015). Carbonates have also been detected within the basin fill materials, around the crater margins, and within several fan-shaped features in the crater (Ehlmann et al., 2008a; Goudge et al., 2012, 2015, 2017; Brown et al., 2016, 2017). At least one of the fans has been

* Corresponding author at: 550 Stadium Mall Dr., West Lafayette, IN 47907, USA.
E-mail address: briony@purdue.edu (B.H.N. Horgan).

https://doi.org/10.1016/j.icarus.2019.113526
Received 17 September 2018; Received in revised form 29 October 2019; Accepted 30 October 2019
Available online 11 November 2019

shown to exhibit sedimentary structures consistent with a lacustrine delta (Goudge et al., 2017), and the presence of valleys leading both in and out of the crater has been interpreted as evidence for an open basin paleolake (Fassett and Head, 2005, 2008). The upstream valleys are part of a large watershed, and crater densities in this watershed suggest cessation of fluvial activity around the Noachian/Hesperian boundary (Fassett and Head, 2008).

The presence of multiple carbonate-bearing units within a Noachian to early Hesperian paleolake basin in Jezero raises the possibility that some of these carbonates may have precipitated in the paleolake. On Earth, carbonates are frequently deposited as marine or lacustrine precipitates and evaporites. These types of carbonate deposits have high morphologic, organic, and isotopic biosignature preservation potential (e.g., Cady et al., 2003; Summons and Hallmann, 2014), and can be biologically mediated (e.g., Capezzuoli et al., 2014). In addition, when these deposits are created in a shallow near-shore environment, they are conducive to the formation and preservation of biological macrostructures like stromatolites and tufas (e.g., Bosak et al., 2013). Thus, potential lacustrine carbonates in Jezero would be a major target for in situ investigation by future missions. These missions will likely include NASA's Mars 2020 mission, which is scheduled to land a rover in Jezero on or proximal to the western delta in 2021 (see Fig. 1 for landing ellipse location). The goals of Mars 2020 include exploring the astrobiological potential of Jezero crater (assessing past habitability and biosignature preservation potential), searching for potential biosignatures, and collecting a suite of samples that may one day be returned to Earth via a Mars Sample Return mission (Williford et al., 2018).

In this study, we seek to constrain the origin of carbonate-bearing terrains in Jezero crater based on new analyses of their visible/near-infrared spectral properties, small scale physical texture, and stratigraphic relationships. We also compare Jezero carbonate-bearing terrains to olivine- and carbonate-bearing terrains in the surrounding plains and the NE Syrtis area to the southwest. Through this detailed comparison, we test the hypothesis that some of the carbonate-bearing terrains in Jezero could be related to fluvio-lacustrine activity, as well as the competing hypothesis that all of these terrains are just slightly different expressions of the same large regional carbonate-bearing unit.

2. Background

2.1. Regional and local geologic units

Jezero crater impacted into a regional unit referred to as the basement unit, which is the stratigraphically lowest unit in the area. The basement unit is composed of a complex assemblage that includes megabreccia potentially sourced from the Isidis impact (~3.96 Ga; Werner, 2008) and, in some locations, large fracture systems (Bramble et al., 2017). In visible/near-infrared orbital spectra (VNIR; 0.3–2.5 μm), the basement unit exhibits strong and broad absorptions near 0.9 and 1.8 μm consistent with low-Ca pyroxene, suggesting a primitive igneous composition sourced from the lower crust (Mustard et al., 2007). The unit also exhibits narrow absorptions near 1.9 and 2.3 μm consistent with Fe/Mg-smectites, suggesting pervasive alteration by groundwater or hydrothermal fluids (e.g., Mangold et al., 2007). The basement unit is mantled by the regional olivine- and carbonate-bearing unit.

Carbonate was previously identified along the NW rim of Isidis based on covarying absorption bands in orbital VNIR spectra at 2.3 and 2.5 μm, consistent with Mg-carbonate (Ehlmann et al., 2008a). These areas also typically exhibit a hydration band at 1.9 μm, and while this could be due to some varieties of hydrous carbonates (e.g., Calvin et al., 1994; Harner and Gilmore, 2015), this more likely suggests the presence of an additional hydrated phase such as an Fe/Mg-smectite (Ehlmann et al., 2008a; Bishop et al., 2013). The carbonate signatures are consistently associated with a strong and broad absorption between 1 and 1.3 μm similar to the absorption due to iron in olivine (Ehlmann et al., 2008a; Mustard et al., 2007, 2009), and thermal infrared spectra of the unit support the presence of a Mg-rich olivine (~$Fo_{50–75}$; Koeppen and Hamilton, 2008). Models of thermal-infrared spectra (8–25 μm) in the region suggest that the carbonate and olivine are both present in abundances of ~9% at the 2–3 km scale, and as this number includes significant sub-pixel mixing with aeolian cover and other units, both the carbonate and olivine are likely much more abundant in individual outcrops (Salvatore et al., 2018). Regional analyses based on thermal-infrared and visible/near-infrared spectra suggest carbonate abundances of up to ~20% at the decameter scale (Edwards and Ehlmann, 2015).

Hypotheses for the origin of the olivine-bearing unit include an intrusion (Hoefen et al., 2003), lava flows (Hamilton and Christensen, 2005), and an impact melt sheet (Mustard et al., 2007, 2009). More recently, the mantling nature and other properties of the deposit have been interpreted as evidence for an airfall origin, perhaps as volcanic tephra (Kremer et al., 2018). The Mg-rich carbonate in the unit was most likely derived from in situ alteration of the Mg-rich olivine, but the alteration process is poorly constrained. Proposed mechanisms for carbonate formation include hydrothermal systems, low-grade crustal metamorphism, serpentinization, and surface weathering (Ehlmann et al., 2008a, 2009; Viviano et al., 2013; Mcsween et al., 2015).

Within Jezero crater, previous work has divided the carbonate-bearing terrains into two separate geomorphic units: the Mottled Terrain and the Light-toned Floor (Fig. 1b; Goudge et al., 2015). The Mottled Terrain is texturally diverse with multiple sub-units ("eroded", "dusty", "lineated") that has been mapped around the margin of Jezero and in the broader watershed by Goudge et al. (2015). The Mottled Terrain is light toned, appears heavily degraded, and has likely been exhumed based on the presence of circular features interpreted as degraded impact craters. Some banding has been observed but no clear layering. This unit may be equivalent to the olivine- and carbonate-bearing "Fractured Unit" in the NE Syrtis area to the south (Bramble et al., 2017), and may be representative of the regional olivine- and carbonate-bearing terrains.

The Light-toned Floor is distinct from the Mottled Terrain based on location within the crater and aeolian dune cover. The Light-toned Floor is the lowest exposed unit that fills the basin, and grades into the surrounding Mottled Terrain. The Light-toned Floor exhibits similar spectra to the Mottled Terrain, with hydrated, Mg-carbonate, and olivine signatures. However, the Light-toned Floor exhibits stronger olivine signatures, which are attributed to variable mantling by olivine-bearing aeolian bedforms, interpreted to be sourced from the Light-toned Floor itself (Ehlmann et al., 2008b; Goudge et al., 2015). The Light-toned Floor has been hypothesized to be a sub-unit within the Mottled Terrain (and thus likely formed along with the regional carbonate-bearing terrains), although previous studies could not rule out a detrital origin in the Jezero crater paleolake (Goudge et al., 2015). In this study, we compare the spectral and physical properties of the Mottled Terrain within and beyond the crater to the Light-toned Floor to better constrain the relationship between these two units.

The Light-toned Floor is overlain by a dark-toned capping unit with lobate margins and mafic VNIR spectral signatures that have previously been hypothesized to be volcanic in origin, potentially a lava flow (Goudge et al., 2015). Here we refer to this unit as the "Mafic Floor". The Light-toned Floor is exposed in windows through the Mafic Floor, and while these windows may be erosional in origin, these areas may also represent former topographic highs that were never covered by the Mafic Floor (similar to a "kipuka" in a lava flow on Earth; Ruff, 2017).

2.2. Fluvio-lacustrine history

Jezero is interpreted as once containing an open basin paleolake, based on the presence of both inlet and outlet valleys cut into the crater rim (Fassett and Head, 2005; Goudge et al., 2012; Fig. 1c). The outlet valley exhibits meanders and bar deposits, which are inconsistent with only a high flow rate dam-breach channel, suggesting that the crater was

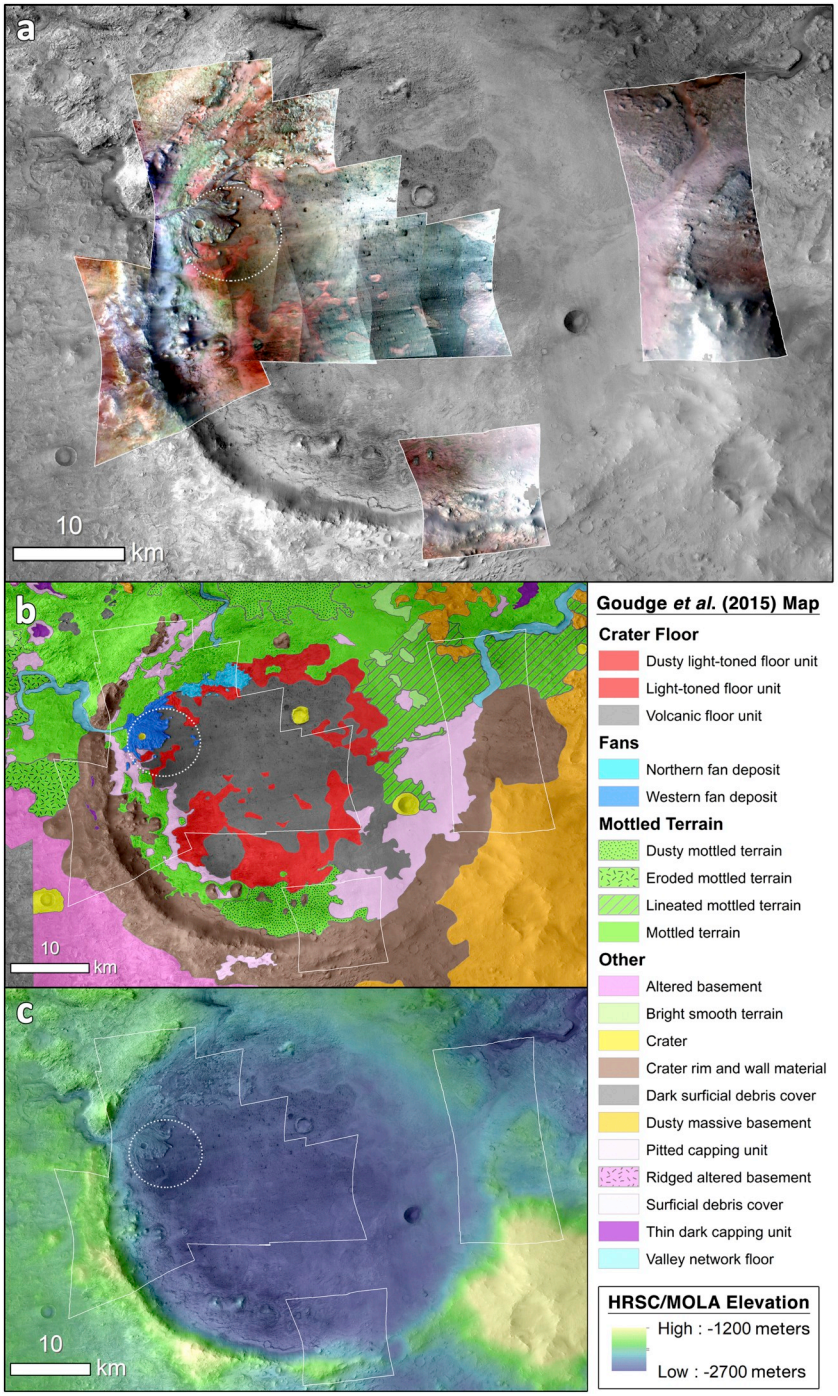

Fig. 1. CRISM MTRDR coverage over Jezero crater, as indicated by white outlines. Dashed circle indicates Mars 2020 landing ellipse as of October 2019. (a) CRISM false color mosaic of ten cubes used in this study over CTX mosaic, see Table 1 for wavelengths. (b) Geologic map of Jezero crater, modified from Goudge et al. (2015). (c) CTX image of Jezero crater, colors from HRSC and MOLA elevation.

filled and outflowed for an extended period of time (Schon et al., 2012). The elevation of the outlet valley suggests a sustained lake level near −2400 m. Prior to breach, high stand lake levels may have been as high as a notable break in slope in the crater rim near −2260 m (Fassett and Head, 2005).

There are also several deposits in Jezero that have been mapped as fans or deltas (Fassett and Head, 2005; Ehlmann et al., 2008b; Goudge et al., 2015). We refer to the farthest west and best-known of these as the "western delta". Orbital geomorphic analysis of the western delta supports a deltaic origin for this feature based on large scroll bars and epsilon cross-bedding (Schon et al., 2012). Detailed bedding geometry analysis of the delta has shown the presence of inclined bedding planes with dips (2–9°) that increase with elevation on the delta. These beds are interpreted as foreset beds and are underlain by more flat-lying planes (<2°) that are interpreted as bottomset beds (Goudge et al., 2017).

Goudge et al. (2018) identified three different facies within the western delta and proposed that the stratigraphy of these facies is most consistent with a record of increasing lake levels (perhaps due to basin filling) during one relatively continuous phase of lacustrine activity. In their model, facies interpreted as point bar strata are the oldest, formed by laterally migrating channels, perhaps at some distance (100's of meters) upstream from a shallower lake level. The overlying facies are interpreted as inverted channels, formed by avulsing linear channels. These deposits were most likely subaerial and relatively close to a deeper lake level, where the channels stepped upward and backward as lake levels rose up to the elevation of the originally confining basin topography, prior to overflowing and forming the outlet valley at the breach elevation of −2395 m. Lastly, the inverted channels are cut by an incised valley, which is the youngest feature, and may have formed during much lower lake levels later on.

The western delta is fed by a large fluvial watershed to the NW that incises the basement unit as well as the Mottled Terrain. The delta is hypothesized to be composed largely of detrital phases from these units (as opposed to authigenic alteration phases precipitated in the lake or fluvial system). The delta exhibits spectral signatures consistent with Fe/Mg-smectites, interpreted as sourced from the basement unit (Ehlmann et al., 2008b; Goudge et al., 2015), as well as patches of carbonates in light-toned exposures interpreted as point bar deposits, interpreted as sourced from the regional olivine/carbonate-bearing unit (Schon et al., 2012; Goudge et al., 2017). If the observed mineralogy is purely detrital, the mineralogical variability observed in the western delta is due to either variations in source mineralogy or grain-size dependent sorting by variable flow velocities through space and/or time (Goudge et al., 2015). Fluvial activity in the watershed of the western delta is inferred to have ceased by around 3.8 ± 0.1 Ga, based on crater counts on the incised valleys (Fassett and Head, 2008). This date is similar to the cessation date for the majority of the valley networks on Mars, which are inferred to have been most active during the late Noachian to early Hesperian eras (Howard et al., 2005; Irwin et al., 2011).

The remaining fan-shaped features along the northern crater margin are much more degraded than the western delta and have not been confirmed as deltaic in origin. These features have been previously mapped together as the "northern fan", but for clarity here we split the feature where needed into the "northwestern fan" and the "northeastern fan". The northwestern fan has been shown to exhibit some areas with olivine, carbonate, and hydrated VNIR spectral signatures similar to the Mottled Terrain (Goudge et al., 2015), but the mineralogy of the northeastern fan has not been investigated. The prevalence of olivine/carbonates in the northwestern fan compared to the prevalence of LCP/smectite in the western delta has been attributed to different relative surface areas of the various source units in the watershed (Goudge et al., 2015). The northern fans have been inferred to be the same age as the western delta, with the difference in degradation due to the mineralogical difference between the features (i.e., the carbonate-rich fan is more friable than the LCP/smectite-dominated western delta; Goudge et al., 2015). In this study we compare the spectral properties and morphology of the three fan/delta landforms in Jezero to constrain their role in the fluvio-lacustrine history of Jezero crater.

2.3. The Marginal Carbonates

The strongest carbonate signatures in Jezero occur on the northwest inner margin of the crater, between the western delta and the crater rim (Goudge et al., 2012; Fig. 3). We refer to these carbonate-bearing portions of the marginal region as the "Marginal Carbonates" but emphasize that this term is not meant to carry any connotations about their origin. This area was previously mapped as part of the Mottled Terrain (Goudge et al., 2015). The location of the Marginal Carbonates along the inner rim of the crater could be consistent with deposition in the near-shore region (the littoral zone) of a possible paleolake. If correct, this interpretation would have major implications for biosignature preservation in Jezero, as shallow lacustrine and marine carbonates on Earth in modern environments and in the geologic record are often biologically mediated and can effectively preserve a variety of biosignatures, including macro- and microscopic textures, isotopes, organics, and biominerals (Cady et al., 2003; Benzerara et al., 2006; Webb and Kamber, 2011; Summons and Hallmann, 2014; Flannery et al., 2018; Section 7.3 and Table S3). In this study we compare the properties of the Marginal Carbonates to other carbonate-bearing units in the crater and surrounding region in order to determine whether or not they have unique properties that could suggest a separate origin related to lacustrine activity.

3. Methods

The primary datasets used in this study to investigate the fine-scale morphology and mineralogy of carbonate-bearing terrains in Jezero crater are CRISM (Compact Reconnaissance Imaging Spectrometer for Mars; Murchie et al., 2007, 2009a) visible/near-infrared (~0.3–2.6 μm) hyperspectral images and HiRISE (High Resolution Imaging System; Mcewen et al., 2007) ~25 cm/pixel visible imagery. Supporting datasets in this study include a 20 m/pixel CTX (Context Camera) Digital Terrain Model and accompanying 6 m/pixel orthoimage (Fergason et al., 2017), a broader CTX mosaic of the Jezero region (Dickson et al., 2018), as well as 200 m/pixel blended HRSC and MOLA topography processed by the U.S. Geological Survey (USGS) (Fergason et al., 2018; Fig. 1).

CRISM images in this study were all acquired at the most recent calibration level (MTRDR - Mapped Targeted Reduced Data Record; Seelos et al., 2016) from the Planetary Data System (PDS). Ten unique images are available over the crater, as shown in Fig. 1a: eight ~18 m/pixel FRT images (Full Resolution Targeted) and two ~36 m/pixel HRL (Half Resolution Long) images. All images are delivered with a set of precalculated spectral parameters, derived from I/F cubes, and refined to reduce noise (Viviano-Beck et al., 2014). RGB composites were generated from these spectral parameters to evaluate spectral diversity within the carbonates and related units, as listed in Table 1 and shown in Figs. 3, 4, 6, and 8. All spectral parameters as shown were initially stretched from approximately their average value to 98% of their maximum value to enhance spectral differences; for mosaics shown in Figs. 3, 4, 6, and 8, these stretches were modified to improve continuity across the map.

Spectral variability inferred from the RGB composites was verified using detailed spectral analysis and comparison to laboratory endmembers (Fig. 2). CRISM MTRDR images on the PDS have been processed to suppress atmospheric and instrumental effects (Seelos et al., 2016), but still require ratioing with spectrally neutral terrains to bring out subtle spectral features. An advantage of the MTRDR images is that the majority of column-dependent (i.e., detector element) variability has been suppressed. Thus, unlike the previous TRR3-level images (e.g., Murchie et al., 2009a), the spectrally neutral reference terrain does not need to be within the same detector column and can be from anywhere

within the image (Seelos et al., 2012), although should ideally be extracted from a similar elevation to remove any residual atmospheric bands. To take advantage of this flexibility, here we have implemented a new ratioing technique that quantitatively determines the most spectrally neutral pixels from throughout the image, as determined by the CRISM spectral parameters of Viviano-Beck et al. (2014). We then average the spectra from these pixels together to create one "neutral" reference spectrum, and then the entire reflectance cube can be divided by this spectrum to create a ratio image cube. The advantages of this technique are both that spectral analysis after ratioing is much more straightforward and that all spectra from the same cube are ratioed to the same reference spectrum, so spectrum-to-spectrum differences represents real spectral variability.

All spectra presented in this study were ratioed against an average of all spectra with spectral parameters indicating no major absorption bands due to primary and secondary minerals, which we term a "mineral mask". We also evaluated an alternative mask, a "dust mask", which is an average of all spectra with parameters indicating significant dust as well as low carbonate band depths. Spectral parameters used to create each mask are listed in Table S1, and comparisons of ratio spectra produced using each mask are shown in Fig. S1. The dust mask tends to more effectively preserve the spectral shape of broad iron bands in mafic minerals, especially at short wavelengths. However, the mineral mask more effectively enhances narrow alteration bands, especially weak carbonate bands at 2.5 μm, so for this study we utilize the "mineral mask" method. These differences between the ratio methods are more apparent in higher resolution FRT images than lower resolution HRL images, most likely due to the greater diversity of surface types covered in the larger HRL images. All CRISM spectra shown are 6 × 6 pixel averages. Some spectra retain residual atmospheric bands after atmospheric suppression in the MTRDR pipeline and ratioing, these are apparent based on a sharp triplet around 2 μm.

Five key CRISM observations were used for detailed spectral analysis of Jezero crater (FRT000047A3, FRT00005C5E, FRT00005850, FRT0001182A, HRL000040FF). An additional two images were analyzed in the NE Syrtis area (FRT0001642E and FRT00017103) to compare the spectral properties of carbonates in the two locations. Where possible, spectra from similar locations in overlapping cubes were compared to evaluate image-to-image consistency. While we found that the position of absorption bands and their relative variations in depth between locations did not change between images, their absolute depth can vary significantly. For example, while the Light-toned Floor does not appear to exhibit clear carbonate absorptions in FRT00005C5E, it does exhibit clear carbonate absorptions in FRT000047A3. FRT000047A3 generally has better spectral contrast than the other images, possibly due to lower detector temperatures or lower atmospheric opacity. For this reason, FRT000047A3 served as our reference image for building parameter mosaics as discussed above.

4. Overview of spectral diversity in Jezero

4.1. Mineralogy of the carbonate units

Based on our CRISM parameter maps shown in Figs. 3, 4, 6, and 8, we find that the carbonate units within Jezero are more spectrally variable than previously reported. All of the carbonate-bearing units typically exhibit carbonate bands near 2.31 and 2.51 μm, hydration bands at 1.93 μm, and one or more mafic components indicated by the strong red spectral slope between 1.0 and 1.8 μm and an additional band or shoulder at ~1.3 μm. However, the relative strengths of these parameters vary both within and between the units. As all of these spectral signatures appear to vary at least somewhat independently, we hypothesize that they are largely due to different phases in the overall assemblage. Fig. 3a shows the "Carbonate" RGB CRISM map, in which all colored areas correspond to the units that typically exhibit carbonate and/or olivine signatures, but the variation in color indicates spectral variability within the olivine-carbonates. Some of this variability is due to variation in the strength of the carbonate band at ~2.5 μm (white, cyan, and blue indicate strong carbonate signatures), but the rest is due to variation in the mafic signatures.

Spectral analysis confirms that there are significant variations in the 0.7–1.8 μm mafic signature of the carbonates. The Mottled Terrain, Light-toned Floor, and most olivine-rich dunes in the area exhibit broad and rounded bands that extend out to nearly 2 μm (e.g., spectra 1–4 in Fig. 3c; spectrum 3 in Fig. 6c), but some dunes and many of the carbonates exhibit a much more square band with an apparent shoulder or band near 1.3 μm (e.g., spectrum 5 in Fig. 3c; spectrum 1 in Fig. 6c). These squared bands are most commonly identified in sediments on or proximal to the Marginal Carbonates. In addition, some spectra in the Marginal Carbonates with strong carbonate signatures exhibit a much weaker rounded mafic band centered at 1.3 μm (e.g., spectrum 6 in Fig. 3c).

Representative laboratory spectra of relevant minerals are shown for comparison in Fig. 2. The square spectral shape in the Marginal Carbonates could be consistent with either Fe-rich or coarse-grained olivine (e.g., King and Ridley, 1987; Fig. 2c), but TES models are more consistent with a Mg-rich composition in this area (~$Fo_{50–75}$; Koeppen and Hamilton, 2008), suggesting that a coarse grain size is more likely. Fe-substitution in plagioclase feldspar can also cause a weak ~1.3 μm band (e.g., Adams and Goullaud, 1978), and may help to flatten and square off the olivine band (e.g., forsterite/anorthite in a lunar troctolite, Fig. 2c). Finally, the strong ~1.3 μm shoulder could also be related to iron in the carbonates, as even minor Fe-substitution (>0.01 wt%) in various carbonates, including Mg-carbonates, commonly causes a strong band around 1.3 μm (Fig. 2b; Gaffey, 1987). The more rounded and strong mafic absorptions of the Light-toned Floor, Mottled Terrain, and sandy areas could be due to either a smaller olivine grain size or a lack of one of these other phases. The weaker mafic absorptions near 1.3 μm in some areas of the Marginal Carbonates (e.g., spectrum 6 in Fig. 3c) is consistent with Fe-substitution in either carbonate or plagioclase, but given the strong 2.3 and 2.5 μm carbonate bands in these areas, is more likely to be due to Fe-substitution in carbonate.

The degree of hydration inferred from the depth of the 1.9 μm hydration band varies across the carbonates, as shown in Fig. 4. Previous studies have attributed this hydration to mixing with phyllosilicates, another distinct hydrated phase, or hydrated carbonates (Ehlmann et al., 2008a). A variety of hydrous carbonates exist, and the degree of hydration can strongly influence their spectral properties (e.g., Calvin et al., 1994; Harner and Gilmore, 2015). Hydromagnesite, artinite, nesquehonite, and dypingite are distinct Mg-carbonate phases that include OH as well as H_2O in their crystal structure at various ratios. Because of this structural change, these phases exhibit distinct spectral properties compared to magnesite (Calvin et al., 1994; Harner and Gilmore, 2015). Hydromagnesite is the most stable of these phases and thus also the most common in terrestrial settings (e.g., Königsberger et al., 1999; Russell et al., 1999). Hydromagnesite exhibits sharp OH bands at 0.96 and 1.4 μm, which are superposed on broader H_2O bands at 1.44 and 1.96 μm. The carbonate 2.3 μm band is replaced in hydromagnesite by a shallow triplet at 2.26, 2.32, and 2.43 μm and another shallow band at 2.53 μm. Hydrated magnesites are also found in natural settings, and are spectrally similar to magnesite, but with added hydration bands near 1.4–1.5 and 1.9–2.0 μm (Fig. 2b). These bands have been attributed to mixing with minor hydromagnesite (Hunt and Salisbury, 1971) or to hydration from fluid inclusions (Crowley, 1986). Many hydrated magnesites exhibit a sharp 1.9 μm band, while some natural samples exhibit a rounded band closer to 2.0 μm (Fig. 2b). This 2.0 μm band shifts to 1.9 μm upon dehydration in the laboratory, suggesting that the 2.0 μm band indicates greater water content (Fig. 2b). These hydrated magnesites may have formed from dehydration and/or recrystallization of phases like hydromagnesite.

We have identified several locations in the southern reaches of the Marginal Carbonates that exhibit clear and strong carbonate signatures

and weak mafic signatures, suggesting concentrated carbonates with less olivine. These carbonate-dominated spectra are still hydrated, suggesting that the carbonates themselves are hydrated, at least in this location. The hydration band occurs as a rounded band centered at longer wavelengths near 2.0 μm (spectrum 6 in Fig. 3c; see also Fig. 19), which is consistent with either hydrated magnesite or a magnesite-hydromagnesite mixture (Fig. 2b). However, this weak 2.0 μm band is only detectable because the spectra do not exhibit a sharp 1.9 μm band. Elsewhere, this 2.0 μm band may be present but obscured by more common 1.9 μm hydration bands. Thus, the variability in hydration signatures in the carbonate units may be related to hydration state of the carbonates themselves as well as the presence of other hydrated minerals.

The presence of other hydrated phases in the carbonate-bearing terrains is supported by the observation that the hydration band strength appears to vary independently of carbonate band strength, as indicated by the diversity in the "hydration" RGB shown in Fig. 4. The Mottled Terrain in Jezero, in particular, exhibits strong hydration bands and weak carbonate bands relative to the other units. We have identified at least one location in a possible delta remnant where only strong hydration bands are present without clays or carbonates (spectrum 1 in Fig. 4c), but it is unclear if this is the same hydrated phase as in the carbonates. Other hydrated phases like phyllosilicates could be present, which could potentially be identified by other diagnostic bands in the 2.0–2.5 μm region. Al-phyllosilicate and hydrated silica exhibit bands near 2.20–2.22 μm, but these are not clearly present in the carbonate-bearing terrains. Fe/Mg-phyllosilicates exhibit bands near 2.30 μm, but identifying Fe/Mg-phyllosilicates in mixtures with carbonates is challenging, as this band overlaps with the strong carbonate band near 2.3 μm (e.g., Bishop et al., 2013). However, local occurrences of spectra consistent with the Mg-phyllosilicates serpentine and talc/saponite have been identified in CRISM spectra in a few locations within the regional olivine-carbonate unit, both on the plains surrounding Jezero and in the Nili Fossae region to the northwest (Ehlmann et al., 2009, 2010; Viviano et al., 2013; Amador et al., 2018). Thus, Fe/Mg-phyllosilicates are a likely contender for the cause of the hydration in the carbonate-bearing terrains (Goudge et al., 2015), but it is unclear based on previous work whether or not any of these phases may be present within the Jezero carbonates.

Table 1
RGB composites of spectral parameters (defined by Viviano-Beck et al., 2014) used in this study to evaluate spectral differences between carbonate units and related deposits.

RGB Map	Purpose	Red/Green/Blue Channels	Interpretation of relative mineral assemblage
False Color (Figure 1a)	Correlating maps to surface features	R2529 / R1506 / R1080	**Red:** olivine. **Green to blue:** carbonates. **Purple:** low-calcium pyroxene. **Brown:** mafic floor.
Carbonates (Figure 3)	Variability within the carbonate units	BD1300 / BDI1000IR / MIN_2295_2480	**Red:** olivine. **Cyan/blue:** strong carbonates, weaker olivine. **Yellow/white:** strong carbonates and strong olivine. **Green:** relatively olivine-poor with other Fe-bearing phases (e.g., clays/carbonates). **White:** hydration with carbonates.
Hydration (Figure 4)	Hydration with clays or carbonates	D2300 / BD1900_2 / MIN_2295_2480	**Magenta:** weak or no hydration with carbonates. **Green:** hydration with weak carbonates or other phases like Al-clays and silica. **Yellow/orange:** Fe/Mg-clays. **Red/Yellow:** Fe/Mg-smectites or carbonates.
Phyllosilicates (Figure 8)	Al/Si vs. Fe/Mg alteration minerals	D2300 / D2200 / MIN2250	**Green:** Al-clays. **Cyan:** silica or Al-clays. **Blue:** opal or hydrated silica.
Mafic (Figure 6)	Primary mafic minerals	BD1300 / LCPINDEX/ HCPINDEX	**Red:** olivine and mafic component of carbonates. **Green:** Low- calcium pyroxene. **Blue:** High-calcium pyroxene.

The presence of Fe/Mg-phyllosilicates could potentially be detected based on their effect on the position of the carbonate bands. The carbonate bands in Jezero are predominantly centered between 2.307 and 2.310 and 2.515–2.520 μm – slightly off from the typical band centers for magnesite, which are reported as 2.298–2.300 and 2.497–2.500 μm (Gaffey, 1987). This shift in band center could represent a shift toward another carbonate composition through cation substitution, such as Ca—Mg carbonate (dolomite), which has bands centered at 2.320 and 2.515 μm (Fig. 2b). Alternatively, Mg-phyllosilicates like smectite, serpentine, talc, and saponite could also produce this shift. In particular, serpentine exhibits bands near 2.325 and 2.510 μm that could be shifting the carbonate bands to longer wavelengths. We conducted a search for serpentine bands in Jezero based on the presence of other bands that serpentine often exhibits at 2.12 and 2.38 μm (Fig. 2a). Weak bands at these positions are present in a small number of spectra, and these appear to be strongest in the Marginal Carbonates near the western delta inlet (e.g., spectra 2 and 3 in Fig. 4). However, these detections are weak and not clearly resolved, and while these bands are present in the vast majority of serpentine lab spectra, they exhibit variable strengths and may not always be good indicators of the presence of serpentine (e.g., Ehlmann et al., 2010). Thus, whether or not serpentine is present in Jezero remains unclear.

The Fe/Mg-phyllosilicate that may be more likely to be mixed with the carbonates in significant abundance is Fe/Mg-smectites. Fe/Mg-smectites outside of the carbonate-bearing terrains are recognized by a band near 2.31 μm and no ~2.5 μm band, where a 2.31 μm band center is consistent with Mg-rich smectites (Fe/Mg < 0.5; Michalski et al., 2015). These signatures are present in the western delta and in the basement exposed in the rim as reported previously (Goudge et al., 2015, 2017), but are also present in the northern fans and in portions of the Mottled Terrain. Fe/Mg-smectites may be present elsewhere as well. The position of the 2.31 μm band in the carbonates in Jezero is indistinguishable from the same band in the Fe/Mg-smectites in the western delta and crater rim. Because of this similarity, smectites can only be conclusively identified by the absence of a 2.5 μm carbonate band. Thus, in many locations, weak smectite signatures could be mistaken for weak carbonate signatures, or vice versa.

Some information on the relative variations in carbonate vs. smectite spectral signatures may be gleaned from comparing the depths of the 2.3 and 2.5 μm bands. Carbonates tend to exhibit stronger 2.5 μm bands than 2.3 μm bands, and this is especially true for Mg-rich carbonates (Fig. 2b). Adding Fe/Mg-smectite to a carbonate makes the 2.3 μm band as strong or stronger than the 2.5 μm band (Bishop et al., 2013). Fig. 5 shows the ratio (1 + D2300)/(1 + BD2500) mapped over the western crater. This ratio is similar to a direct band depth ratio but allows for negative parameter values that occur in the refined spectral parameters. This map demonstrates that there are systematic variations in the relative strength of these bands in Jezero, likely indicating variations in the relative abundance of Fe/Mg-phyllosilicates and Mg-carbonates between the different units.

Based on these spectral observations, the mineral assemblage in the Jezero carbonates is consistent with some combination of magnesite or hydromagnesite with some Ca-substitution, Mg-rich smectites, Mg-rich

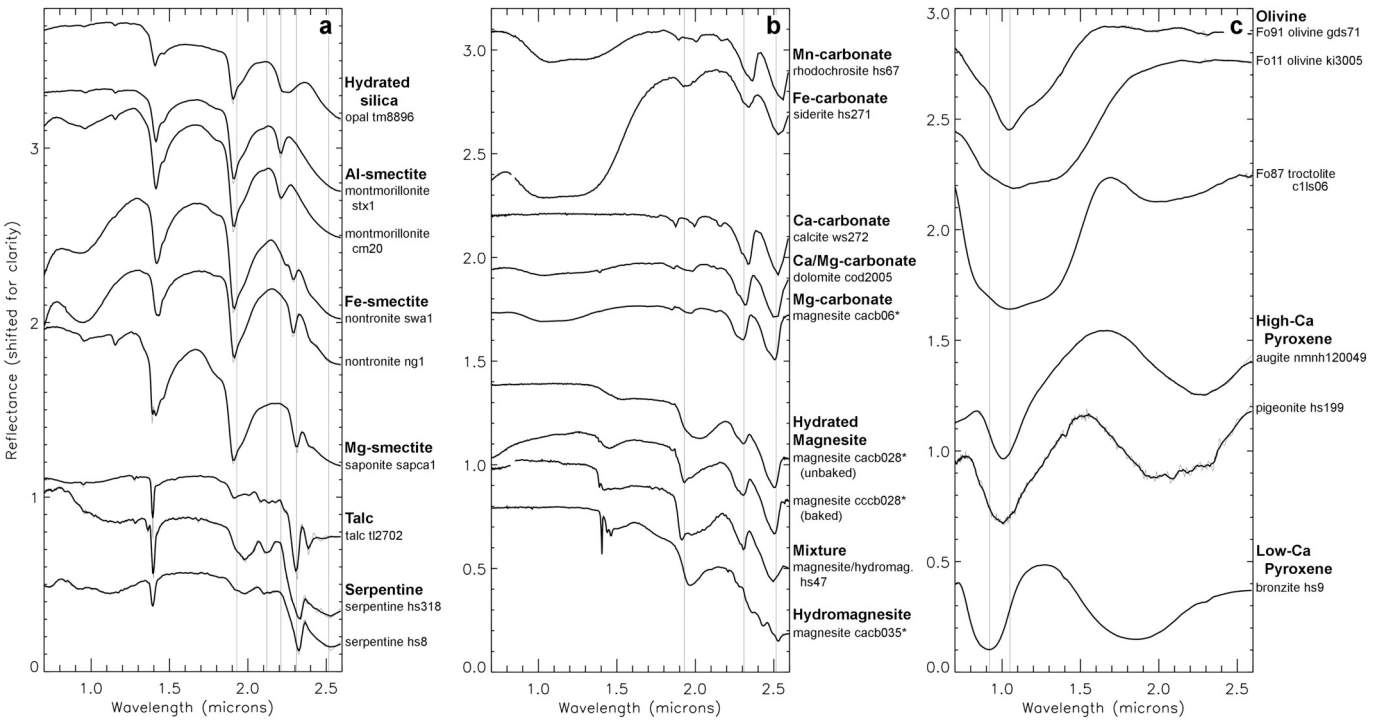

Fig. 2. Laboratory endmember spectra representing the possible spectral diversity in Jezero crater for (a) phyllosilicates and silica, (b) carbonates, and (c) primary mafic minerals. In some cases, spectra have been smoothed with a boxcar smoothing algorithm (width of 3 channels), and the original spectra are shown as thin gray lines. Vertical lines at 0.92, 1.05, 1.93, 2.21, 2.31, and 2.515 μm indicate the typical absorption band positions in CRISM spectra of Jezero. Spectra are from the USGS Spectral Library (Clark et al., 2007), except starred samples, which are from the RELAB Spectral Library (Pieters, 1983).

olivine, and perhaps minor serpentine, in potentially highly variable relative abundances.

4.2. Mafic mineralogy of Jezero

The clearest correlation between spectral properties and geologic units in Jezero is provided by mafic mineralogy, as determined based on the position and shape of broad bands due to iron near 1 and 2 μm (Fig. 2c; e.g., Adams, 1968; Cloutis and Gaffey, 1991; Horgan et al., 2014). Even where carbonate and clay signatures are weak, there are clear differences in mafic mineralogy (Fig. 6). The rim and associated knobs of rim material in the marginal regions exhibit strong low-Ca pyroxene (LCP) signatures consistent with the regional basement unit, as do much of the western delta and northeastern fan. In contrast, the carbonate units exhibit strong olivine signatures (and/or signatures due to minerals that are spectrally similar to olivine, like Fe-bearing carbonate), and these olivine-like signatures are also found in both of the northern fans. However, the delta/fans all exhibit significant variability, as detailed in the next section. Finally, the Mafic Floor itself appears to be enriched in high-Ca pyroxene (HCP), although the underlying mineralogy is difficult to constrain, as the Mafic Floor is frequently obscured by bedforms and surficial mantles.

Bedforms in the crater have diverse compositions, indicating many sediment sources and/or sorting during transport. On the Light-toned Floor, all bedforms are enriched in olivine, whereas bedforms and sediment mantles covering many areas on the Mafic Floor are enriched in LCP, most likely sourced from the delta and fans. Elsewhere, including on much of the Mafic Floor and on some areas of the Mottled Terrain and northeastern fan, bedforms often exhibit HCP spectral signatures, most likely indicating a source in the Mafic Floor, or perhaps the HCP-bearing terrains on the plateau outside of the crater (e.g., spectrum 4 in Fig. 6). These terrains may correspond to previously unidentified occurrences of the HCP-bearing "Pitted Capping Unit" mapped farther to the west by Goudge et al. (2015).

4.3. Mineralogy of the delta and fans

The three fan/delta features in Jezero all exhibit distinct spectral signatures, as shown in Fig. 7. The western delta is the most complex, and exhibits clear regions enriched in different primary and secondary minerals. The majority of the channel deposits mapped by Goudge et al. (2018) are dominated by LCP and Fe/Mg-smectite signatures in CRISM (spectra 3/4 in Fig. 7c), and all of the curvilinear regions interpreted as point bar deposits are dominated by olivine and carbonate signatures. Areas where this correlation does not hold are mapped as channel deposits but exhibit olivine/carbonate signatures; however, these areas appear to be logical extensions of the mapped point bar deposits with more muted surface expressions. We have noted an additional LCP-bearing unit that appears to underlie the olivine/carbonate-bearing point bar deposits at the northwestern margins of the delta (Fig. 7e), which correspond to foreset/bottomset strata mapped in Goudge et al. (2017).

The northwestern fan is dominated by olivine and strong carbonate signatures (spectra 9/10, Fig. 7d), with LCP and weak Fe/Mg-smectite detections limited to light-toned knobs around the eastern margin (spectrum 1, Fig. 7c). The northeastern fan exhibits large areas of both olivine and LCP signatures, but in general, smectite bands are weak or not present (spectrum 2, Fig. 7c). The overall weaker signatures on the northeastern fan may be due to both significant erosion and mantling by surface sediment. Supporting this interpretation, the smoother olivine-bearing eastern portion of the northeastern fan does exhibit carbonate signatures where it is not mantled by LCP-bearing bedforms. These olivine/carbonate-bearing units on both fans appear to overlie the LCP-bearing portions of the fans. This mineral stratigraphy is similar to the stratigraphic relationship observed in parts of the western delta, where the olivine/carbonate-bearing point bar facies overlie LCP/smectite-bearing layers (Fig. 7e). The relationship between the mineral stratigraphies in delta and fans is not well-constrained, except that the farthest margin of the topmost, LCP-bearing inverted channel facies of the

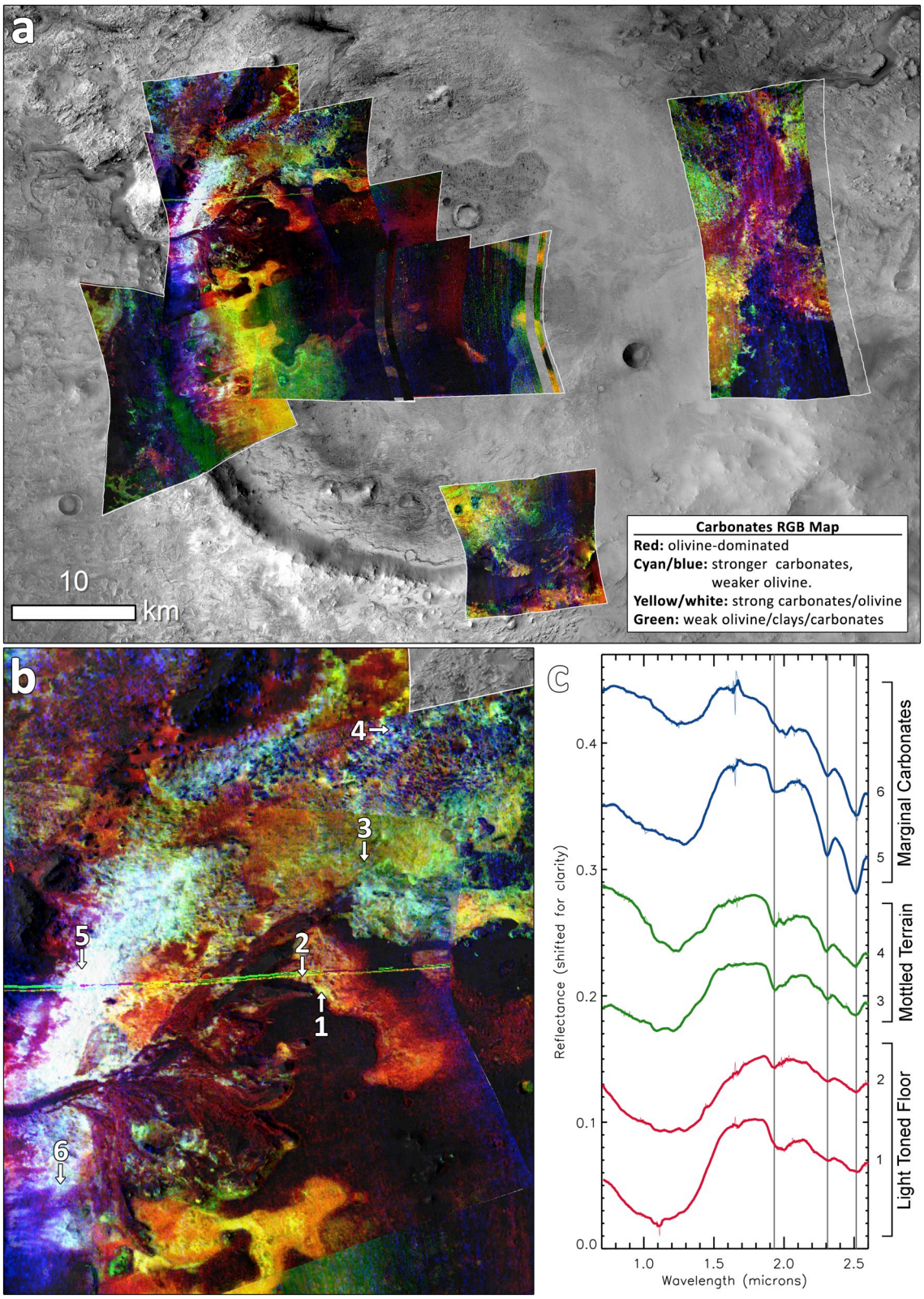

Fig. 3. Spectral diversity in carbonate-bearing terrains in Jezero crater. (a) Mosaic of "carbonate" RGB composite of select CRISM images. Red indicates olivine, yellow/white indicates strong olivine and carbonate signatures, cyan/blue indicates strong carbonates with weaker olivine, green indicates relatively carbonate and olivine-poor, possibly with other Fe-bearing phases (e.g., clays/carbonates). (b) Zoom to show diversity in the region of the western delta. Green horizontal line in center of image is due to noise in some of the spectral parameter maps, which does not adversely affect the extracted spectra. (c) CRISM ratio spectra of carbonate-bearing units from image HRL000040FF at numbered locations in (b), showing variability in the strength and shape of mafic bands at 1.0–1.3 μm, hydration bands at 1.9 μm, and carbonate bands at 2.3 and 2.5 μm. (For interpretation of the references to color in this figure legend, the reader is referred to the web version of this article.)

western delta may overlie the olivine/carbonate-bearing unit on the northwestern fan, as shown in Fig. 7e.

We also report new detections of possible silica or Al-clay bands within the delta, northern fans, and proximal terrains, based on ~2.2 μm shoulders on the 2.3 μm carbonate/smectite band, as shown in Fig. 8. The additional absorption is correlated with geomorphic features, suggesting that it is due to real spectral variability. This band tends to occur along with olivine/carbonate signatures in the delta and fans, including in several exposures of the western delta point bar facies (Fig. 8b). This band could be due to silica, which exhibits a broad doublet at 2.21/2.25 μm (Langer and Florke, 1974; Rice et al., 2013), Al-substitution in Fe/Mg-smectites, which produces a broad shoulder near 2.23–2.24 μm (Bristow et al., 2018), or Al-clays, which exhibit a narrower band at 2.21 μm (Bishop et al., 2002; Cuadros and Michalski, 2013). However, a definitive identification is challenging when mixed with carbonate.

5. Properties of the carbonate units

All of the carbonate units exhibit a grossly similar morphology characterized by a rough surface texture, often with craters, and a light tone compared to other regional bedrock. Because of this similarity, most of the carbonate-bearing terrain was grouped into the Mottled Terrain in previous studies at CTX-scales (Goudge et al., 2015). This grouping is supported by their strong spectral similarity in CRISM data, including the mafic, hydration, and carbonate absorptions discussed above. However, there are HiRISE-scale variations in texture between and within units that correlate with spectral variability, as summarized in Fig. 9.

5.1. Mottled terrain: textures

Both within and to the north and west of Jezero, the Mottled Terrain unit is primarily characterized by an erosional texture of numerous small (tens to hundreds of meters) linear ridges, often with a northeast/southwest orientation (Fig. 10a/b). These ridges are responsible for the mottled appearance at CTX scales (and thus the name of the unit). In the plains to the west of Jezero, the Mottled Terrain exhibits some linear features that follow this same northeast/southwest orientation (Fig. 10c), but if these are equivalent to the ridges in and around Jezero, they have undergone much more erosion. At finer scales, the Mottled Terrain is generally fractured with a highly variable texture. In some areas, the surface is relatively smooth with fractures traceable for hundreds of meters, or the surface exhibits smaller-scale polygonal or "honeycomb" fracture patterns, or the surface is dominated by a rubbly texture. The Mottled Terrain also includes rings of rough, raised topography surrounding knobs of crater wall material in the southwestern portion of the crater. In general, the Mottled Terrain appears to be a broad and textural properties exhibited by the Fractured Unit could help determine which other "catch-all" map designation for a variety of surface textures and expressions, and may include multiple geologic units that are difficult to distinguish clearly, even at higher resolutions. There does not appear to be any clear correlation between Mottled Terrain morphology and whether it is inside or outside Jezero crater. The sub-unit designations from Goudge et al. (2015) are generally unclear at HiRISE scale, and some may be misleadingly named (e.g. some "dusty Mottled Terrain" areas are clean exposures of bedrock with high thermal inertia, inconsistent with dust cover).

The Mottled Terrain may be stratigraphically equivalent to the Fractured Unit, the olivine/carbonate unit in the plains to the south of Jezero, in the vicinity of the candidate NE Syrtis landing site (Bramble et al., 2017). Bramble et al. (2017) described the Fractured Unit as exhibiting a corrugated surface texture of light-toned, fractured blocks surrounded by dark-toned material in HiRISE images - similar to the general description that could be used to describe virtually all of the carbonate-bearing terrains both within and beyond Jezero.

In a survey of the textural characteristics of the Fractured Unit across the NE Syrtis region in HiRISE images, we observe that the unit is highly variable and generally less morphologically distinctive than the Mottled Terrain. In some locations, the Fractured Unit does exhibit the characteristic ridges of the Mottled Terrain, but only in isolated occurrences a few hundred meters wide (e.g., Fig. 11 location 2). In other isolated locations, the Fractured Unit exhibits distinct rectilinear to subpolygonal fracture patterns, with the fractures visible as darker-toned than the surrounding outcrop (possibly because fractures are recessive and shadowed and/or have been filled by darker sands; Fig. 11 location 6). Occasionally, these fractures are visible in raised relief as "boxwork" patterns of ridges, which have been interpreted elsewhere on Mars as forming via mineralization during fluid flow through the fractures (Siebach and Grotzinger, 2014; Fig. 11 location 3). The most prevalent texture of the Fractured Unit in NE Syrtis, however, is less distinct, with patchy outcrops of fractured, light-toned rock visible beneath various amounts of darker-toned mantles and aeolian bedforms (Fig. 11 location 4).

5.2. Mottled terrain: spectral signatures

The spectral properties of the Mottled Terrain are as variable as its textural properties, as demonstrated by the heterogeneity of the Mottled Terrain that mantles the northern portion of the crater, as shown in the maps in Fig. 12b–c. The main spectral characteristic of the Mottled Terrain in this area is strong hydration bands, as shown by the strong green color in Fig. 4, often along with weaker carbonate and olivine bands than other carbonate units. However, some locations do not exhibit carbonate bands and instead exhibit only 2.3 μm bands with no 2.5 μm bands, consistent with Fe/Mg-smectite (spectrum 6 in Fig. 12d). Indeed, the relative strength of smectite relative to carbonate appears to be generally higher throughout most of the northern Mottled Terrain away from the fans, based on the relative band depth of their 2.3 and 2.5 μm bands, as shown in Fig. 5 and discussed in Section 4.1. Both smectite and carbonate spectral signatures are strongest around the margin of the northern Mottled Terrain (large yellow/orange arc at the location of spectrum 1 in Fig. 12d).

On the plains just outside of Jezero to the northwest, the Mottled Terrain exhibits stronger and generally more consistent spectral signatures compared to the Mottled Terrain in the interior (spectra 7–9 in Fig. 12d): moderate mafic signatures, variable but typically strong hydration bands, and moderate carbonate signatures. Compared to the interior, the 2.3 μm band is somewhat weaker than the 2.5 μm band (visible in the upper left of Fig. 5), more consistent with carbonate and perhaps minor Fe/Mg-smectite (or another Fe/Mg-phyllosilicate).

Beyond the crater, only one CRISM MTRDR image currently exists that includes the Mottled Terrain, located upstream along the main drainage valley of the western inlet watershed (Fig. 13). Within this area, the Mottled Terrain is spectrally similar to the plains just beyond the rim of Jezero, with clear carbonate bands and limited evidence for Fe/Mg-smectite, but also clear and sharp hydration bands (Fig. 13; Goudge et al., 2015). Mafic signatures are quite variable, which is also a common characteristic of the Mottled Terrain in many locations both within and beyond Jezero. While the Mottled Terrain beyond the crater does exhibit scattered small areas with clear smectite detections (e.g., spectrum 5 in Fig. 13), these are associated with uplifted knobs, presumably of basement materials, or mantles within fields of secondary craters consistent with impact ejecta from the large nearby crater.

In CRISM observations, the Fractured Unit to the south of Jezero exhibits strong hydration bands, moderate to strong mafic signatures, and variably strong carbonate bands (Fig. 11a–b). Some areas within the Fractured Unit exhibit ~2.2 μm shoulders on the 2.3 μm carbonate band, suggesting the presence of Al-clays or silica (e.g., spectra 2 and 5 in Fig. 11). However, neither the Mottled Terrain or Fractured Unit outside of Jezero exhibit the smectite and mixed smectite/carbonate signatures found in the Mottled Terrain in the northern interior of Jezero, nor do other areas of Mottled Terrain covered by CRISM in the southwest,

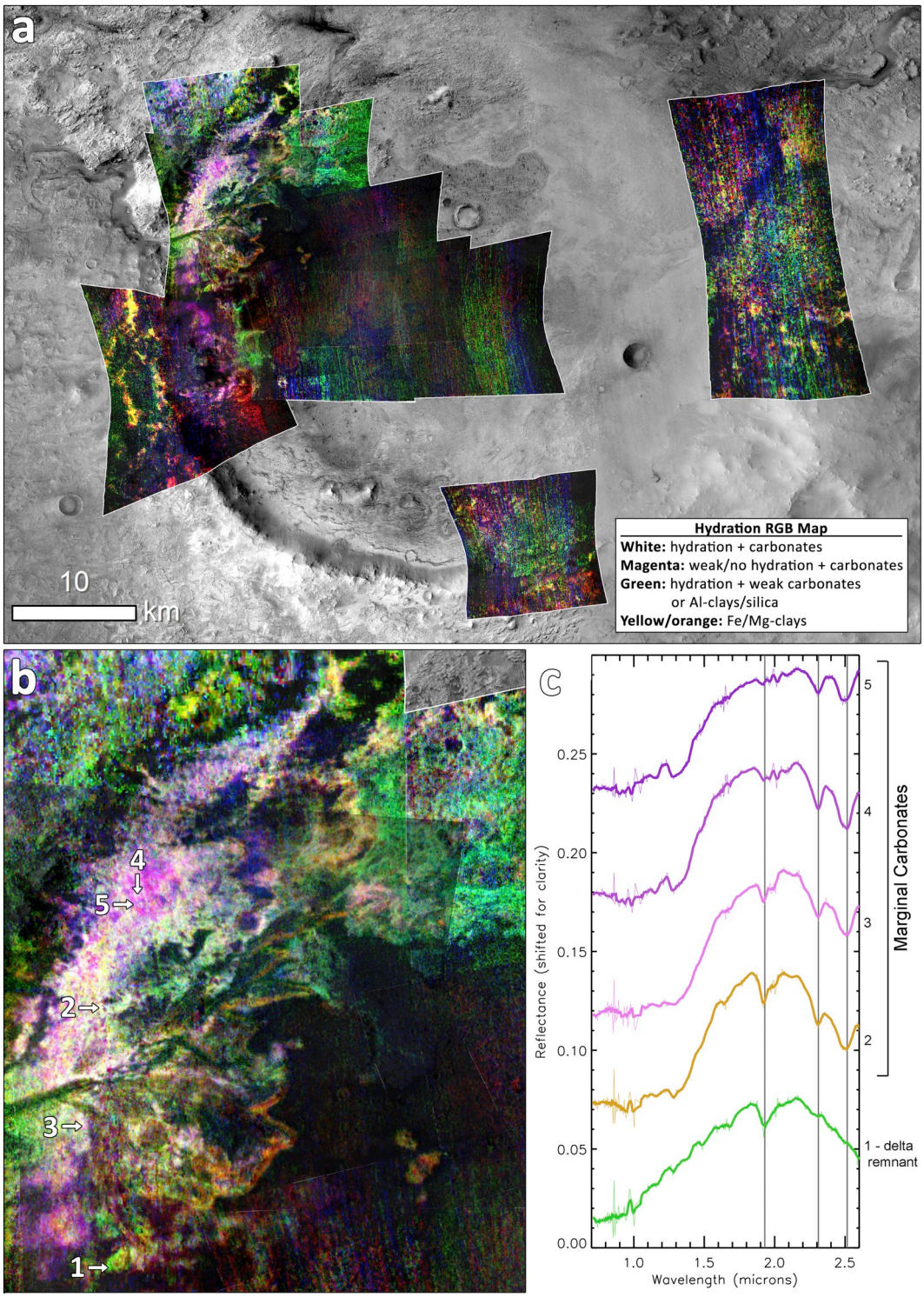

Fig. 4. Variation in hydrated spectral signatures. (a) Mosaic of "hydration" RGB composite of select CRISM images. White indicates hydration with carbonates, magenta indicates weak or no hydration with carbonates, green indicates hydration with weak carbonates or other phases like Al-clays and silica, and yellow/orange indicates Fe/Mg-clays. (b) Zoom to show diversity in the region of the western delta. (c) CRISM spectra showing increasing 1.9 μm hydration band depth from top to bottom, from image FRT5C5E at numbered locations in (b). Color corresponds to approximate color in alteration RGB. (For interpretation of the references to color in this figure legend, the reader is referred to the web version of this article.)

southeast, or eastern portions of the crater. This suggests that these smectite exposures are unique to the northern interior of Jezero.

To summarize, the regional olivine/carbonate-bearing terrains of the Mottled Terrain and Fractured Unit outside of Jezero crater tend to exhibit moderate carbonate bands with limited evidence for Fe/Mg-smectite, variable but strong hydration signatures, and variable mafic signatures. This is in contrast to the Mottled Terrain in the northern interior of Jezero, which in exhibits weak mafic bands and is more strongly dominated by smectite instead of carbonate.

5.3. Light-toned floor

The Light-toned Floor generally lacks the larger ridges and fractures characteristic of the Mottled Terrain. The Light-toned Floor often has a characteristic "pock-marked" texture but elsewhere is smoother (Fig. 14). Morphologically, the boundary between the Light-toned Floor and the Mottled Terrain is often unclear, though in some cases a possible textural contact can be identified (see Fig. 18d). In some areas, such as the northern portion of the crater, the Light-toned Floor does exhibit faint ridges similar to those observed in the neighboring Mottled Terrain. Spectrally, the Light-toned Floor exhibits strong olivine signatures that correlate with aeolian cover (Fig. 15), supporting the hypothesis that the olivine-bearing sand is sourced from the Light-toned Floor itself (Ehlmann et al., 2008b; Goudge et al., 2015). The 2.3 and 2.5 μm carbonate bands are generally weak in the Light-toned Floor (even in locations with strong hydration bands, e.g., spectrum 7 in Fig. 15). Typically the 2.3 μm band is as strong or stronger than the 2.5 μm band (Fig. 5), likely indicating significant Fe/Mg-clay content, much like the Mottled Terrain in the north of Jezero.

5.4. Marginal Carbonates

The "Marginal" Carbonates are differentiated from other carbonate units in Jezero based on much stronger and clearer carbonate signatures (Figs. 3 and 5), and the fact that these signatures appear to be restricted to a narrow strip along the base of the crater wall. Although the most distinct exposure of the Marginal Carbonates is to the west of the western delta, outcrops with similar spectra and textures occur all along the base of the western crater rim (Fig. 3).

Along the western inner crater rim, the Marginal Carbonates are restricted to elevations between approximately −2420 m and −2260 m (Fig. 16), where the upper limit corresponds to the break in slope associated with the crater rim. The lower limit is just below the breach elevation (−2395 m) for the outlet valley reported by Fassett and Head (2005), and is also just below the highest elevation measured for inverted channels on the western delta (approximately −2380 m; Goudge et al., 2018). A few isolated areas to the south that may or may not be consistent with the Marginal Carbonates fall outside of this range; however, the lowermost isolated area is within the range of lake levels based on the minimum elevation of the main body of the western delta. These isolated occurrences are within and upslope from rough concentric terraces around knobs and buttes of LCP-bearing rim material in the southwest crater.

Although they were mapped as part of the Mottled Terrain by Goudge et al. (2015), the Marginal Carbonates lack the characteristic ridged erosional texture of the Mottled Terrain, appearing smooth at CTX scale and heavily fractured and blocky at HiRISE scale (Fig. 17), with a more "rubbly" appearance than most exposures of the Mottled Terrain. The Marginal Carbonates also lack the "pock-marked" texture characteristic of the Light-toned Floor. These textural differences are clearest at the northeastern edge of the Marginal Carbonates (Fig. 16a), where the edge of the strong carbonate signatures in Figs. 3 and 5 also corresponds to a textural boundary. Areas to the east of the boundary exhibit a brighter tone and smoother surface texture than the Marginal Carbonates, as well as some NE/SW-trending ridges potentially similar to the Mottled Terrain (Fig. 18c). Thus, this textural and spectral boundary may correspond to a boundary between these units. Further east, this smooth texture transitions into the.

"pockmarked" texture characteristic of the Light-Toned Floor (Fig. 18d). Lastly, the valley leading to the western delta appears to cut through the Marginal Carbonates, exposing a light-toned layered unit that appears to be beneath them (Fig. 17d). Outcrops of the Marginal Carbonates above this layered outcrop are rubbly with no clear bedding visible.

The Marginal Carbonates exhibit several spectral characteristics that are distinct from the other carbonate-bearing terrains within the crater. First, their carbonate signatures are consistently much stronger and narrower than either the Mottled Terrain or the Light-toned Floor (Fig. 3c). While the absolute band depths vary from image to image, and can vary across images due to local variations in, e.g., atmospheric opacity, these signatures are strong relative to other terrains in all three CRISM images that include the Marginal Carbonates (FRT00005C5E; FRT000047A3; HRL000040FF). The stronger band depths in the Marginal Carbonates could potentially be due to differences in texture and/or dust cover – for example, while the Marginal Carbonates are rough at HiRISE scales, they are smooth at CTX/MOLA scales, which could result in more wind erosion, less dust, and stronger spectral signatures. Grain size differences between the units could also influence band depth, as coarser grains tend to result in relatively deeper bands (Pieters, 1983). However, the Marginal Carbonates also consistently exhibit stronger 2.5 μm bands relative to their 2.3 μm bands compared to other terrains in Jezero, suggesting a higher carbonate:clay ratio (Fig. 5). This suggests that there are real mineralogical differences between the Marginal Carbonates and other carbonate units in the crater.

The strength of the 1.9 μm hydration band also varies significantly across and locally within the Marginal Carbonates. Some spectra with strong carbonate signatures in the Marginal Carbonates exhibit strong 1.9 μm bands, others do not exhibit a 1.9 μm band at all, and some instead exhibit a rounded 2.0 μm band consistent with a hydrated Mg-carbonate or a magnesite-hydromagnesite mixture.

Finally, mafic signatures are also much more variable within the Marginal Carbonates than other units. The Marginal Carbonates do not exhibit the broad and rounded olivine absorptions exhibited by the Light-toned Floor, Mottled Terrain, and Fractured Unit, but spectral shapes include a squared-off band consistent with coarse olivine (spectra 4 and 7–9 in Fig. 19), or an isolated narrower Fe-band centered at 1.3 μm consistent with a weaker olivine band, Fe-substitution in carbonates or plagioclase feldspar (spectra 1–3 in Fig. 19).

The spectral properties of the Marginal Carbonates vary spatially and appear to correlate with distance from the inlet valley (Fig. 19). These variations are similar in both CRISM images that cover the extent of the Marginal Carbonates (FRT00005C5E; HRL000040FF), and do not appear to be correlated with variations in albedo, sand cover, or surface texture, suggesting that they are due to real variations in mineralogy or physical properties (abundances, grains sizes, etc.). Proximal to the inlet valley, the Marginal Carbonates exhibit clear carbonate signatures, moderate hydration bands, and strong olivine bands (spectra 4/5 in Fig. 19). Moving to the north, the Marginal Carbonates exhibit somewhat stronger spectral signatures, including clear hydration bands and more squared-off mafic signatures consistent with coarse-grained olivine (white in "carbonates" RGB, yellow in "hydration" RGB, and spectrum 6 in Fig. 19). This area may also be a source of some olivine-bearing sands, supporting greater abundances of coarse-grained olivine. To the north, hydration bands become significantly weaker (magenta in "hydration" RGB, and spectrum 7 in Fig. 19), and aeolian bedforms are LCP-bearing, suggesting that this area is not a major source of olivine sands (Fig. 18b). The Marginal Carbonates may include an arcuate carbonate-bearing region to the northeast along the inner crater rim, but these areas exhibit much weaker spectral signatures than the rest of the Marginal Carbonates (spectra 8–9 in Fig. 19).

A clearer spectral trend extends to the south of the inlet valley. While the 2.5 μm carbonate band maintains similar band depths throughout

the "southern" Marginal Carbonates, mafic signatures, the 1.9 μm band, and the 2.3 μm band all rapidly decrease with distance from the inlet valley. In addition, the shape of the broad mafic band and 1.9 μm band change, respectively, to a narrower 1.3 μm band and a weaker and broader 2.0 μm band, consistent with hydrated magnesite or a magnesite-hydromagnesite mixture. The southernmost terrace that is clearly associated with the Marginal Carbonates exhibits the spectrum most consistent with hydrated magnesite (spectrum 1 in Fig. 19), without obscuration by strong olivine, clay, or hydrated spectral signatures, suggesting a relative lack of these phases. Clear hydrated magnesite spectral signatures without apparent olivine or clay contributions are unique to the southern Marginal Carbonates, and have not been detected in the other terrains within or beyond the crater.

In summary, the Marginal Carbonates are primarily distinctive compared to other carbonate-bearing terrains within Jezero because they occur only within a narrow range of elevations, whereas the regional carbonate-bearing terrains drape and mantle underlying topography (Kremer et al., 2019). In addition, the Marginal Carbonates exhibit much stronger carbonate signatures than elsewhere in the crater, and strong 2.5 μm bands relative to their 2.3 μm bands that may indicate more carbonate relative to clay. Finally, the southern Marginal Carbonates uniquely exhibit strong carbonate signatures without strong clay and olivine signatures. More subtle characteristics of the Marginal Carbonates include their rubbly surface texture, darker tone, and their spatial variations in spectral properties. However, the spectral and textural properties alone are less distinctive when placed in the context of the wide range of textures and spectral properties of the regional olivine/carbonate-bearing terrains. Thus, it is the correlation of elevation with the spectral and textural properties of the Marginal Carbonates that may suggest that they were emplaced and/or modified by processes distinct from the regional olivine/carbonate-bearing terrains.

6. Constraints on the origin and timing of units in Jezero crater

6.1. Mottled Terrain

The Mottled Terrain unit appears to be the local stratigraphic equivalent of other widespread olivine-bearing units throughout the circum-Isidis region, including the NE Syrtis Fractured Unit to the south, and the Nili Fossae olivine-bearing unit to the northwest (Mustard et al., 2007, 2009; Ehlmann et al., 2009; Bramble et al., 2017). Thus, given its large regional extent beyond Jezero, the Mottled Terrain is perhaps the most enigmatic of the units in this study. Previous hypotheses for the regional olivine-bearing units include Isidis impact melt, ultramafic lava flows, and ultramafic tephra (Hamilton et al., 2003; Hoefen et al., 2003; Hamilton and Christensen, 2005; Mustard et al., 2005, 2007, 2009; Tornabene et al., 2008; Poulet et al., 2009; Bramble et al., 2017; Kremer et al., 2018). The timing of the unit places the first key constraint on its origin, as the unit drapes the highly eroded northern rim of Jezero crater (e.g., Mustard et al., 2009; Goudge et al., 2015). This suggests that some significant period of time passed between the Isidis impact and the emplacement of the Mottled Terrain, in order to allow for the Jezero impact and erosion of the northern rim. Thus, the Mottled Terrain and related units are unlikely to be related to the Isidis impact, and a volcanic origin is more likely. In particular, ultramafic tephra is the most consistent with the regional properties of the olivine-bearing units, including their draping relationship with local topography, significant topographic extent, and measured thicknesses that appear to decrease away from Syrtis Major (Kremer et al., 2019).

This scenario may also place constraints on the proposed alteration processes that lead to carbonate formation in the unit, which have included surface weathering, surface ponds, low-T groundwater alteration, hydrothermal alteration, and contact metamorphism (Ehlmann et al., 2008a, 2009; Murchie et al., 2009b; Mustard et al., 2009; Brown et al., 2010; Ehlmann and Mustard, 2012; Viviano et al., 2013; Edwards and Ehlmann, 2015; Bramble et al., 2017). While all of these processes could have produced the observed alteration assemblage, here we suggest that the distribution of the alteration signature across the region and topography may be more consistent with top down alteration by precipitation (rain or snow melt), perhaps even at elevated temperatures if the alteration occurred while the unit was still hot. Possible terrestrial analogs for this process are kimberlite lavas and tephras of the Igwisi Hills in Tanzania, which were altered by rain shortly after emplacement, and exhibit a low-temperature hydrothermal mineral assemblage dominated by calcite, olivine, and a serpentine-like mineral, along with minor smectites (Willcox et al., 2015). In this scenario, local variability in the strength of alteration could be due to variations in porosity, drainage, etc., or to later diagenetic processes.

Within Jezero crater, the most extensive outcrops of the Mottled Terrain are located in the northern crater interior and drape the northern degraded rim; however, this area may have been modified compared to the regional unit on the plateau. The Mottled Terrain north of the northern fans exhibits strong hydration bands, weak olivine bands, and strong clay signatures relative to carbonate (Fig. 5), including areas with clear Fe/Mg-smectite absorption bands and no clear carbonate signatures (Fig. 12). This is in contrast to both the Fractured Unit to the south and the Mottled Terrain outside of the crater, which exhibit clear and consistent carbonate bands along with strong hydration and olivine (Figs. 11, 12, and 13). The presence of smectites in the Jezero Mottled Terrain could be due to exposure of underlying basement materials, either via erosion or impact processes. However, the weak mafic spectral signature of these areas is more consistent with olivine than LCP, and LCP is consistently observed in basement exposures in the crater and surrounding plains. It is also possible that these smectites are due to local alteration of the Mottled Terrain by subsequent diagenetic fluids or fluvio-lacustrine activity. Fluvio-lacustrine activity may be consistent with the fact that these olivine/smectite detections are restricted to this area of the crater, which is closely associated with the eroded northern fans.

6.2. Light-toned Floor

Previous studies have suggested that the Light-toned Floor is either a sub-unit of the Mottled Terrain or a lacustrine deposit likely sourced from within the Mottled Terrain (Goudge et al., 2015). In support of these hypotheses, the spectral signatures of the Light-toned Floor (Fig. 15) are broadly similar to those in the regional olivine-carbonate units on the plateau (e.g., Fig. 11), with stronger olivine signatures and weaker carbonate signatures that are probably due to more extensive coverage by olivine sands. While these spectral signatures are somewhat distinct from the smectite and weak olivine signatures observed in the Mottled Terrain within northern Jezero, the lack of a clear stratigraphic contact between the two units suggest that they may be related. However, because the Light-toned Floor is a major source of sand (e.g., Ehlmann et al., 2008b), it is likely to contain a significant component of sand sized sediments. We suggest that it is unlikely that the Light-toned Floor was initially deposited as fluvio-lacustrine sediment, as coarse grained (sand-sized) detrital sediments would be concentrated near the fluvial inlet, and not throughout the basin. However, if the lake was at least transiently dry, aeolian processes could have distributed sand across the basin. In this scenario, the carbonate in the Light-toned Floor could have been formed in a playa setting.

Thus, we find that two plausible origins for the Light-toned Floor are (1) that it formed as an aeolian deposit due to reworking of the Mottled Terrain, perhaps in association with a playa system, or (2) that it is a sub-unit of the Mottled Terrain, and formed at the same time as the larger regional unit. In the latter case, differences between the two sub-units in Jezero could be due to a variety of factors, including variations in erosion or diagenesis, or direct airfall deposition of tephra into a lake.

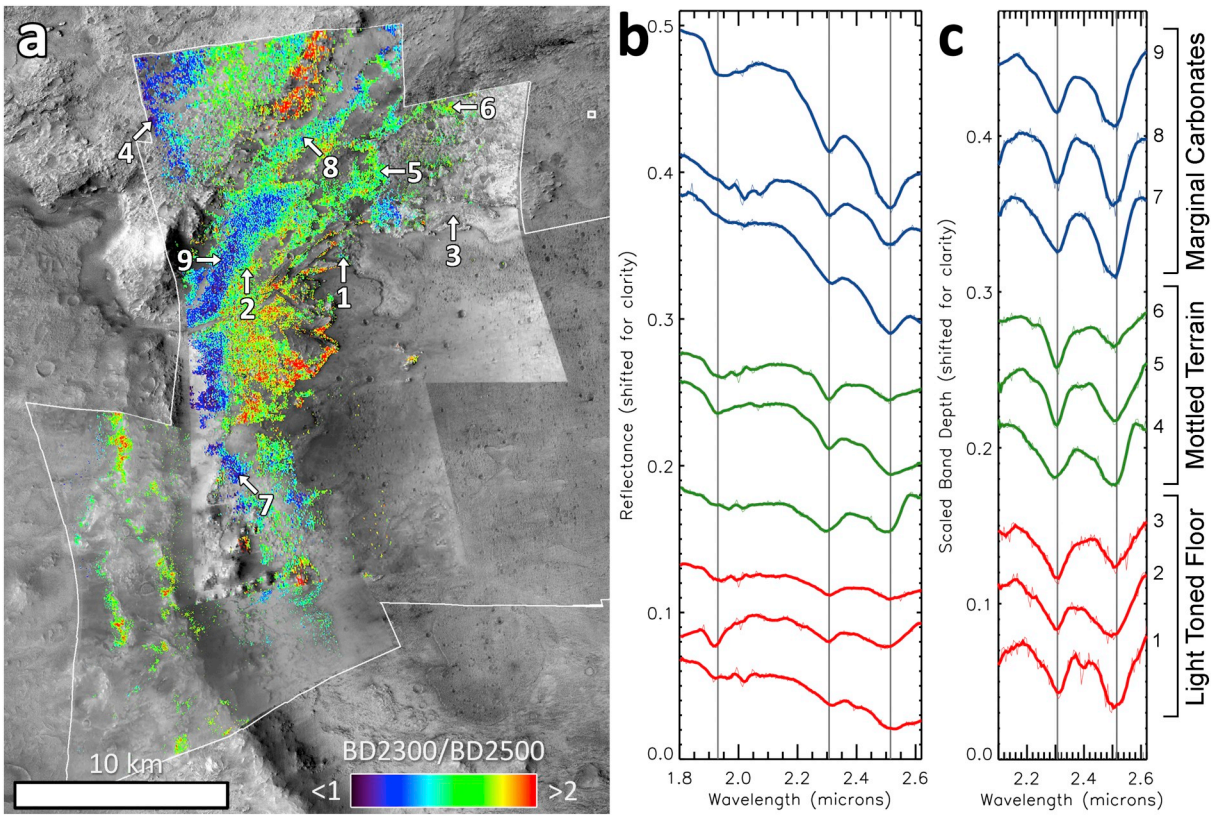

Fig. 5. Comparison of 2.3 and 2.5 μm band depths. (a) Mapped for CRISM cubes FRT000047A3, FRT00005850, and HRL000040FF, calculated as (1 + D2300)/(1 + BD2500), stretched from 1.000 to 1.027, and masked to show only D2300 > 0.01. High values of this parameter (red) correspond to 2.3/2.5 μm band depth ratios in ratio spectra of 2 or more, indicating a stronger 2.3 μm band likely due to more dominant smectite. Low values (purple) correspond to ratio values <1, indicating a stronger 2.5 μm band due to more dominant carbonate. Similar trends are apparent in Fig. 8. (b) Ratio spectra of selected locations in (a) showing differences in absolute band depths. (c) Differences in relative band depths are illustrated in continuum removed versions of these spectra, which have been scaled to have the same 2.3 μm band depth. (For interpretation of the references to color in this figure legend, the reader is referred to the web version of this article.)

6.3. Marginal Carbonates

Here we discuss three hypotheses for the origin of the materials that make up the Marginal Carbonates unit: lacustrine, detrital, and non-lacustrine. In the lacustrine hypothesis, the enhanced carbonate signatures in the Marginal Carbonates are due to carbonate precipitation in the near-shore environment of the Jezero paleolake. In the detrital hypothesis, the Marginal Carbonates were sourced from the western watershed, and emplaced in the Jezero paleolake via fluvial deposition. In this scenario, the carbonate could be entirely detrital, and thus not geochemically related to the lake waters. In the non-lacustrine hypothesis, the Marginal Carbonates are a sub-unit of the Mottled Terrain, and the carbonate could be entirely unrelated to any paleolakes that existed in Jezero. Ultimately, we find that a combination of these processes is most consistent with the observed properties of the Marginal Carbonates.

The hypothesis that the Marginal Carbonates are at least partially related to near-shore lacustrine processes is based on the observation that the Marginal Carbonates are restricted to a narrow range of elevations (−2420 to −2260 m) that are comparable to the pre-breach upper stand (−2260 m) and minimum elevation during outlet breach (−2395 m) for a Jezero paleolake reported by Fassett and Head (2005). This is the zone of elevations in which we would expect shorelines prior to the breach, during an early closed-basin phase of the lake. One process that could produce near-shore carbonate during this phase is authigenic carbonate precipitation.

As discussed in detail in Section 7, authigenic lacustrine carbonate is most efficiently deposited in shallow, warm, and agitated waters with high levels of dissolved ions from weathering in the river catchment, and can form along the shoreline in the form of layered structures (e.g., stromatolites; Golubic, 1991; Grotzinger and Knoll, 1999), clay to sand-sized concretions (e.g., ooids; Halley, 1977), cemented sediments (e.g., beach rocks; Stoddart and Cann, 1965), and other precipitates (e.g., tufas; Capezzuoli et al., 2014). Thus, we would expect authigenic lacustrine carbonate deposition in Jezero in the shallowest portions of the lake (the littoral zone) and in proximity to the inlet valley(s). This prediction is consistent with the overall location of the Marginal Carbonates along the western and northwestern inner margin of the crater, close to both the western and northern inlet valleys, and just below the highstand for the lake. In particular, we would expect strong carbonate signatures near the inlet where incoming waters contained the highest concentration of dissolved solutes, leading to the most authigenic carbonate precipitation. This prediction may be consistent with the location of the strongest carbonate signatures in the central Marginal Carbonates, just north of the western inlet, suggesting that these signatures could correspond to areas of at least some lacustrine carbonate deposition. If concentrations of bicarbonate in the lake were high enough, this could also produce areas of isolated carbonate precipitation, beyond the region where detrital materials would be deposited. This prediction may be consistent with the presence of strong and relatively uncontaminated carbonate signatures (hydrated magnesite, possibly mixed with hydromagnesite) on the far southern extent of the Marginal Carbonates, making these isolated carbonate-bearing terraces the most likely marginal lacustrine carbonate deposits in the crater.

The possible detection of relatively isolated hydrated magnesite in the southern Marginal Carbonates is also mineralogically consistent with a lacustrine origin. Hydrated Mg-carbonate minerals form in abundance during evaporation of Mg-rich waters with high Mg:Ca ratios

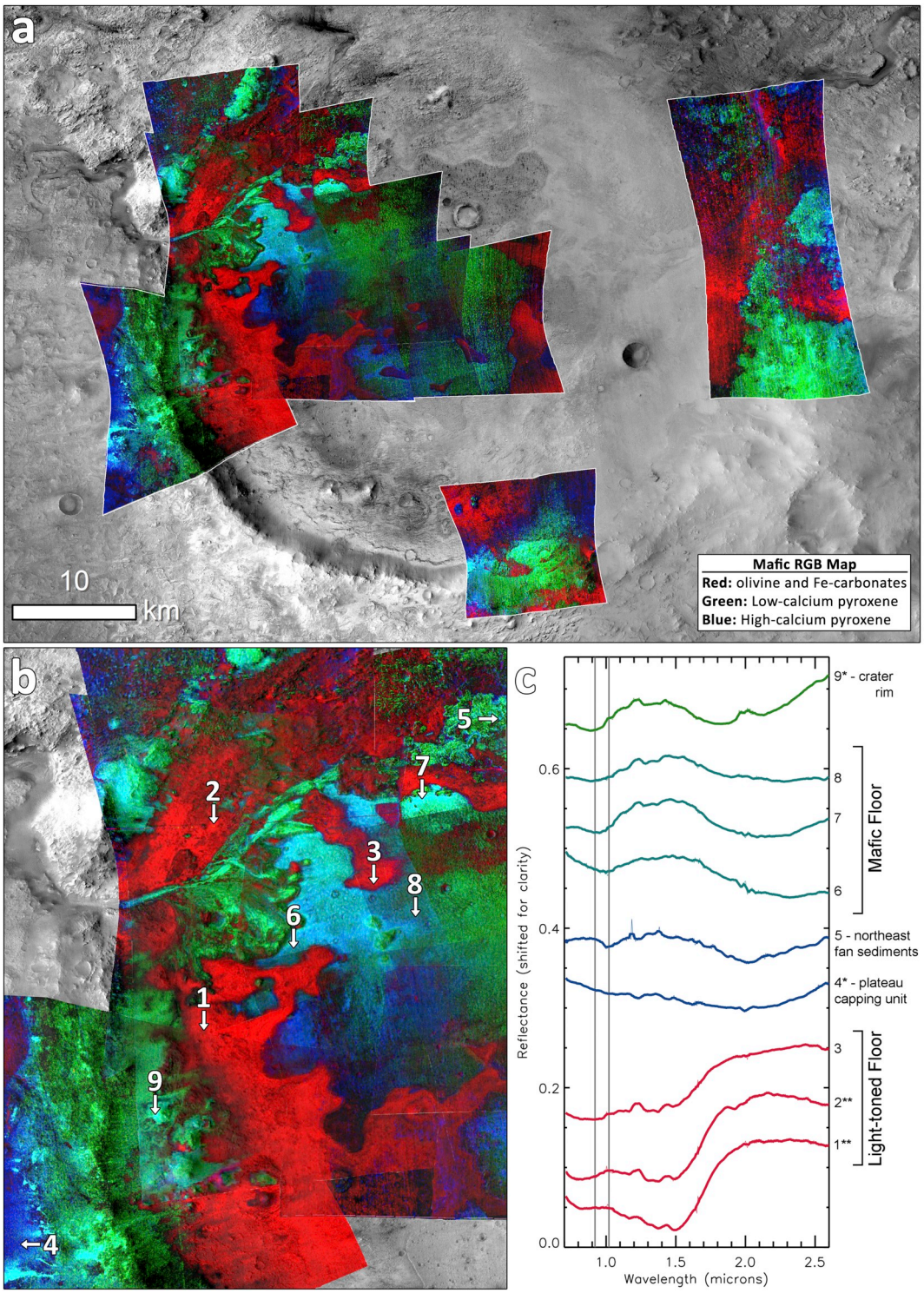

Fig. 6. Mafic signatures from primary minerals in surface sediments and bedrock units. (a) Mosaic of "mafic" RGB composite of select CRISM images. Red indicates olivine or the mafic component of the carbonates, green indicates low-calcium pyroxene (LCP), and blue indicates high-calcium pyroxene (HCP). (b) Zoom to show diversity in the region of the western delta. (c) CRISM spectra showing strong mafic mineral signatures associated with different units and sediment covers in the crater, from images FRT000047A3, FRT00005850 (indicated by *), and HRL000040FF (indicated by **) at numbered locations in (b). Narrow bands or inverted bands between 1.2 and 1.5 μm are artifacts emphasized by ratioing in these dark (low signal) spectra. (For interpretation of the references to color in this figure legend, the reader is referred to the web version of this article.)

(Müller et al., 1972), which typically occur in mafic terrains with abundant Mg. Hydromagnesite is a common mineral along the evaporative margins of Mg-rich alkaline lakes (Müller et al., 1972; Walter et al., 1973; Braithwate and Zedef, 1994) and is also found along with other hydrated magnesites in playas fed by Mg-rich groundwater (Vance et al., 1992; Renaut, 1993; Power et al., 2014). However, hydromagnesite does not specifically indicate deposition a lake, as it also forms due to weathering of serpentine-rich outcrops and mine tailings (e.g. Wilson et al., 2009, 2011; Bea et al., 2012) and in speleothems in caves (Fishbeck and Müller, 1971; Canaveras et al., 1999). Hydrated Mg-carbonate minerals like hydromagnesite are metastable and transform to magnesite due to high temperatures, dehydration, and diagenesis (Müller et al., 1972; Hänchen et al., 2008; Spotl and Burns, 1994; Zedef et al., 2000). Thus, it is unlikely that hydromagnesite itself would persist over geologic timescales, so one possible origin for concentrated hydrated magnesite or magnesite-hydromagnesite mixtures in the Marginal Carbonates is dehydration or diagenesis of pre-existing hydromagnesite.

We suggest that all of these properties together make it plausible that the Marginal Carbonates were influenced in some way by near-shore authigenic carbonate precipitation. This would have occurred during the lacustrine phase when the lake was deepest, most likely in a closed basin prior to formation of the outlet valley. A closed (endorheic) basin at the time of deposition may have helped achieve and maintain the high levels of alkalinity required for carbonate deposition.

Authigenic lacustrine carbonate precipitation cannot explain the origin of all materials in the Marginal Carbonates, however, as the bulk of the unit is composed of a mixture of olivine, a hydrated phase, and carbonates that cannot all have formed through lacustrine processes. Thus, carbonate precipitation could have occurred either at the same time or long after the bulk of the material in the Marginal Carbonates was deposited. One possibility is that the Marginal Carbonates were deposited as part of the regional olivine/carbonate unit, and then later experienced additional carbonate precipitation from nearshore lake waters. This could occur either because they were deposited into a pre-existing lake or were later submerged by rising lake levels. However, the Marginal Carbonates could also have been deposited as fluvial sediments and lacustrine precipitates in a near-shore environment. The two origin scenarios have different predictions for the distribution of other minerals within the deposit. If the Marginal Carbonates were deposited as part of the Mottled Terrain, then olivine, clay, and hydration signatures should either be consistent throughout the unit, or possibly increase away from the inlet where alteration and/or carbonate precipitation was less intense. In contrast, fluvio-lacustrine deposition would produce stronger signatures closer to the source inlet from detrital materials derived from the catchment.

While the Marginal Carbonates exhibit relatively strong carbonate bands all along the western margin, the strength of their hydration and olivine absorption bands generally decreases with distance from the western inlet (Fig. 19). The clear decrease in olivine and hydration signatures to the south of the western inlet may be consistent with fluvio-lacustrine deposits proximal to the western inlet and decreasing to the south, leading to a greater relative proportion of lacustrine precipitates in the southern Marginal Carbonates. In comparison, the northern Marginal Carbonates exhibit much weaker hydration bands and slightly weaker carbonate signatures than the proximal deposits, but still exhibit strong mafic signatures. Thus, the spectral variability in the northern Marginal Carbonates could also be consistent with decreasing fluvial deposition away from the western inlet, but the trend is much weaker than in the south. This could be due to the fact that this northwestern corner of the crater is equidistant from both the western and northern inlets – if both inlets were active sources of detrital materials, this would produce a more complex depositional environment in the intermediate regions.

Farther to the north, in the vicinity of the northern fans, there are exposures of the Mottled Terrain at elevations comparable to the Marginal Carbonates. These areas tend to show very weak carbonate and stronger clay absorption bands even compared to exposures of the Mottled Terrain outside of the crater. This could be the result of post-depositional modification, but if so, under different geochemical conditions than those that produced the Marginal Carbonates. Thus, either lacustrine modification was restricted to the Marginal Carbonates because of their location relative to fluvial/solute inputs, or the Marginal Carbonates were emplaced largely due to secondary transport/precipitation processes that did not occur or are not preserved in the northern part of the crater.

Based on these observations, if the Marginal Carbonates are at least partially lacustrine in origin, we find that the southern Marginal Carbonates are most likely to be dominated by lacustrine carbonate precipitation, and that the central and northern Marginal Carbonates are consistent with either a combination of fluvial deposition and lacustrine carbonate precipitation or localized lacustrine modification of pre-existing Mottled Terrain.

If the Marginal Carbonates are fluvio-lacustrine in origin, they would have formed in the near-shore environment when lake levels were highest, prior to the breach. But it is unclear when this occurred relative to the other fluvio-lacustrine deposits in Jezero. In the Goudge et al. (2018) scenario of increasing lake depth, the Marginal Carbonates would be associated with the highest lake levels, and thus could be a fluvio-lacustrine deposit contemporaneous with the highest elevation avulsing channel bodies. However, this hypothesis does not explain why the Marginal Carbonates exhibit a distinctly different primary and secondary mineral assemblage (olivine/carbonates) compared to the channel deposits (LCP/smectites). Alternatively, the mineralogy of the Marginal Carbonates could suggest that the unit formed as a fluvio-lacustrine deposit during an earlier lacustrine phase, perhaps part of the lacustrine sequence that formed the olivine/carbonate-bearing point bar deposits, as discussed in the next section. The Marginal Carbonates do appear to underlie the LCP-bearing inverted channels and are cut by the incised valley where it emerges from the western inlet, which is consistent with this sequence of events.

While we cannot entirely rule out the possibility that the Marginal Carbonates were formed by other processes and thus are not related to lacustrine carbonate precipitation, these other processes require significant assumptions that decrease their likelihood. For example, in the detrital hypothesis, it is possible that the Marginal Carbonates were entirely derived from erosion and fluvial transport of the regional olivine/carbonate unit. A similar detrital origin has been proposed for the clays and carbonates detected in the western delta (Ehlmann et al., 2008a, 2008b; Goudge et al., 2015). In this scenario, the compositional trends that we observe could be due to processes like grain size sorting, where fine-grained detrital carbonates are concentrated in the most distal areas to the south. While fluvial deposition alone cannot easily explain the lateral and topographic distribution of the Marginal Carbonates (as compared to the fluvial patterns of the western delta or northern fans), it is possible that their current expression could have been created by later processes – for example, by wave erosion along shorelines.

We also find it unlikely but not impossible that the Marginal Carbonates are a sub-unit of the Mottled Terrain or the Light-toned Floor without any genetic relationship to the lake itself. The main supporting argument for this hypothesis is that because the morphology and spectral properties of the Mottled Terrain and Fractured Unit are highly variable throughout the region (Goudge et al., 2015; Bramble et al., 2017), the Marginal Carbonates could just be a slightly different expression of this large-scale variability, and thus may not require any interaction with a lake in Jezero crater. While it is unclear what mechanisms in this scenario could have concentrated strong carbonate signatures in the Marginal Carbonates, caused their clear topographic restriction, and generated their observed spectral trends, these properties could perhaps be due to more pervasive diagenetic processes along the inner rim of the crater, e.g., the emergence of carbonate-rich

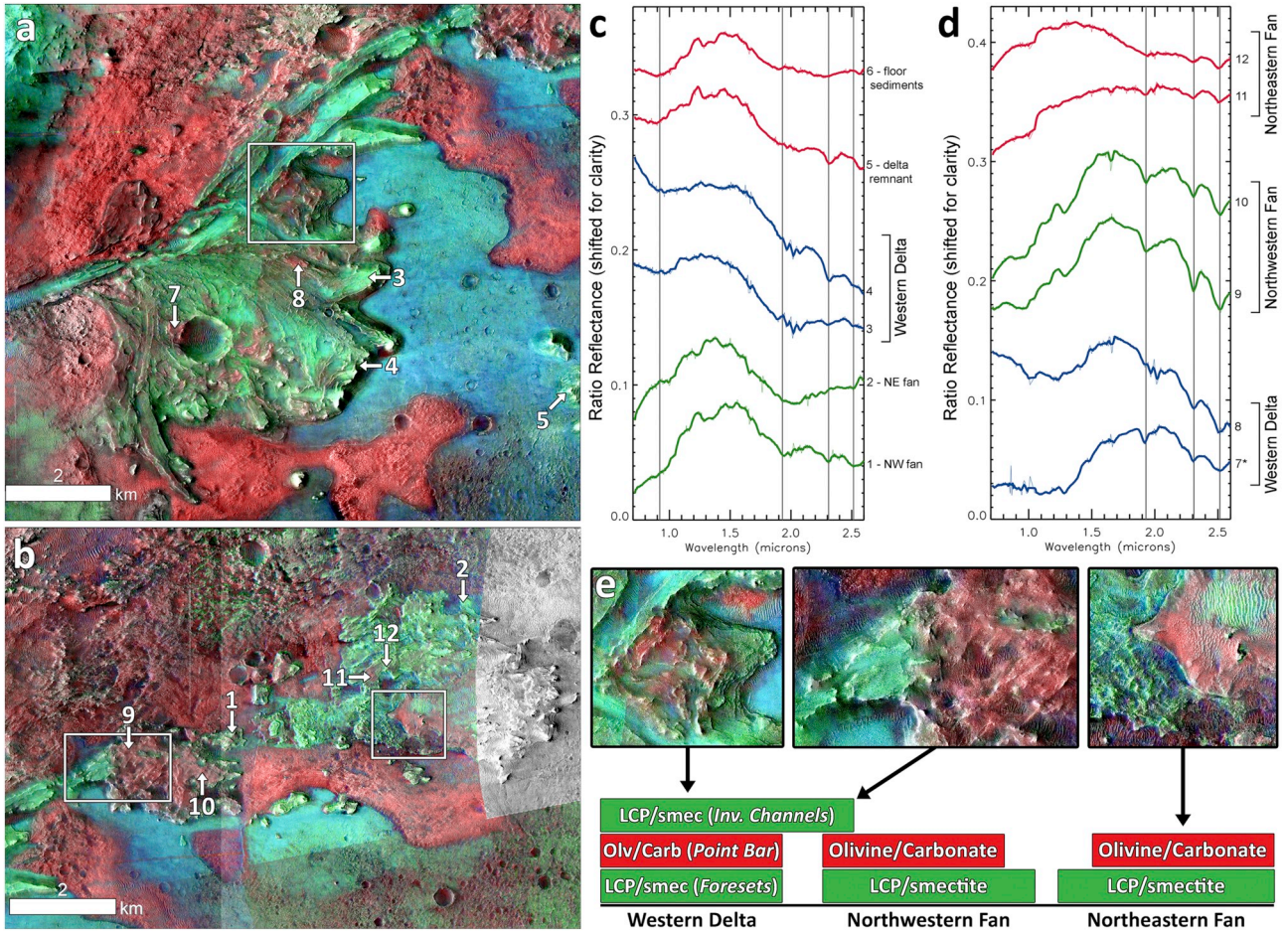

Fig. 7. Spectral diversity of delta, fans, and related deposits. Mafic RGB composite mosaics over CTX mosaic, showing (a) the western delta and (b) the northern fan complex. Boxes indicate the location of zooms shown in (e). (c) LCP and variable Fe/Mg-smectite from green regions in the western delta (blue spectra), the delta remnants and widespread sediments on the Mafic Floor (red spectra), and the majority of the northeastern fan (green spectra). Spectrum 6 is spectrum 8 in Fig. 6c, see Fig. 6b for location. (d) Carbonate, hydration, and olivine signatures from red regions in the western delta (blue spectra) and both northern fans (green and red spectra). Spectra are from FRT47A3 and FRT5C5E (indicated by *), at locations indicated in (a) and (b). (e) Inferred general spectral stratigraphy of the western delta and northern fans, with zooms from (a) and (b) illustrating the relationship between the spectral units. Units in the western delta are labeled with closely correlated morphologic facies from Goudge et al. (2017, 2018). (For interpretation of the references to color in this figure legend, the reader is referred to the web version of this article.)

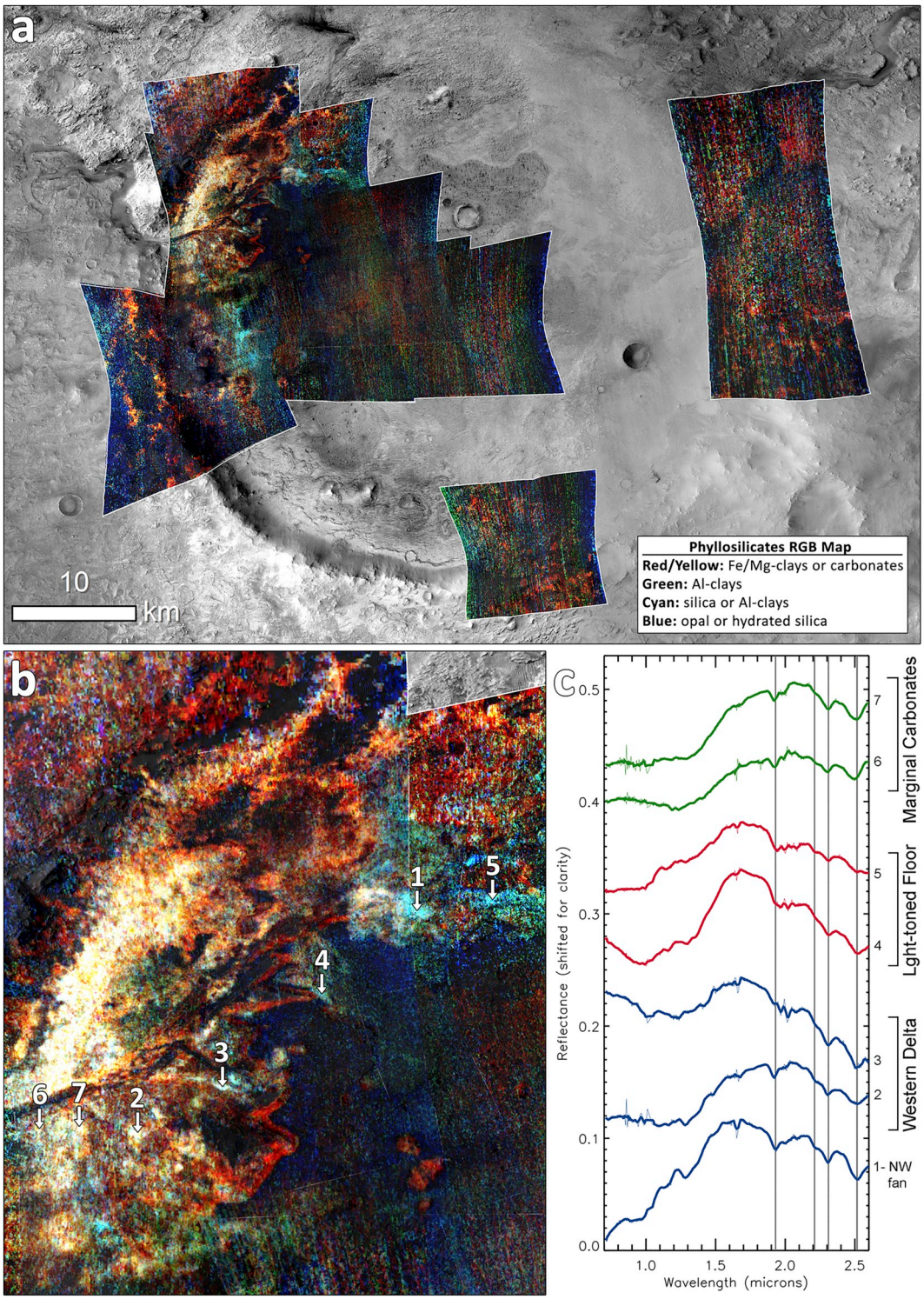

Fig. 8. Al/Si-OH and Fe/Mg-smectite spectral signatures in Jezero. (a) Mosaic of "phyllosilicates" RGB composite of select CRISM images. Red/Yellow indicates Fe/Mg-smectites or carbonates, green indicates Al-clays, and cyan indicates silica or Al-clays. Red indicates Fe/Mg-smectites or Mg-carbonates, cyan indicates silica or Al-clays, and yellow/white may indicate a mix of carbonates and silica or Al-clay. (b) Zoom to show diversity in the region of the western delta. (c) CRISM spectra illustrating 2.21 μm shoulder on the 2.31 μm carbonate band, from images FRT47A3 (blue and red spectra) and FRT5C5E (green spectra) at numbered locations in (b). Note that all spectra are acquired on or next to delta or fans. (For interpretation of the references to color in this figure legend, the reader is referred to the web version of this article.)

groundwater at springs.

6.4. Fluvio-lacustrine deposits

The various facies of the western delta identified by Goudge et al. (2018) exhibit distinct mineralogies. While previous studies had noticed a correlation between the facies and alteration minerals (Goudge et al., 2015, 2017), our results show that there is also a much stronger relationship between the facies and primary mineralogy (Fig. 7). The point bar strata consistently exhibit olivine and carbonate, and often also silica or Al-clay spectral signatures, while the overlying channel deposits and incised valley consistently exhibit LCP and often Fe/Mg-smectite spectral signatures. In addition, some stratigraphically lower outcrops without a facies designation exhibit LCP/smectite spectral signatures. The northern fans exhibit similar clear compositional units, with olivine/carbonate-bearing deposits overlying LCP/smectite-bearing deposits (Fig. 7e), perhaps similar to the lower two units of the western delta. Here we evaluate possible origins of these stark compositional variations within the delta and fans.

The watershed for the western delta includes a variety of units but is areally dominated by the LCP-bearing basement unit (Goudge et al., 2015). This unit is highly heterogeneous (clays, megabreccia, sedimentary layers, etc.; e.g., Bramble et al., 2017) and is unlikely to be dominated by a single grain size, so an average sampling of the watershed at any grain size should include significant LCP. LCP is a particularly strong absorber in the VNIR, so even small amounts of LCP tend to spectrally dominate CRISM spectra (~10–40%; e.g., Horgan et al., 2014). So we would expect that sediments from across the watershed at any grain size would exhibit spectra primarily consistent with LCP. This hypothesis may explain the detection of LCP throughout the inverted channel facies, as this could actually be consistent with a much more heterogeneous composition. Given that these are some of the most recent fluvial deposits and the most recently preserved fluvial network incises across many different units, these uppermost deposits may integrate materials from across the watershed. Similar arguments may apply to some stratigraphically lower outcrops in the western delta, which are also LCP-dominated.

Based on these arguments, it is unlikely that the basement unit contributed significantly to the sediments in the olivine/carbonate-bearing units of the western delta or northern fans, as there is no evidence for LCP in spectra of these units (Fig. 7). One hypothesis to explain the clear dominance by olivine/carbonate in the point bar facies of the western delta and the uppermost unit of the northern fans is that these units correlate with emplacement of the regional olivine/carbonate-bearing unit. If the fluvial system was active during and/or shortly after deposition of the regional unit, it is plausible that this unit dominated the watershed for some period of time, and thus also dominated the corresponding fluvial deposits.

Alternatively, variations in alteration mineralogy across the delta and fans have previously been attributed to variations in grain size sorting between the facies (Goudge et al., 2017). In this scenario, differences in mineralogy are not due to changes over time in the exposed lithology of the watershed, but rather due to changes over time and/or space in flow velocity in the depositional environment. This could help create the different sedimentary facies observed in the western delta, and if there was a strong correlation between grain size and composition, could also cause strong compositional gradients within the depositional system. This hypothesis was primarily based on the observation that the strongest Fe/Mg-smectites are located on the margins of the western delta, while carbonates are detected in the point bar facies in the interior of the delta (Goudge et al., 2015). This separation in composition is potentially consistent with concentration of detrital clays in distal bottomset beds at the base of the delta and coarser-grained carbonate or carbonate cement in the point bar deposits (Goudge et al., 2017).

Grain size sorting may indeed have strongly influenced the distribution of alteration phases, but we find it less likely that it would have produced the observed stark compositional difference in primary mineralogy between the LCP- and olivine-bearing units in the delta and fans. The regional olivine/carbonate-bearing unit is a major source of olivine sand, so it likely contains a significant sand-sized component and could be strongly segregated by grain size sorting. However, as discussed above, the basement unit is highly heterogeneous and likely erodes into a variety of grain sizes. Thus, we would expect LCP to be detected in virtually any grain size fraction that included the basement unit. For this reason, we favor a change in watershed lithology over grain size sorting to explain the observed differences in primary mineralogy within the fans and deltas.

Also new in this study is the observation that the northern fans exhibit the same compositional units as the western delta, but lack the topmost LCP/smectite-bearing unit, which corresponds to the inverted channel facies in the western delta. This relationship is the same in both the northwestern and northeastern fans. The northwestern and northeastern fans may have been two separate deposits, but the lack of a clear spectral or morphological boundary between the two suggests that they may be the remnants of one larger fan or delta. While both fans are too eroded to clearly preserve deltaic structures, they do exhibit clear sedimentary structures of either deltaic or alluvial origin (Goudge et al., 2015). In addition, their location within the crater and association with the extensive northern fluvial system and watershed mapped by Goudge et al. (2015) is consistent with fluvio-lacustrine deposits. The origin and timing of the northern fan complex is much less well constrained than the western delta, but could be consistent with deltaic or alluvial activity contemporaneous with the western delta, significantly predating the western delta, or both.

The only location where a possible stratigraphic relationship between the western delta and the northern fans may be preserved is at the end of the farthest lobe of the LCP-bearing inverted channel deposits of the western delta, which may overlie the uppermost olivine/carbonate-bearing units of the northern fans (Fig. 7e). If this is true, then the inverted channel facies likely postdate the preserved portions of the northern fans. This relationship between the delta and fans also raises the possibility that the respective olivine/carbonate-bearing units and lowermost LCP/smectite-bearing units of the western delta were each formed contemporaneously with their corresponding mineral unit in the northern fans.

Based on these observations, one possible sequence of events that could have led to the observed mineral stratigraphies in the delta and fans is as follows:

First, fluvio-lacustrine activity at Jezero may have begun quite early, as soon as immediately after the Jezero impact. The extensive erosion of the northern rim of Jezero could be due to fluvial activity, as proposed to explain the erosion of the ejecta and rims of many Noachian craters (e.g., Mangold et al., 2012). This would require that initial fluvial activity predated the deposition of the Mottled Terrain, which drapes the eroded northern rim. In this scenario, we would expect any detrital fluvial materials to be dominated by the LCP of the basement unit, which is consistent with the observed mineralogy of the lowest unit of the delta and northern fans. An important test of this stage of the model is the relationship between the lower LCP-bearing units of the northern fans and the Mottled Terrain – if the fans overlie the Mottled Terrain, then they must have formed after the emplacement of the regional unit, and may instead be composed of a mixture of materials. This relationship is unclear based on our observations.

Next, the olivine/carbonate unit was deposited across the region, and for some time, may have dominated fluvial sediments coming into Jezero from both watersheds, forming the olivine/carbonate units within both the delta and northern fans.

Finally, after fluvial and other erosion had removed some of the regional olivine/ carbonate unit from the surrounding landscape, the basement unit was once again exposed in the watersheds. At some time after this point, the inverted channel facies were formed. While these fluvial deposits are spectrally dominated by LCP, they may be composed

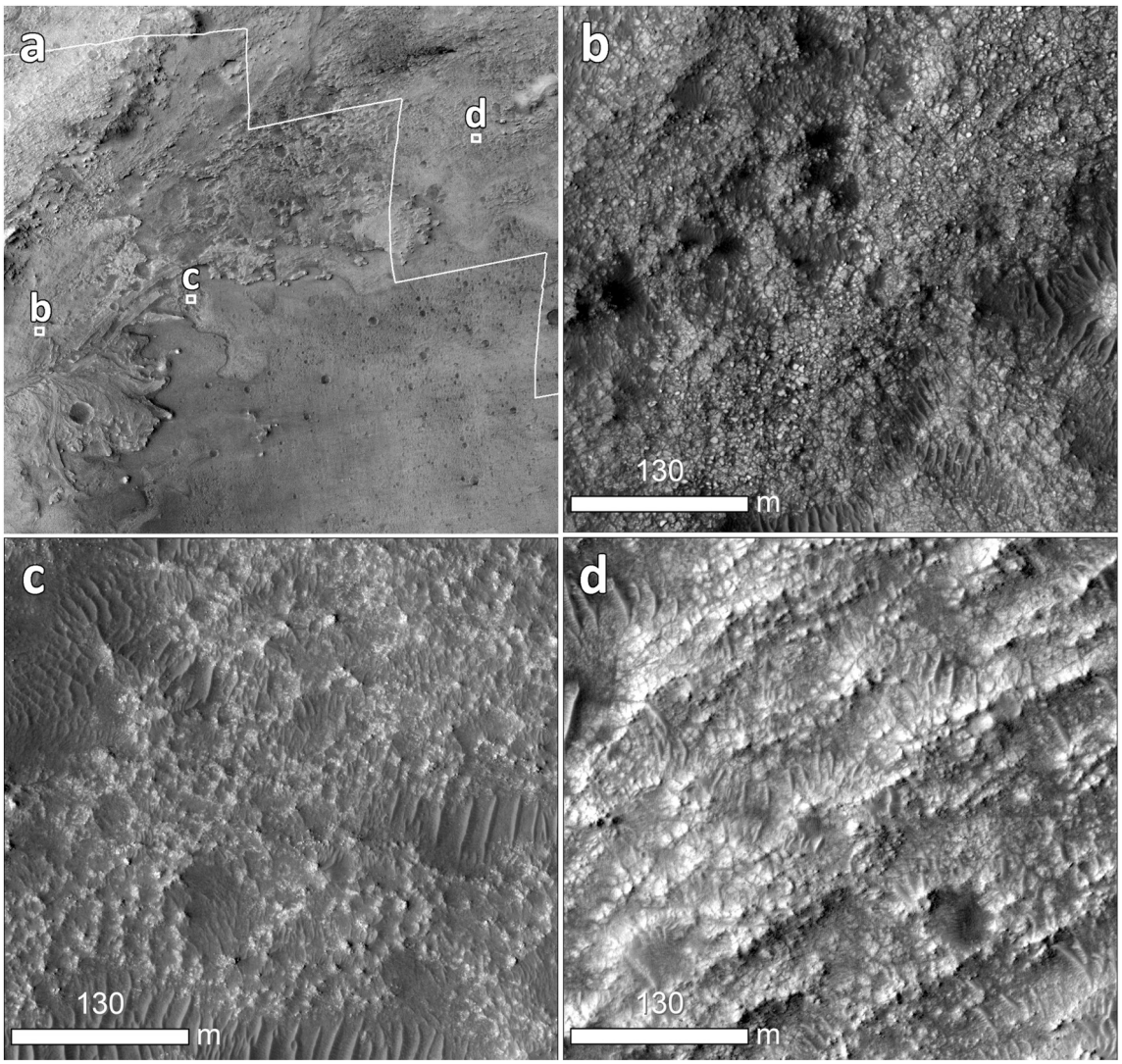

Fig. 9. Comparison of typical texture of carbonate-bearing units in Jezero. (a) CTX mosaic for context, white lines indicate outline of CRISM mosaic. At HiRISE scales, (b) the Marginal Carbonates exhibit a rough blocky texture not observed in the other units with variable sand cover, (c) the Light-toned Floor exhibits pockmarked textures and significant sand cover, and (d) the Mottled Terrain exhibits long ridges and patchy sand cover.

of a mixture of materials. These facies are not observed on the top of the northern fan, suggesting either that they have been eroded, or that the northern watershed was not active during this stage of lake activity.

Our model is potentially consistent with the model presented by Goudge et al. (2015, 2018), in which the delta and fans were formed during one extended lacustrine phase. Our observations would require two modifications to this model: (1) that fluvio-lacustrine activity may have begun somewhat earlier, before emplacement of the olivine/carbonate unit, and (2) that an early period of high lake levels must have occurred to form the Marginal Carbonates, although it is unclear how sediment input into the basin during this period would be related to the observed deltaic deposits. Alternatively, our model could also be consistent with a series of paleolakes, perhaps separated in time by arid periods with little fluvial activity.

Indeed, one explanation for the remarkable preservation of the western delta in Jezero is that the uppermost LCP-rich inverted channel facies are significantly younger that the underlying units, perhaps because they formed after an extended period without fluvial activity. The significant erosion of the northern fans relative to the western delta could also be consistent with this scenario, since if they never experienced this final late phase of fluvial activity, they would have never developed this younger protective capping unit. Goudge et al. (2015) suggested that the northwestern fan underwent more severe erosion than the western delta due to a mineralogy more dominated by olivine and carbonates, as opposed to the LCP/smectite assemblage that appears to gird the margins of the western delta. We find that this hypothesis can only partially explain the current state of the delta and fans. While the inverted channels do appear to be more resistant, this may not be entirely a function of mineralogy, as the northern fans do actually include extensive LCP-bearing areas in their lower units, and these units are still highly degraded. Instead, we suggest that either a shorter exposure age for the deposits and/or their sedimentology (e.g., more resistant inverted channels) may have been the driving factor behind the preservation of the western delta.

Lastly, we have also detected Al-clays and/or silica in association with the delta/fan landforms and their proximal terrains. These signatures are weak or absent throughout the rest of Jezero, but they appear to be nearly ubiquitous throughout the olivine/carbonate-bearing portions of the western delta and northern fans. Although Al-clays and/or silica signatures are not apparent in the Mottled Terrain on the plains outside of Jezero, we have identified similar signatures in some regions within the Fractured Unit to the south, suggesting that they may be present elsewhere in the regional olivine-carbonate unit. Thus, these phases may be detrital, and are present in the delta/fans because they

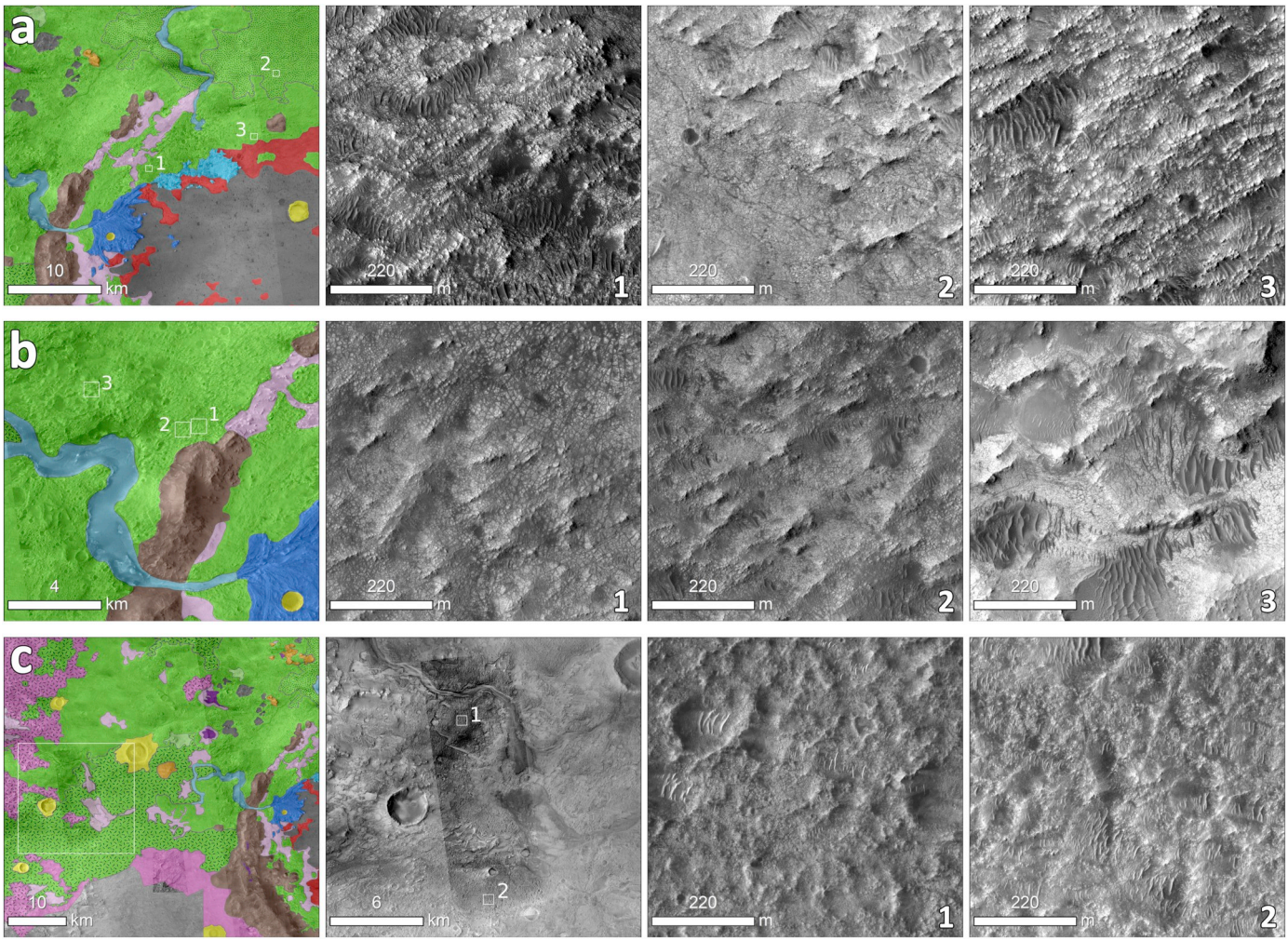

Fig. 10. Ridged texture of the Mottled Terrain in HiRISE, where left columns show context in the Goudge et al. (2015) geologic map. (a) Fractured ridges in the northern interior of the crater. (b) Clear ridges just outside of the crater. (c) Eroded ridge texture in the watershed to the northwest of the crater, with CTX image in second column for added context.

were concentrated during transport, perhaps due to a smaller average grain size than the olivine component of the Mottled Terrain.

Alternatively, the ubiquity of silica or Al-clay detections in the delta/fans and proximal terrains could also support an authigenic origin in the delta/fans. The strongest detections are associated with features interpreted as point bar deposits on the western delta, suggesting either a sub-aerial or very shallow aqueous environment. If these phases are authigenic, they could have formed via weathering in the delta surface environment, which would have important implications for the climate and duration of activity of the fluvial system. Al-clays detected elsewhere on Mars are typically inferred to form either through long-term pedogenic leaching in a surface environment or through high-temperature alteration in a hydrothermal system (e.g., Bishop et al., 2008; Arvidson et al., 2014; Bishop et al., 2018). Al-clays (kaolinite) have been detected in at least one other proposed lacustrine deposit in Columbus crater (Wray et al., 2011). Silica is thought to have been highly mobile on ancient Mars (Mclennan, 2003), and silica detections have been reported across a wide range of geologic contexts on Mars (e.g., Ehlmann and Edwards, 2014; Sun and Milliken, 2018), including within deltaic deposits in Eberswalde crater (Poulet et al., 2014). In surface weathering environments on mafic terrains, enhanced silica deposition could be a sign of short-lived cold climate weathering by snow or ice melt (Rutledge et al., 2018). In either case, this suggests that the Al-clay or silica of the western delta could be a unique record of surface-atmosphere interactions.

6.5. *Mafic Floor*

The Mafic Floor has been hypothesized to be volcanic in origin, potentially a lava flow from an unknown source (Goudge et al., 2015). The physical characteristics of the Mafic Floor are mostly consistent with this hypothesis, including layered lobate margins and apparent embaying relationships with the topographically highest portions (kipukas) of the Light-toned Floor (Ruff, 2017). The major argument against this hypothesis is that the Mafic Floor is highly topographically variable over large scales, and does not create an obvious flow surface. In addition, some textural properties of the Mafic Floor (e.g., crater morphology and preservation, erosional properties, lobate margins) are similar to dark capping units on the crater rim and surrounding plains (Sun and Stack, 2019).

Spectrally, the Mafic Floor is dominated by signatures that appear to be the result of significant sediment cover, including a clear olivine-enriched wind streak extending across the unit from the Light-toned Floor exposure near the western delta, and LCP-enriched sediments that appear to originate on the western delta and delta remnants. Outside of these clear spectral zones, the Mafic Floor exhibits weak HCP signatures. The HCP is most likely derived from the Mafic Floor itself, as the only other unit in the region with this composition is the dark capping unit scattered across the surrounding plains (e.g., spectrum 4 in Fig. 6; Goudge et al., 2015), but no occurrences of this unit have been mapped within Jezero.

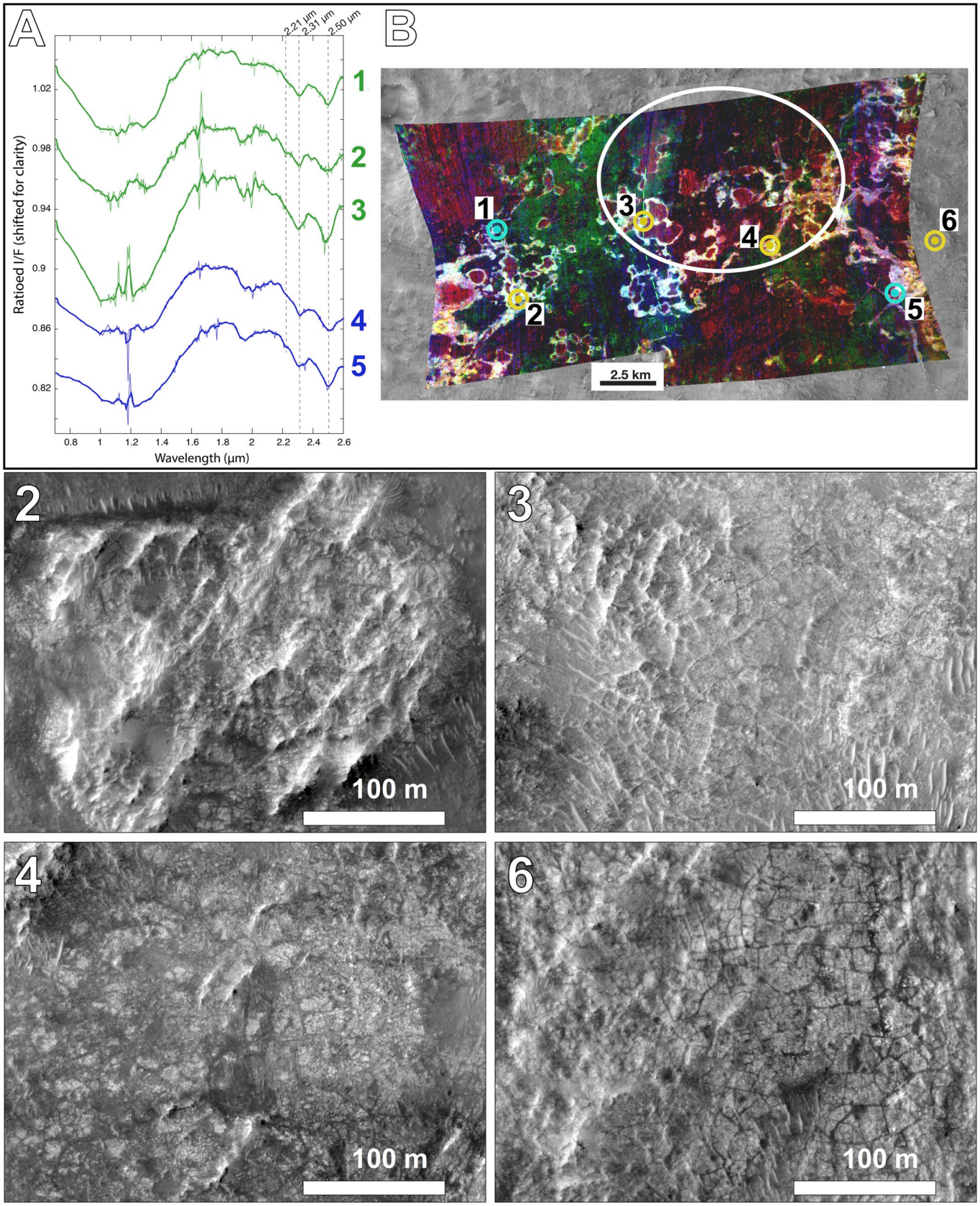

Fig. 11. CRISM spectra and HiRISE textures of the carbonate-bearing Fractured Unit in the NE Syrtis area south of Jezero. (a) Representative spectra showing mafic, hydration, and carbonate bands, as well as some 2.2 µm shoulders; from locations indicated on (b) "Carbonates" RGB composite of CRISM images FRT0001642E and FRT00017103, with local stretch applied to bring out diversity. Ellipse indicates candidate NE Syrtis Mars 2020 landing site. The textures at a subset of these locations in HiRISE images are shown in the following panels, numbered according to their position in (a): (2) rare example of ridges similar to those in the Mottled Terrain in Jezero; (3) example of raised ridges; (4) the variable, patchy appearance that is most common; (6) example of rectilinear fractures.

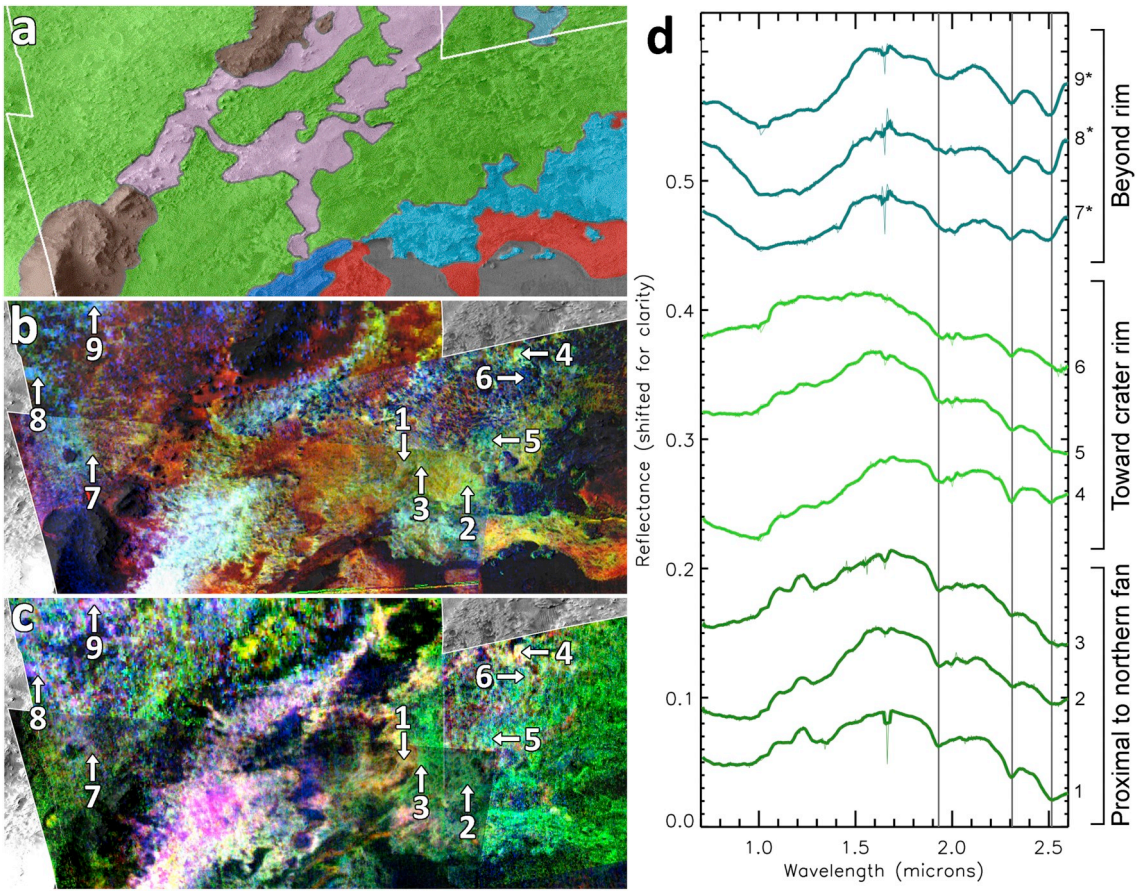

Fig. 12. Spectral diversity in the Mottled Terrain on the northern interior and exterior of Jezero. (a) Portion of Goudge et al. (2015) geologic map over northern Jezero crater, which is largely mapped as Mottled Terrain (green; see Fig. 1b for legend). (b) "Carbonates" and (c) "hydration" RGB composites are variable throughout the Mottled Terrain. (d) CRISM spectra from within the Mottled Terrain in CRISM image FRT000047A3 and HRL000040FF (indicated by *), showing hydration throughout and stronger 2.3 μm bands relative to their 2.5 μm bands to the north and beyond the rim, suggesting increasing Fe/Mg-smectite content throughout the majority of the Jezero Mottled Terrain. (For interpretation of the references to color in this figure legend, the reader is referred to the web version of this article.)

The likely HCP-bearing composition of the Mafic Floor is distinct from the other units in the crater and the fluvio-lacustrine deposits and is consistent with more evolved magma compositions often associated with Hesperian and Amazonian volcanics (e.g., Mustard et al., 2005; Mangold et al., 2010). However, even the areas with HCP spectral signatures still shows a subdued surface texture consistent with sediment cover. Counterintuitively, a tendency to trap and accumulate sediments is a common characteristic of lava flows on Mars, due to their much higher local surface roughness than more friable sedimentary units (Rogers et al., 2018). Thus, while an origin as a tephra deposit or other basaltic sedimentary accumulation cannot be ruled out from orbital data, and may be supported by the similarities between the Mafic Floor and dark capping materials on the surrounding plains (Sun and Stack, 2019), the characteristics of the Mafic Floor are otherwise generally consistent with one or a series of lava flows. The source of the possible flows is unclear based on orbital data and could be from dikes and fissures in the crater floor now covered up by the unit. However, there is also a conical edifice with a summit crater on the southeastern rim of Jezero (apparent in the lower right of Fig. 1c) that could perhaps be the source of flows to create the Mafic Floor.

The timing of the Mafic Floor based on crater counts is debated, as one estimate relying on larger craters suggested an age on the order of 3.45 Ga (Goudge et al., 2012), but a separate count not including several larger craters that may be embayed or covered by the Mafic Floor suggested a much younger age, on the order of 1.4 Ga (Schon et al., 2012). A more recent detailed study of the crater population suggests an intermediate age of 2.6 ± 0.2 Ga, which would put emplacement of the Mafic Floor in the early Amazonian (Shahrzad et al., 2019). Stratigraphically, the only clear constraint on the Mafic Floor is that it is younger than the Light-toned Floor, as the other carbonate units do not exhibit clear contacts with the Mafic Floor. The relationship with the fans and delta is also unclear, as their contact is obscured by sediments in many locations and all of the features have experienced significant erosion. Previous studies have hypothesized that the relationships between the Mafic Floor and the fans/deltas could be consistent with either emplacement prior to the fans/deltas (Ruff, 2017) or much later after cessation of all lacustrine activity (Schon et al., 2012; Goudge et al., 2012, 2015).

Here we suggest a third hypothesis for the timing of the Mafic Floor. Based on the extended history of lacustrine activity that we suggest may be consistent with the physical and compositional diversity of fluviolacustrine features in Jezero, it is also possible that the Mafic Floor was emplaced between lacustrine phases. For example, the delta remnants to the east of the western delta may actually lie on top of the Mafic Floor, which in a history including only a single lacustrine phase would suggest that the entire western delta is younger than the Mafic Floor (Ruff, 2017). However, this could also be consistent with deposition and erosion of much of the delta early on, followed by emplacement of the Mafic Floor, and later emplacement and erosion of another extensive deltaic deposit to form the deltaic remnants. Similarly complex cycles of erosion and deposition have been proposed as a common feature of the martian geologic record (e.g., Malin and Edgett, 2001; Edgett and Malin,

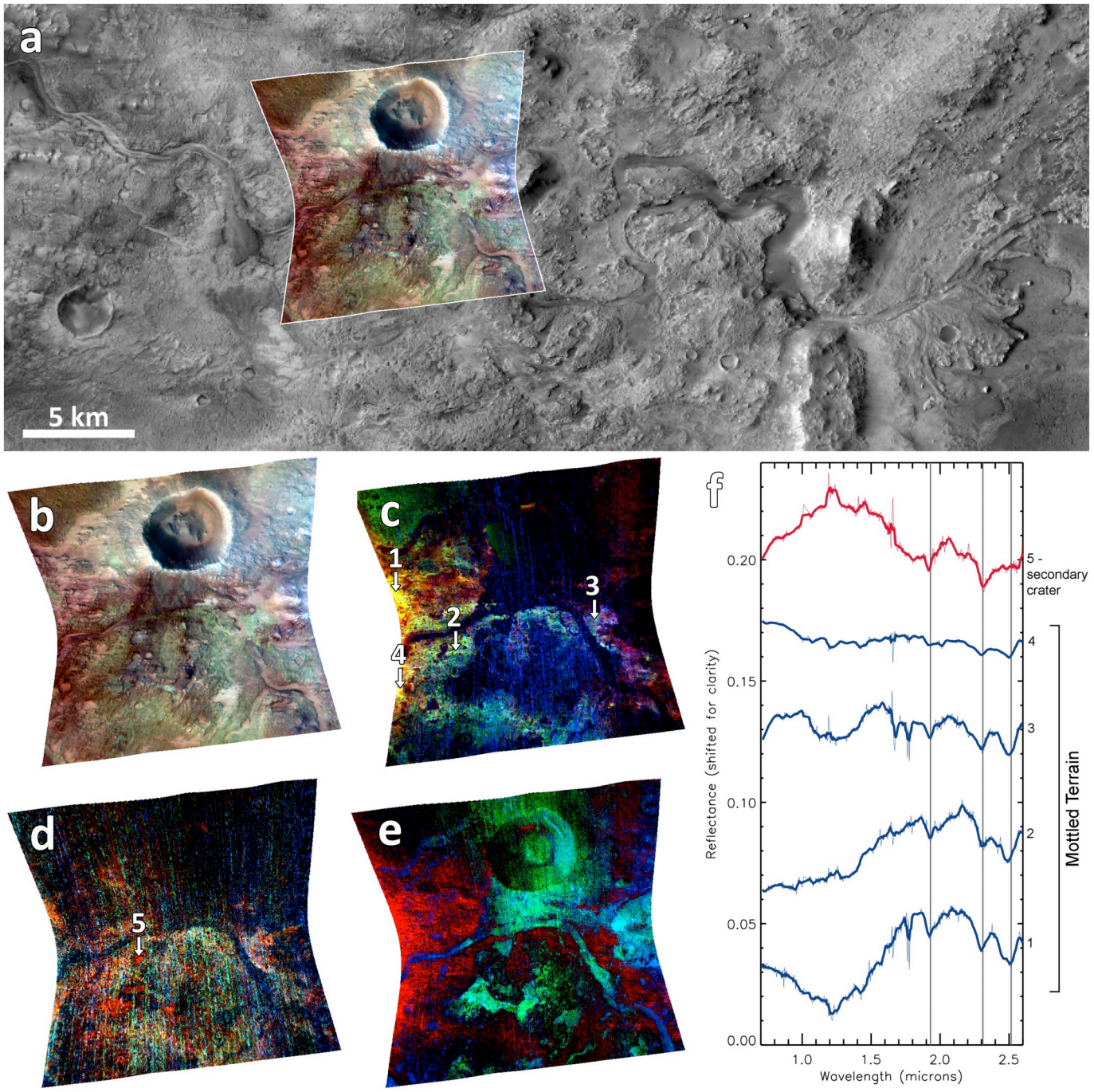

Fig. 13. Spectral diversity in the Mottled Terrain beyond Jezero in the watershed, CRISM image FRT0001182A. (a–b) False color RGB over CTX regional mosaic. Although the region is mapped as Mottled Terrain, it is also disrupted by a young impact crater. (c) The "Carbonate" RGB composite shows variability within the Mottled Terrain. (d) "Phyllosilicate" RGB shows local (red) patches of Fe/Mg-smectite in secondary craters. (e) The "Mafic" RGB shows the extent of olivine-bearing Mottled Terrain in red and LCP-bearing crater ejecta in green. (f) CRISM spectra showing an example of clay-bearing ejecta as well as variability within the Mottled Terrain. Sharp spikes near 1.2 and 1.7 μm are artifacts. (For interpretation of the references to color in this figure legend, the reader is referred to the web version of this article.)

2002; Edgett et al., 2018).

If the Mafic Floor was emplaced between or during lacustrine phases, then it could be critical for constraining the timing of lacustrine activity in Jezero, as a dateable marker bed in stratigraphy with the fluvio-lacustrine deposits. However, dating the unit might require quantitative geochronology as opposed to age inferred from crater density. For example, in the scenario posed above, the small crater counts on the Mafic Floor would not indicate an emplacement age, but rather a cumulative exposure age from both the time prior to emplacement of the last fluvio-lacustrine sediments and the time since erosion of those deposits. In situ investigation of the stratigraphic relationship between the Mafic Floor and both the delta and delta remnants might be necessary to constrain these various timing hypotheses.

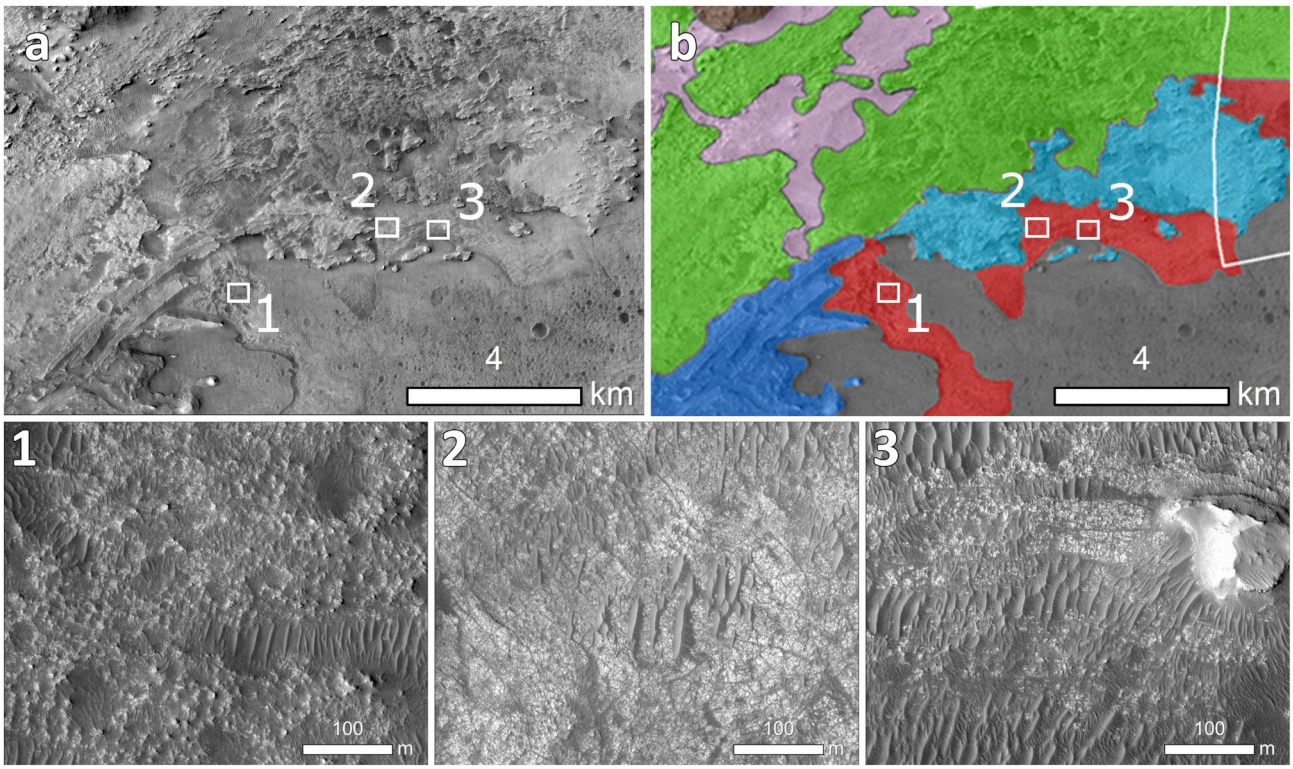

Fig. 14. Textures of the Light-toned Floor. (a) Context view of CTX mosaic and (b) Goudge et al. (2015) geologic map, where red is the Light-toned Floor. The typical "pockmarked" texture in HiRISE (location 1) transitions (3) to a smoother texture (2) in some locations. (For interpretation of the references to color in this figure legend, the reader is referred to the web version of this article.)

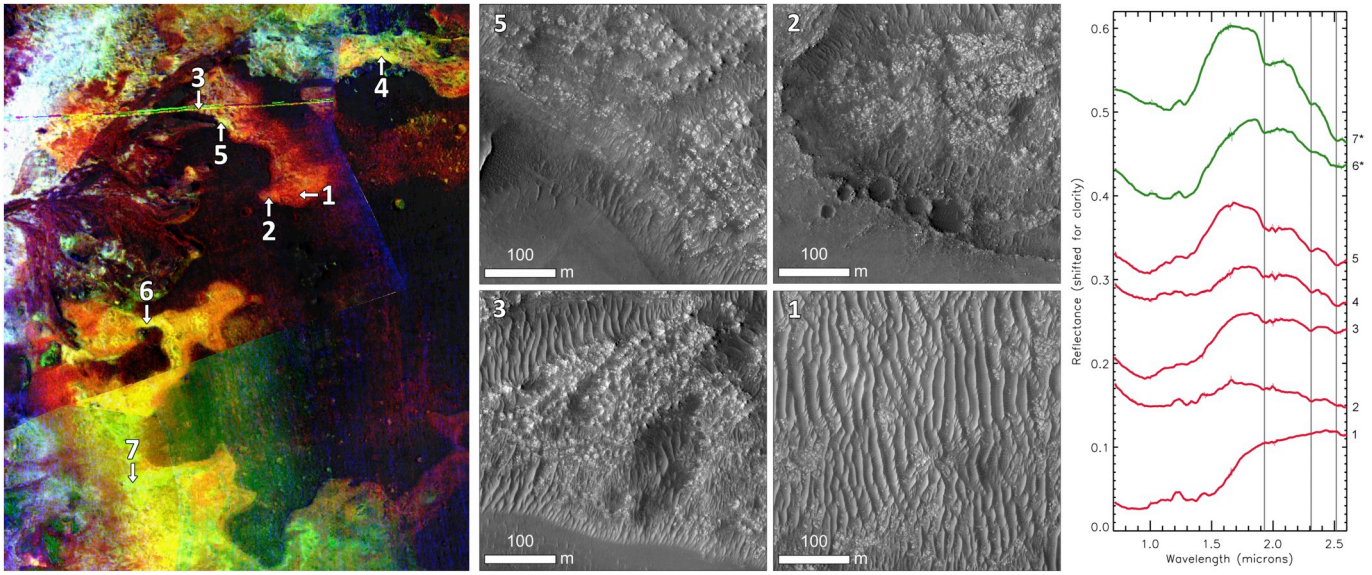

Fig. 15. Olivine signatures in the Light-toned Floor. (left) Olivine is red in the "carbonates" RGB, (middle) and this signature correlates with cover by aeolian bedforms as observed in HiRISE. (right) The carbonate-bearing Light-toned Floor (green in the RGB, spectra 4/5/7) exhibits the strong 1.3 μm band that is not as clearly expressed in the olivine sands (red in the RGB, spectra 1/2). Intermediate spectra (yellow in the RGB, spectra 3/6) exhibit weak carbonate bands. Spectra are from FRT000047A3 and HRL000040FF (indicated by *). (For interpretation of the references to color in this figure legend, the reader is referred to the web version of this article.)

7. Lacustrine carbonates as biosignature repositories

The possibility that the Marginal Carbonates are compositionally and topographically consistent with a near-shore lacustrine carbonate deposit presents a unique opportunity for future in situ astrobiological investigations. One key question for investigations at Mars is which types of deposits are most likely to preserve possible biological signals of interest (e.g., Hays et al., 2017; Summons et al., 2011). In the following section, we evaluate based on terrestrial analogs whether and how marginal lacustrine carbonates are prone to encase biosignatures, and more specifically, to investigate what special hydrochemical environments and taphonomic processes may have been conducive to the

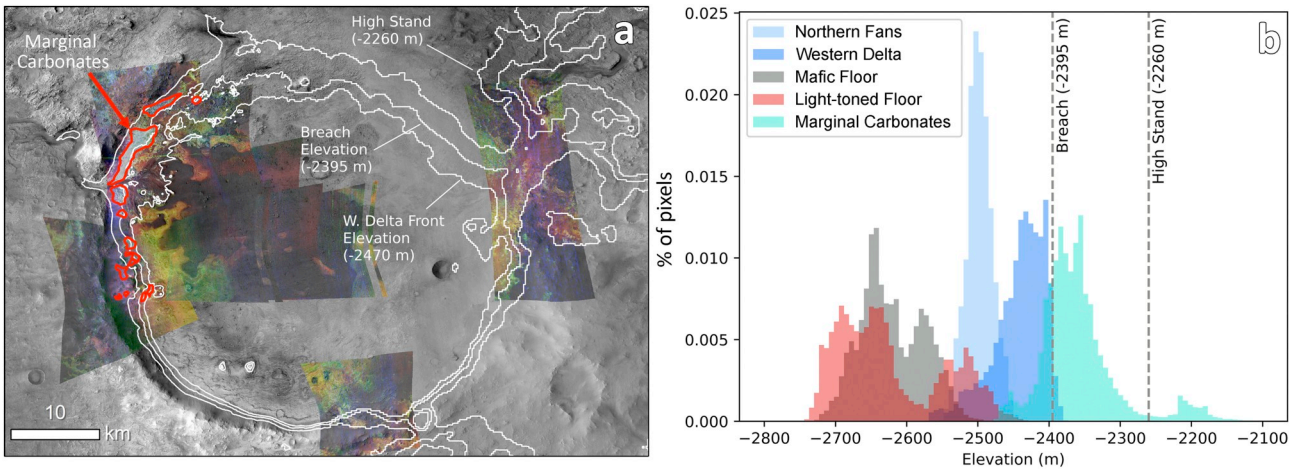

Fig. 16. (a) Distribution of possible occurrences of the "Marginal" Carbonates. In the "Carbonates" RGB composite, the Marginal Carbonates have a distinct light yellow/white/blue color, and all areas with spectral character potentially consistent with the Marginal Carbonates are outlined in red. Contours mark the approximate elevations of the western delta front, crater rim breach, and potential high stand. Elevations are from Fassett and Head (2005), and extracted from the HRSC DTM. (b) Plot of the distribution of elevations in selected units from the geologic map, as well as the Marginal Carbonates. In the vicinity of the western delta, the Marginal Carbonates are restricted to a narrow range of elevations (−2420 to −2260 m) along the inner rim. The small groups of relatively high (−2200 m) and low (−2475 m) Marginal Carbonate elevations correspond to potential occurrences within and upslope from rough concentric terraces around knobs and buttes in the southwest crater that may or may not be part of this unit. (For interpretation of the references to color in this figure legend, the reader is referred to the web version of this article.)

development of biomasses and preservation of microfossil bodies. To best fit with the Jezero geological context, we have focused our review on modern and ancient endorheic (closed basin) perennial lakes, excluding terrestrial coastal salinas.

7.1. Marginal carbonates of recent endorheic hypersaline and soda lakes

A great number of carbonate rocks have been documented from marginal settings of terrestrial, modern and recent, endorheic perennial lakes, and a representative subset of 13 lakes and their key properties are listed in Table S2. These marginal carbonates occur across diverse latitudinal, elevational, and hydrochemical conditions: 41°S to 43°N; 127 to 3016 m; fresh to alkaline waters. Marginal carbonate deposits are a hallmark of the alkaline lakes also referred to as soda lakes, which are defined as exhibiting a pH $\gtrsim$ 9 ($[HCO_3^-] \approx [CO_3^{2-}]$).

Carbonates are deposited in terrestrial lakes when cations (e.g., Ca^+, Mg^{2+}) are sufficiently supersaturated and the fluid contains bicarbonate. The cations are derived from weathering (hydrolysis) of common silicate minerals, which occurs when CO_2 is dissolved in rain to form carbonic acid (Eq. 1). The carbonic acid in the rain deprotonates to form bicarbonate (Eq. 2) which releases free hydrogen to drive hydrolysis and dissolution of silicate minerals, placing liberated cations in solution (e.g., Eby, 2016). Carbonate precipitation occurs as CO_2 degasses and escapes to the atmosphere, and both the bicarbonate and carbonate cation become supersaturated (Eq. 3). Thus, carbonate precipitation is most effective in warm, shallow, and agitated waters where CO_2 degassing rates are higher. In Jezero, the presence of carbonates near the margin of the maximum extent of the lake and in proximity to the largest inlet valley appears to be consistent with carbonate precipitation from lake waters.

$$CO_2 + H_20 \geq H_2CO_3 \quad (1)$$

$$H_2CO_3 \geq H^+ + HCO_3^- \quad (2)$$

$$Mg^{2+} + 2HCO_3^- \geq MgCO_3 + H_20 + CO_2 \quad (3)$$

These processes can result in either the production of ooids nucleated on particles in the water column, or direct precipitation of carbonate onto subaqueous or subaerial surfaces in the form of tufa, travertines, and stromatolites. On Earth, biomediation may play an important role in many of these low-temperature deposits (especially in locations with sub-saturated conditions), through a variety of mechanisms including indirectly through the removal of CO_2 from the water for photosynthetic respiration and production of particles for nucleation, as well as directly through organomineralization in biofilms and precipitation in shells and casings (e.g., Dupraz et al., 2009; Capezzuoli et al., 2014; Zhu and Dittrich, 2016).

Low-magnesium calcite is the prevalent lacustrine carbonate mineral, but high-magnesium calcite and aragonite are also widespread. In addition, normally rare polyhydrated carbonate minerals have been reported in terrestrial lake settings: ikaite ($CaCO_3.6H_2O$) in Mono Lake, or hydromagnesite ($Mg_5(CO_3)_4(OH)_2{\cdot}4H_2O$; Fig. 2b) in Lake Salda, Turkey (Braithwate and Zedef, 1996; Russell et al., 1999) and the playas of the Cariboo Plateau in British Columbia, Canada (Renaut and Stead, 1990; Power et al., 2009). In both cases, the source of the Mg to form the hydromagnesite is ultramafic or mafic rocks in the catchment or groundwater system. The most relevant analogy to the Jezero Marginal Carbonates may be provided by Lake Salda, around which hydromagnesite strandline terraces lie, including a hydromagnesite-cemented fan delta with beach deposits of hydromagnesite, including stromatolites, and pebbles of lizardite, and for which the catchment area is composed of partially serpentinized ultramafic rocks, i.e. ophiolites (Braithwate and Zedef, 1996; Russell et al., 1999).

There are three key types of marginal lacustrine carbonate deposits that have been described in terrestrial lakes, in a decreasing order of relative occurrence (e.g., Riding, 2000): microbialites, tufas, and beach sediments (Fig. 20). Carbonate "microbialites" (e.g., Burne and Moore, 1987) show variable internal structures or fabrics that can be classified as stromatolitic (fine, planar, domal, wavy lamination), oncolitic (irregular, concentric lamination), thrombolitic (clotted fabric), or cryptic (no obvious internal structure). These structures are referred to as "microbialites" because they typically form in the presence of microbial mats (e.g., Noffke et al., 2001); however, microbial activity is not necessarily required in order to form these structures, and carbonate precipitation in microbial mats can still be driven by abiogenic processes (e.g., Brasier, 2011). Microbialites are a very common feature of

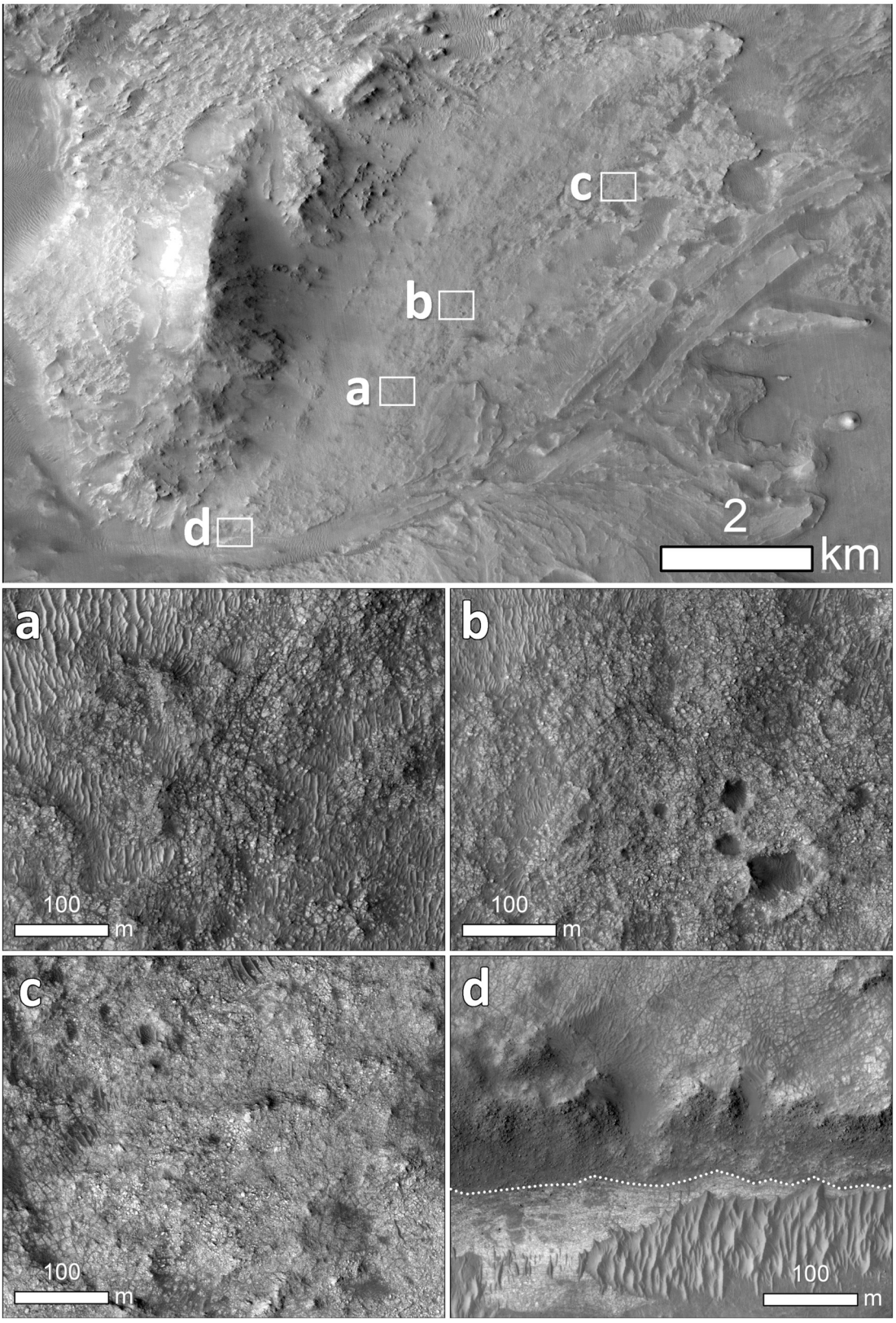

Fig. 17. Texture of the Marginal Carbonates at HiRISE scales.(a–c) Rubbly texture typical of Marginal Carbonates, (d) possible contact between Marginal Carbonates and possibly underlying layered materials in inlet channel, as indicated by dashed line.

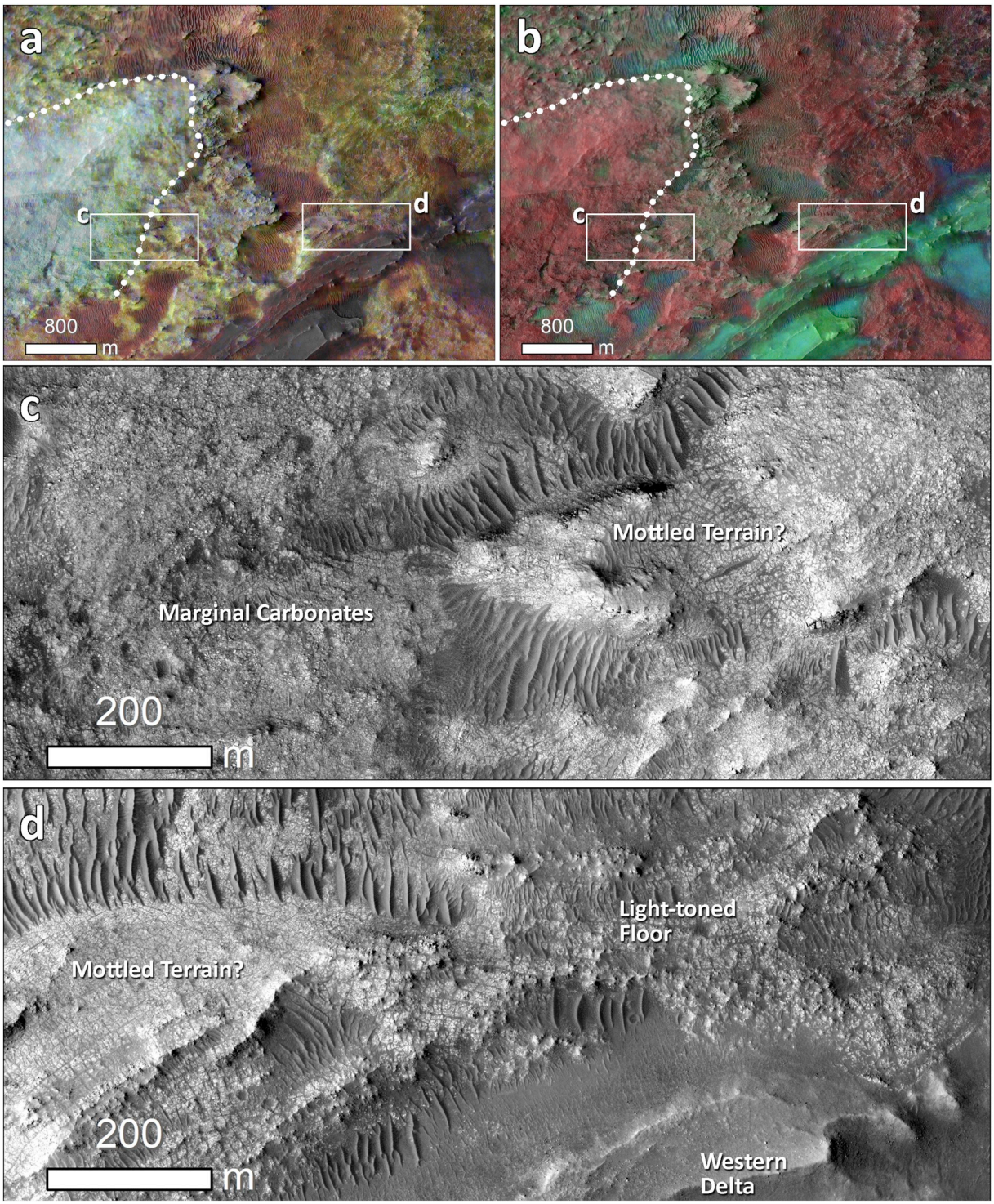

Fig. 18. Possible contacts at the northeastern edge of the Marginal Carbonates inferred from transitions in texture and tone, highlighting differences in texture between all three carbonate units. (a) The northern Marginal Carbonate appear cyan while adjacent terrains to the east appear purple to green in the "carbonates" RGB, and (b) also do not exhibit as strong of olivine signatures in the "mafic" RGB. (c) The contact between the northern Marginal Carbonates and the smoother, brighter terrain to the east, which may correspond to the Mottled Terrain, and (d) the contact between the possible Mottled Terrain and the Light-toned Floor. (For interpretation of the references to color in this figure legend, the reader is referred to the web version of this article.)

shallow, marginal areas of our set of lakes (8/13 cases), where they typically encrust firm substrates: pebbles in Lake Natron (Casanova, 1994), carbonate pinnacles in Lake Van (Lopez-Gargia et al., 2005) and Pyramid Lake (Benson, 1994), and bedrock in Fayetteville Green Lake (Thompson et al., 1990).

Carbonate tufas are carbonate precipitates localized at the emergence of cation-rich springwaters (Capezzuoli et al., 2014), either into subaerial environments, or in lacustrine settings, into alkaline CO_3^{2-} rich waters. In some studies, "tufa" and "travertine" are used interchangeably for spring-related carbonate deposits (Pentecost, 2005), but recent attempts to separate the two terms have suggested that travertines form where supersaturated (e.g., hydrothermal) fluids emerge,

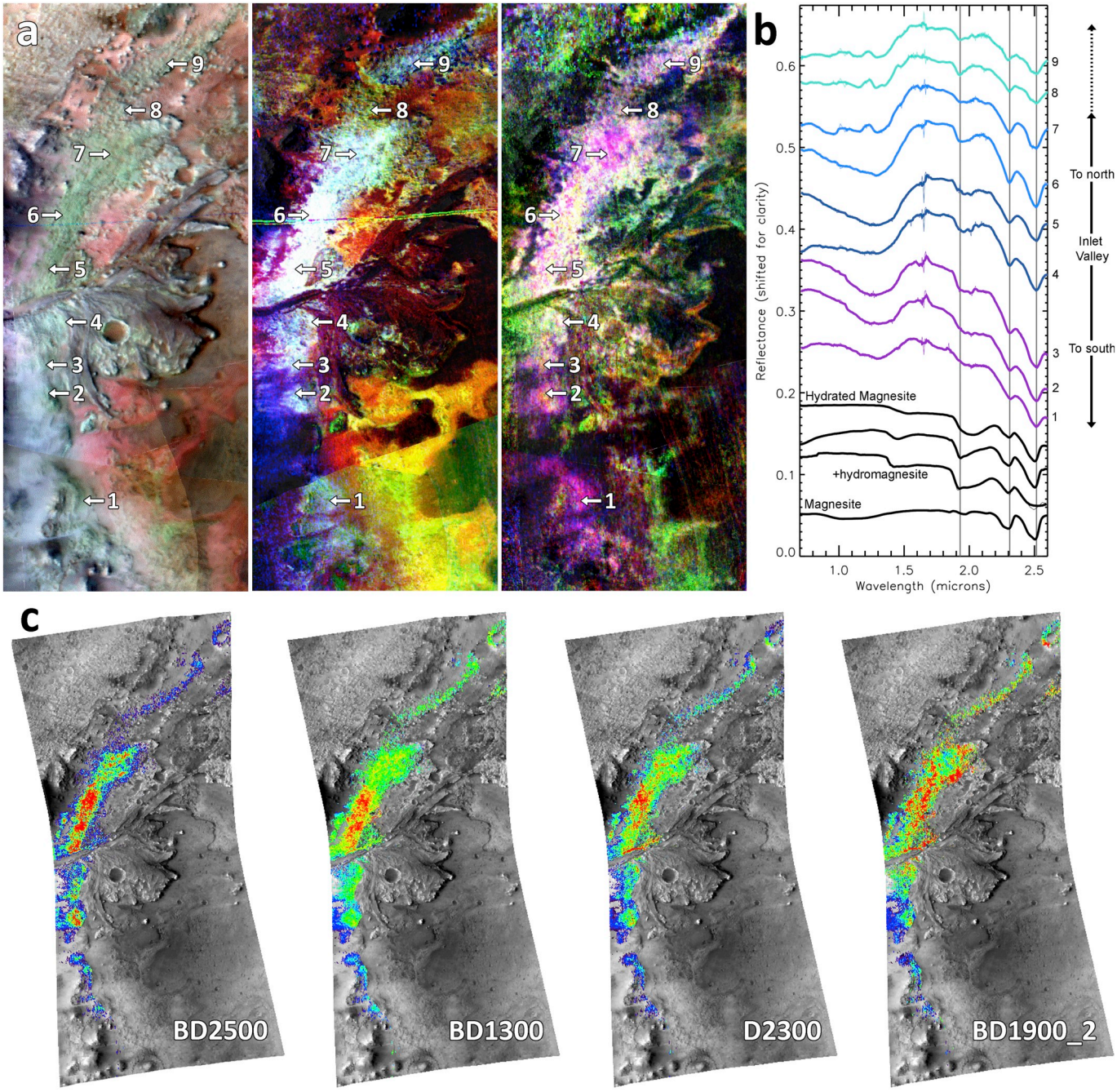

Fig. 19. Spectral variability of the "marginal" carbonates from south to north. (a) False color, "Carbonates", and "hydration" RGB mosaics. (b) Spectra of the Marginal Carbonates from HRL000040FF from locations indicated on maps. The main exposure of the Marginal Carbonates to the north of the inlet valley exhibits strong carbonate, hydration, and olivine bands, which all weaken to the north. To the south, 1.9 μm hydration and broad olivine signatures gradually weaken, terminating in spectra consistent with a relatively uncontaminated hydrated magnesite or magnesite-hydromagnesite mixture. (c) Spectral variability of specific band parameters within the Marginal Carbonates, restricted based on MOLA elevations between −2420 and − 2260 m. BD2500 indicates carbonate, BD1300 in this area indicates olivine and Fe-substitution in carbonate, D2300 indicates carbonate and Fe/Mg-smectite, and BD1900_2 indicates hydration.

Fig. 20. Examples of terrestrial lacustrine carbonates from the Great Basin in Utah. (a) Carbonate tufa on basalt, Tabernacle Hill flow. (b) Carbonate beach rocks partly covered with loose ooid sands and (c) eroded recent stromatolites at the shore of the Great Salt Lake. (d) Well-developed ancient stromatolites, Green River formation, stripes indicate 10 cm intervals.

while tufas form where more dilute (e.g., ambient temperature groundwater) fluids emerge (Capezzuoli et al., 2014). In lacustrine settings, tufas occur as a variety of forms including low relief mounds and high-relief chimneys or pinnacles. The most spectacular occurrences are encountered in lakes in the Western US (e.g. Mono Lake; Shearman et al., 1989) and East African Rift (Lake Abhe).

Marginal carbonates can also be concentrated through sedimentary processes, and lacustrine carbonate sedimentary deposits include: (i) beach-rocks, which are formed via syndepositional and/or early diagenetic cementation of loose beach sands and pebbles and may have a substantial siliciclastic component (e.g., Stoddart and Cann, 1965); (ii) oolitic and skeletal sands (e.g., the large oolitic beaches in the Great Salt Lake; Halley, 1977); (iii) fine-grained sediments (e.g. aragonitic laminated muds in Lake Son Kul and chalks sourced from whiting events in Fayetteville Green Lake; Pacton et al., 2015; Thompson and Ferris, 1990).

Despite >100 years of micropaleontologic, sedimentologic, isotopic and now experimental and metagenomic analyses, the relative roles of different biotic and abiotic processes in accretion of tufa, travertines, and stromatolites are still disputed, and significant debate continues regarding their biogenicity (e.g., Grotzinger and Rothman, 1996; Grotzinger and Knoll, 1999; Brasier, 2011). For example, it is clear that microorganisms live on and in tufa towers, but the role biology might play in tufa precipitation remains uncertain. The current consensus is that tufas form a continuum of abiotic and biologically influenced or induced processes during mixing of groundwater and lake water (e.g., Della Porta, 2015). Whether the nano- and microorganisms associated with the microbialites and tufas triggered, controlled, contributed to, or just behaved as opportunistic populations colonizing new substrates, is not the scope of this review. Our practical and present objective is to focus on the less ambiguous class of biosignatures that any biogenic or abiogenic carbonate-cemented sedimentary deposits may enclose, namely the class of microorganism morphologies (cells, body fossils, casts) that recent and ancient lacustrine carbonate deposits can preserve.

7.2. Microbial communities in modern endorheic hypersaline and soda lakes

Study of modern endoreic, perennial lakes has disclosed a high diversity of microorganisms, whether it is in the water column and in sediment pore spaces or as attached biofilms (e.g., Edwardson and Hollibaugh, 2018; Cabestrero et al., 2018). In particular, restricted, alkaline lake basins with high salinity have fostered the growth of microbial communities (and were not conducive to the ecological success of large multicellular organisms; Hickson et al., 2018). For example, in Lonar Lake, India, a hyperalkaline soda lake that is the only meteorite impact crater in the world situated in basalt rocks, microbial diversity analysis revealed the existence of diverse, yet largely consistent communities: Proteobacteria (30%), Actinobacteria (24%), Firmicutes (11%), and Cyanobacteria (5%) (Paul et al., 2016).

A plethora of phototrophic and non-phototrophic microorganisms are commonly associated with lacustrine microbialites. For example, living cyanobacteria and diatoms in thrombolites or thrombolitic stromatolites of Lake Van, Great Salt Lake, Salda Lake (see the compilation by Chagas et al., 2016); bacteria and cyanobacteria in recent stromatolites of East African lakes (Casanova, 1994); and a diverse array of cyanobacteria in the microbialites of the Fayetteville Green Lake (Wilhelm and Hewson, 2012). Recently, Pacton et al. (2014) have documented that viruses occur in high diversity, vastly outnumbering

prokaryotes, within a modern microbial mat from the hypersaline Lagoa Vermelha lake, Brazil. Their experimental results have shown that mineral precipitation occurs directly on free viruses and on cell debris resulting from cell lysis. Viruses are initially mineralized by amorphous magnesium silicates, which turns to magnesium carbonate nanospheres during diagenesis.

7.3. Microbial structures in recent and ancient terrestrial lacustrine carbonates

We have so far identified a total number of 17 lacustrine cases through the stratigraphic record for which likely microfossils have been documented, mostly in association with microbialites (Table S3). Microfossils of terrestrial lacustrine carbonates occur as three basic classes of microstructures: (1) filaments or tubes (erect and evenly spaced or organized as shrubs); (2) spheres (scattered or clustered); and (3) alveolar, honeycomb-like networks. There is no apparent trend or any long-term evolution of the lacustrine microfossil communities, and similar forms have been encountered in shallow, marginal marine microbialitic mounds of the Proterozoic and Paleozoic sequences. For example, the Paleoproterozoic microsphere Eoentophysalis belcherensis which is the oldest microfossil whose morphology is diagnostic for cyanobacteria (Knoll, 1996); tubular structures, and coalescent microspheres resembling Renalcis in "Algal" reefs of the Middel/Upper Proterozoic (Aitken, 1989); and shruby Epiphton and Renalcis in reef mounds of the Lower Cambrian (Narbonne and Arbuckle, 1989). It can thus be stated that the occurrences of these calcified microfossil forms neither reflect specific Earth environments nor milestones in the evolution of microbial communities, but rather appropriate sedimentary and diagenetic circumstances conducive to their preservation.

Biosignature preservation is enhanced by rapid mineralization, and there are several lines of evidence that marginal lacustrine deposits were the loci of an early, massive, and sometimes very rapid mineralization and lithification. An exceptionally fast growth rate greater than or equal to 30 mm/yr has been reported for the <100 yr old tufa mounds on the margin of Big Soda Lake, Nevada, USA (Rosen et al., 2004). A second generation of stromatolitic bioherms (ca 28–23 ka) encrusted an underlying former generation of bioherms, 90 ka in age, in L. Manyara, East Africa (Casanova, 1994). Beachrocks can form quickly as is testified by the inclusion of anthropogenic objects such as beer cans (Tucker, 1991) or ancient Greek grave remains (Bernier et al., 1987). There are also the spectacular petrified bird corpses of L. Natron, East Africa. The precipitation of carbonate is higher in soda lakes due to a stronger alkalinity engine and probably a higher degradation rate of exopolymeric substances (Cabestrero et al., 2018).

A combination of processes maximize the probability of preserving organic molecules, body fossils and sedimentary textures in marginal lacustrine carbonate settings on both Earth and Mars. First, marginal lacustrine settings provide hydrochemical environments and substrates that are very suitable for development of microbial communities. Second, the early, rapid, and massive calcification hampers any internal fluid circulation and thus protect the microbial structures from any mineral corruption. This early mineralization process would also shield organic molecules that are trapped between carbonate minerals (Benzerara et al., 2006) from destruction by surface oxidants and UV radiation. Finally, the marginal position of those deposits will make any burial-related thermal alteration of the organic components and microstructures unlikely, and Ostwald ripening (partial recrystallization) of carbonates is capable of preserving microbial fossils in carbonates on geologic timescales (Potter-McIntyre et al., 2017). Among this suite of favorable processes, the rapid mineralization appears to be the key factor, which facilitates preservation of microfossils by early encapsulation.

Based on the suite of terrestrial analogs presented here, marginal lacustrine carbonate deposits constitute a type of deposit that have a high probability of preserving microfossil bodies and organic components. The potential to preserve evidence of diverse microlife makes lacustrine microbialites, tufas, and beachrocks high priority biosignature repositories for in situ investigations on Mars. In addition, many of the key types of biosignatures preserved in these deposits (mm-scale textures, microbial fossils, and associated organics) can be of sufficient scale to be detected by a rover. Thus, the Marginal Carbonates of Jezero may represent a high-priority target for future in situ astrobiology investigations.

8. Conclusions

Our detailed spectral and morphological analyses of the major geologic units in Jezero crater combined with a synthesis of previous studies shows that the geological history of the basin has the potential to be much more complex than previously hypothesized. In particular, it was unclear from previous studies whether or not the carbonate-bearing terrains in the crater had any genetic relationship to the past lake activity that is indicated by the presence of the western delta. We find that the carbonate-bearing terrains in Jezero are all generally spectrally and morphologically similar, in line with previous mapping studies that largely grouped these units together. However, we also find that topographic properties, variations in the relative strength of key spectral signatures, erosional surface textures, and geologic context varies sufficiently across the crater to suggest different emplacement and/or modification histories for the carbonate-bearing units, some of which may be related to fluvio-lacustrine activity.

The olivine and carbonate-bearing Mottled Terrain along the northern rim and interior of Jezero exhibits spectral and morphological characteristics that are all comparable to similar properties of the regional olivine/carbonate-bearing unit on the plains to the west and south of Jezero, but the presence of localized Fe/Mg-smectite signatures within this unit in Jezero suggests that this portion of the unit may have undergone fluvial and/or lacustrine modification. The Light-toned Floor may also be part of the regional olivine/carbonate-bearing unit, as we find that the significant olivine sand component is unlikely to have accumulated via fluvial transport. Recent studies of the regional olivine-bearing unit have suggested that it has properties consistent with an ultramafic tephra deposit, which, in Jezero, is consistent with the draping relationship between the Mottled Terrain and the eroded northern rim. Alteration of the regional unit to form carbonates may have occurred through a number of different processes, but the widespread distribution and local variability of alteration across the unit along with the alteration assemblage is consistent with low to moderate temperature alteration of fresh ultramafic tephra by rain or snow melt.

The primary characteristic that distinguishes the Marginal Carbonates from the Mottled Terrain and Light-toned Floor is that they are located on the western inner margin of the crater, close to the western inlet, and within a narrow range of elevations that would correspond to the highest shorelines during the closed-basin phase of the Jezero lake sequence. In contrast, the regional olivine/carbonate unit drapes and mantles topography over a large range of elevations. The Marginal Carbonates exhibit much stronger carbonate spectral signatures throughout the unit than the other carbonate-bearing terrains, with olivine and hydration spectral signatures that are strong near the inlet but fade to the south, terminating in relatively uncontaminated hydrated carbonate spectral signatures in terraced deposits along the inner rim and around local knobs. Their surface texture is also somewhat distinct from the other carbonate terrains in the crater. While these spectral and textural properties could be attributed to the variability that has been observed across the regional olivine/carbonate-bearing unit, together with the topographic distribution of the Marginal Carbonates they are also consistent with fluvial transport of the regional olivine/carbonate-bearing unit into the crater and lacustrine precipitation of carbonate in the near-shore environment of a closed lake basin. Based on comparison to terrestrial analogs, the Marginal Carbonates are consistent with a combination of fluvial and beach or strandline

carbonate deposits, which can include microbialites, tufas, and oolitic sediments.

All three carbonate units would make excellent targets for in situ investigation by Mars 2020 or other future landed missions. As geological targets, both the Mottled Terrain/Light-toned Floor and the Marginal Carbonates contain carbonates that were most likely produced directly or indirectly through weathering by carbonic acid derived from the atmosphere. These units all thus represent key chemical and isotopic records of the late Noachian atmosphere, which could be used to better constrain the composition, thickness, and loss rates of the atmosphere during the peak of martian surface aqueous activity (Hu et al., 2015). The chemistry and sedimentology of the Marginal Carbonates and of the sedimentary facies preserved in the western delta could also help to constrain the chemistry and hydrogeology of Noachian fluvio-lacustrine systems, and their links to Noachian paleoclimate. However, perhaps the most compelling reason for detailed future in situ investigations in Jezero crater is the astrobiological potential of these units. If the Marginal Carbonates are indeed lacustrine shoreline deposits, they would be a particularly high priority target for future in situ investigations and sample return, as near-shore carbonate deposits on Earth are commonly biologically mediated (e.g., carbonate reefs, microbialites, and perhaps tufa), and have high biosignature preservation potential. In particular, lacustrine carbonates are capable of preserving morphological and textural biosignatures at scales that may be detectable by a landed mission.

Carbonates are just one part of the fluvio-lacustrine history in Jezero, as revealed by the mineral stratigraphy of the western delta and northern fans. The different sedimentological facies within the western delta exhibit distinct mineral assemblages that suggest changes in the source units in the watershed. The northern fans exhibit a similar mineral stratigraphy, suggesting that they either record the same regional trends in watershed mineralogy or were once part of the western delta. Based on these observations, there may be as many as four distinct lacustrine phases preserved in Jezero. Lacustrine activity in Jezero may have started early, with fluvial erosion of the regional basement unit and the northern rim of Jezero to form the lowermost units of the delta and fans. The second lacustrine phase may have begun either after or contemporaneous with deposition of the regional olivine/carbonate-bearing unit, resulting in erosion of this unit on the plains to form the current uppermost units on the northern fans, the point bar facies of the western delta, and the Marginal Carbonates. The third lacustrine phase is represented by the inverted channels that cap much of the western delta, and corresponds to additional transport of the basement unit, likely via incision through overlying units. The timing of the breach to form the outlet valley is only constrained to sometime after deposition of the Marginal Carbonates, but may have occurred during this third phase. The last lacustrine phase would then have formed the incised valley on the western delta, corresponding to a final shallow lake level well below the breach. This proposed history may be consistent with the relatively continuous scenario put forward by Goudge et al. (2018), in which the western delta represents gradually increasing lake levels and shoreline transgression, followed by the breach to form the outlet valley, and potentially later deposition in a shallower lake. However, the mineral diversity in the fans, delta, and Marginal Carbonates could also be consistent with a much more complex and long-lived fluvio-lacustrine history in Jezero, with distinct lacustrine sequences separated in time by fluctuating climatic conditions, resulting in fluctuating or even periodic lacustrine activity.

Ultimately, fully determining the relationships between the different geologic units at Jezero, their origin, and their astrobiological potential will require in situ investigation, and the hypotheses presented in this study should be testable on the ground using high resolution imagery, chemical, and spectral data produced by Mars 2020. A more detailed accounting of the rich history of aqueous alteration and fluviolacustrine activity that occurred at the site would provide many new insights into the nature of surface environments, climates, and habitability on early Mars.

Acknowledgements

We would like to thank Ken Williford and Katie Stack for inspiring and initiating this project, Tim Goudge and Vivian Sun for excellent reviews that significantly improved the clarity of this manuscript, Robin Fergason and Michael Diggles for internal USGS reviews, the Mars 2020 science team and Steve Ruff for helpful feedback on our analysis and the manuscript, Tim Goudge for providing the geologic map, and Jay Dickson for providing CTX and HiRISE mosaics. This study was funded in part by the Mars 2020 project, via the Mastcam-Z and SuperCam instrument teams.

Data availability

- All figures were derived from CRISM, HiRISE, CTX, and HRSC products available on the NASA Planetary Data System (https://pds.nasa.gov/).
- Laboratory mineral and rock spectra are available from the USGS Spectral Library (https://www.usgs.gov/energy-and-minerals/mineral-resources-program/science/usgs-high-resolution-spectral-library) and the PDS Geosciences Spectral Library (http://speclib.rsl.wustl.edu/)
- All CRISM spectral data shown in plots is available in the supplementary data file, which is also available at the linked Mendeley Data repository.
- High resolution versions of all CRISM RGB maps are also available at the linked Mendeley Data repository.

Appendix A. Supplementary data

Supplementary data to this article can be found online at https://doi.org/10.1016/j.icarus.2019.113526.

References

Adams, J.B., 1968. Lunar and Martian surfaces: petrologic significance of absorption bands in the near-infrared. Science 159 (3), 1453–1455. https://doi.org/10.1126/science.159.3822.1453.

Adams, J.B., Goullaud, L.H., 1978. Plagioclase feldspars - Visible and near infrared diffuse reflectance spectra as applied to remote sensing. In: Lunar and Planetary Science Conference, 9, pp. 2901–2909.

Aitken, J.D., 1989. Giant "algal" reefs, Middle/Upper Proterozoic Little Dal Group, Mackenzie Mountains, N.W.T., Canada. In: Geldsetzer, James, Tebbutt (Eds.), Reefs, Canada and Adjacent Area, 13. Canadian Society of Petroleum Geologists Memoir, pp. 13–23.

Amador, E.S., Bandfield, J.L., Thomas, N.H., 2018. A search for minerals associated with serpentinization across Mars using CRISM spectral data. Icarus 311, 113–134. https://doi.org/10.1016/j.icarus.2018.03.021.

Arvidson, R.E., et al., 2014. Ancient aqueous environments at Endeavour Crater, Mars. Science 343 (6169), 1248097. https://doi.org/10.1126/science.1248097.

Bandfield, J.L., Glotch, T.D., Christensen, P.R., 2003. Spectroscopic identification of carbonate minerals in the Martian Dust. Science 301 (5636), 1084–1087. https://doi.org/10.1126/science.1088054.

Bea, S.A., Wilson, S.A., Mayer, K.U., Dipple, G.M., Power, I.M., Gamazo, P., 2012. Reactive Transport Modeling of Natural Carbon Sequestration in Ultramafic Mine Tailings. Vadose Zone J. 11 (2), 0–17. https://doi.org/10.2136/vzj2011.0053.

Benson, L., 1994. Carbonate deposition, Pyramid Lake Subasin, Nevada: sequence of formation and elevational distribution of carbonate deposits (Tufas). Palaeogeogr. Palaeoclimatol. Palaeoecol. 109, 55–87.

Benzerara K., Menguy N., Lopez-Garcıa P., Yoon T-H, Kazmierczak J., Tyliszczak T., Guyot F. & Brown Jr. G. (2006) Nanoscale detection of organic signatures in carbonate microbialites. PNAS, 103, 25. doi:https://doi.org/10.1073/pnas.0603255103.

Bernier, P., Dalongeville, R., Duchêne, H., Rougemont, G., 1987. Les littoraux de Délos et de Rhénée. In: Bulletin de Correspondance Hellénique, 111.2, p. 655.

Bishop, J., Madejova, J., Komadel, P., Froschl, H., 2002. The influence of structural Fe, Al and Mg on the infrared OH bands in spectra of dioctahedral smectites. Clay Miner. 37 (4), 607–616. https://doi.org/10.1180/0009855023740063.

Bishop, J.L., et al., 2008. Phyllosilicate diversity and past aqueous activity revealed at Mawrth Vallis, Mars. Science 321 (5), 830. https://doi.org/10.1126/science.1159699.

Bishop, J.L., Perry, K.A., Darby Dyar, M., Bristow, T.F., Blake, D.F., Brown, A.J., Peel, S. E., 2013. Coordinated spectral and XRD analyses of magnesite-nontronite-forsterite mixtures and implications for carbonates on Mars. Journal of Geophysical Research Planets 118 (4), 635–650. https://doi.org/10.1002/jgre.20066.
Bishop, J.L., Fairén, A.G., Michalski, J.R., Gago-Duport, L., Baker, L.L., Velbel, M.A., Gross, C., Rampe, E.B., 2018. Surface clay formation during short-term warmer and wetter conditions on a largely cold ancient Mars. Nat Astron 115, 665–668. https://doi.org/10.1038/s41550-017-0377-9.
Bosak, T., Knoll, A.H., Petroff, A.P., 2013. The meaning of stromatolites. Annual Rev Earth Planet Sci 41 (1), 21–44. https://doi.org/10.1146/annurev-earth-042711-105327.
Boynton, W.V., et al., 2009. Evidence for calcium carbonate at the Mars Phoenix Landing Site. Science 325 (5), 61. https://doi.org/10.1126/science.1172768.
Braithwaite, C.J.R., Zedef, V., 1994. Living hydromagnesite stromatolites from Turkey. Sediment. Geol. 92 (1-2), 1–5. https://doi.org/10.1016/0037-0738(94)90051-5.
Braithwate, Zedef, 1996. Hydromagnesite stromatolites and sediments in an alkaline lake, Salda Golu, Turkey. Jour. of Sed. Research A 66, 991–1002.
Bramble, M.S., Mustard, J.F., Salvatore, M.R., 2017. The Geological History of Northeast Syrtis Major, Mars, Icarus, 293, pp. 1–28. https://doi.org/10.1016/j.icarus.2017.03.030.
Brasier, M.D., 2011. Towards a null hypothesis for stromatolites. In: Earliest Life on Earth: Habitats, Environments and Methods of Detection. Springer Netherlands, Dordrecht, pp. 115–125.
Bristow, T.F., et al., 2018. Clay mineral diversity and abundance in sedimentary rocks of Gale crater, Mars. Sci. Adv. 4 (6), eaar3330 https://doi.org/10.1126/sciadv.aar3330.
Brown, A.J., Hook, S.J., Baldridge, A.M., Crowley, J.K., Bridges, N.T., Thomson, B.J., Marion, G.M., de Souza Filho, C.R., Bishop, J.L., 2010. Hydrothermal formation of Clay-Carbonate alteration assemblages in the Nili Fossae region of Mars. Earth Planet. Sci. Lett. 297 (1), 174–182. https://doi.org/10.1016/j.epsl.2010.06.018.
Brown, A.J., Viviano-Beck, C.E., Bishop, J.L., Cabrol, N.A., Andersen, D., Sobron, P., Moersch, J., Templeton, A.S., Russell, M.J., 2016. A Serpentinization Origin for Jezero Crater Carbonates, 47th Lunar and Planetary Science Conference, #2165.
Brown, A.J., Viviano-Beck, C.E., Goudge, T.A., Putirka, K.D., 2017. Carbonate Mineralogy of the Jezero Crater Watershed. In: 48th Lunar and Planetary Science Conference, #2346.
Burne, R.V., Moore, L.S., 1987. Microbialites: Organosedimentary Deposits of Benthic Microbial Communities. PALAIOS 2 (3), 241. https://doi.org/10.2307/3514674.
Cabestrero, O., Sanz-Montero, M.E., Arregui, L., Serrano, S., Visscher, P.T., 2018. Seasonal variability of mineral formation in microbial mats subjected to drying and wetting cycles in alkaline and hypersaline sedimentary environments. Aquat. Geochem. 24 (1), 79–105.
Cady, S.L., Farmer, J.D., Grotzinger, J.P., Schopf, J.W., Steele, A., 2003. Morphological biosignatures and the search for life on Mars. Astrobiology 3, 351. https://doi.org/10.1089/153110703769016442.
Calvin, W.M., King, T.V.V., Clark, R.N., 1994. Hydrous carbonates on Mars? Evidence from Mariner 6/7 infrared spectrometer and ground-based telescopic spectra. J. Geophys. Res. 99 (E7), 14. https://doi.org/10.1029/94JE01090.
Canaveras, J.C., Hoyos, M., Sanch, S., 1999. Microbial Communities Associated With Hydromagnesite and Needle-Fiber Aragonite Deposits in a Karstic Cave (Altamira, Northern Spain). Geomicrobiol J. 16 (1), 9–25. https://doi.org/10.1080/014904599270712.
Capezzuoli, E., Gandin, A., Pedley, M., 2013. Decoding tufa and travertine (fresh water carbonates) in the sedimentary record: the state of the art. Sedimentology 61 (1), 1–21. https://doi.org/10.1111/sed.12075.
Casanova J. (1994) Stromatolites in East African Lakes. In Phanerozoic Stromatolites II (Bertrand-Sarfati & Monty eds). Kluwer Academic Publishers, 193–226.
Chagas, A.A.P., Webb, G.E., Burne, R.V., Southam, G., 2016. Modern lacustrine microbialites: towards a synthesis of aqueous and carbonate geochemistry and mineralogy. Earth Sci. Rev. 162, 338–363.
Clark, R.N., Swayze, G.A., Wise, R., Livo, K.E., Hoefen, T.M., Kokaly, R.F., Sutley, S.J., 2007. USGS digital spectral library splib06a. In: U.S. Geological Survey Data Series, 231.
Cloutis, E.A., Gaffey, M.J., 1991. Spectral-compositional variations in the constituent minerals of mafic and ultramafic assemblages and remote sensing implications. Earth Moon Planets 53, 11–53. https://doi.org/10.1007/BF00116217.
Crowley, J.K., 1986. Visible and near-infrared spectra of carbonate rocks: Reflectance variations related to petrographic texture and impurities. J Geophys Res-Sol Ea 91 (B), 5001–5012. https://doi.org/10.1029/JB091iB05p05001.
Cuadros, J., Michalski, J.R., 2013. Investigation of Al-rich clays on Mars: evidence for kaolinite-smectite mixed-layer versus mixture of end-member phases. Icarus 222 (1), 296–306. https://doi.org/10.1016/j.icarus.2012.11.006.
Della Porta, G., 2015. Carbonate build-ups in lacustrine, hydrothermal and fluvial settings: comparing depositional geometry, fabric types and geochemical signature. In: Bosence, et al. (Eds.), Microbial Carbonates in Space and Time: Implications for Global Exploration and Production, Geological Society, London, Special Publications, 418, pp. 17–68.
Dickson, J.L., Kerber, L.A., C. F. L. A. Planetary, 2018, 2018. A Global, Blended CTX Mosaic of Mars with Vectorized Seam Mapping: A New Mosaicking Pipeline Using Principles of Non-Destructive Image Editing, 49. LPSC (#2480).
Dupraz, C., Reid, R.P., Braissant, O., Decho, A.W., Norman, R.S., Visscher, P.T., 2009. Processes of carbonate precipitation in modern microbial mats. Earth-Sci. Rev. 96 (3), 141–162. https://doi.org/10.1016/j.earscirev.2008.10.005.
Eby, G.N., 2016. Principles of environmental geochemistry. Waveland Press.
Edgett, K.S., Malin, M.C., 2002. Martian sedimentary rock stratigraphy: Outcrops and interbedded craters of northwest Sinus Meridiani and southwest Arabia Terra. Geophys. Res. Lett. 29 (2), 2179. https://doi.org/10.1029/2002GL016515.
Edgett, K.S., et al., 2018. Multi-Cycle Sedimentary Rocks on Mars and Implications. In: Lunar and Planetary Science Conference, 49, p. #1669.
Edwards, C.S., Ehlmann, B.L., 2015. Carbon sequestration on Mars. Geology 43 (10), 863–866. https://doi.org/10.1130/G36983.1.
Edwardson, C.F., Hollibaugh, J.T., 2018. Composition and activity of microbial communities along the redox gradient of an alkaline, hypersaline, lake. Front. Microbiol. 9, 14.
Ehlmann, B.L., Edwards, C.S., 2014. Mineralogy of the Martian surface. Annual Rev Earth Planet Sci 42 (1), 291–315. https://doi.org/10.1146/annurev-earth-060313-055024.
Ehlmann, B.L., Mustard, J.F., 2012. An in-situ record of major environmental transitions on early Mars at Northeast Syrtis Major. Geophys. Res. Lett. 39 (11) https://doi.org/10.1029/2012GL051594.
Ehlmann, B.L., et al., 2008. Orbital identification of carbonate-bearing rocks on Mars. Science 322 (5), 1828. https://doi.org/10.1126/science.1164759.
Ehlmann, B.L., Mustard, J.F., Fassett, C.I., Schon, S.C., Head, J.W.I., Des Marais, D.J., Grant, J.A., Murchie, S.L., 2008. Clay minerals in delta deposits and organic preservation potential on Mars. Nat. Geosci. 1 (6), 355–358. https://doi.org/10.1038/ngeo207.
Ehlmann, B.L., et al., 2009. Identification of hydrated silicate minerals on Mars using MRO-CRISM: geologic context near Nili Fossae and implications for aqueous alteration. J. Geophys. Res. 114 (5) https://doi.org/10.1029/2009JE003339.
Ehlmann, B.L., Mustard, J.F., Murchie, S.L., 2010. Geologic setting of serpentine deposits on Mars. Geophys. Res. Lett. 37 (6), 6201. https://doi.org/10.1029/2010GL042596.
Farmer, J.D., Des Marais, D.J., 1999. Exploring for a record of ancient Martian life. Journal of Geophysical Research: Planets 104 (E11), 26977–26995. https://doi.org/10.1029/1998JE000540 (1991–2012).
Fassett, C.I., Head, J.W., 2005. Fluvial sedimentary deposits on Mars: ancient deltas in a crater lake in the Nili Fossae region. Geophys. Res. Lett. 32 (14) https://doi.org/10.1029/2005GL023456 n/a–n/a.
Fassett, C.I., Head, J.W., 2008. Valley network-fed, open-basin lakes on Mars: distribution and implications for Noachian surface and subsurface hydrology. Icarus 198 (1), 37–56. https://doi.org/10.1016/j.icarus.2008.06.016.
Fergason, R.L., Hare, T.M., Kirk, R.L., Piqueux, S., Galuzska, D.M., Golombek, M.P., Otero, R.E., Redding, B.L., 2017. Mars 2020 landing site evaluation: slope and physical property assessment. In: 48th Lunar and Planetary Science Conference, held 20–24 March 2017, at The Woodlands, Texas. LPI Contribution No. 1964, id.2163. https://astrogeology.usgs.gov/search/map/Mars/Mars2020/landing_site/J03_045994_1986_J03_046060_1986_20m_DTM.
Fergason, R.L., Hare, T.M., Laura, J., 2018. HRSC and MOLA Blended Digital Elevation Model at 200m v2, Astrogeology PDS Annex. U.S. Geological Survey. http://bit.ly/HRSC_MOLA_Blend_v0.
Fishbeck, R., Müller, G., 1971. Monohydrocalcite, hydromagnesite, nesquehonite, dolomite, aragonite and calcite in speleothems of the Frankische Schweiz, western Germany. Contrib. Mineral. Petrol. 33, 87–92 (Chicago).
Flannery, D.T., Summons, R.E., Walter, M.R., 2018. Chapter 5 - Archean lakes as analogues for habitable martian paleoenvironments. In: From Habitability to Life on Mars. Elsevier Inc.
Gaffey, S.J., 1987. Spectral reflectance of carbonate minerals in the visible and near infrared (0.35–2.55 μm): anhydrous carbonate minerals. J. Geophys. Res. 92 (B), 1429–1440. https://doi.org/10.1029/JB092iB02p01429.
Golubic, S., 1991. Modern stromatolites: a review. In: Riding, R. (Ed.), Calcareous Algae and Stromatolites. Springer, Berlin, Heidelberg.
Goudge, T.A., Head, J.W., Mustard, J.F., Fassett, C.I., 2012. An analysis of open-basin lake deposits on Mars: evidence for the nature of associated lacustrine deposits and post-lacustrine modification processes. Icarus 219 (1), 211–229. https://doi.org/10.1016/j.icarus.2012.02.027.
Goudge, T.A., Mustard, J.F., Head, J.W., Fassett, C.I., Wiseman, S.M., 2015. Assessing the mineralogy of the watershed and fan deposits of the Jezero crater paleolake system, Mars. Journal of Geophysical Research Planets 120 (4), 775–808. https://doi.org/10.1002/2014JE004782.
Goudge, T.A., Milliken, R.E., Head, J.W., Mustard, J.F., Fassett, C.I., 2017. Sedimentological evidence for a deltaic origin of the western fan deposit in Jezero crater, Mars and implications for future exploration. Earth Planet. Sci. Lett. 458, 357–365. https://doi.org/10.1016/j.epsl.2016.10.056.
Goudge, T.A., Mohrig, D., Cardenas, B.T., Hughes, C.M., Fassett, C.I., 2018. Stratigraphy and paleohydrology of delta channel deposits, Jezero crater, Mars. Icarus 301, 58–75. https://doi.org/10.1016/j.icarus.2017.09.034.
Grotzinger, J.P., Knoll, A.H., 1999. Stromatolites in Precambrian carbonates: evolutionary mileposts or environmental dipsticks? Annual Rev Earth Planet Sci 27 (1), 313–358. https://doi.org/10.1146/annurev.earth.27.1.313.
Grotzinger, J.P., Rothman, D.H., 1996. An abiotic model for stromatolite morphogenesis. Nature 383 (6), 423–425. https://doi.org/10.1038/383423a0.
Halley, R.B., 1977. Ooid fabric and fracture in the Great Salt Lake and the geological record. Jour. of Sed. Petr. 47 (3), 1099–1120.
Hänchen, M., Prigiobbe, V., Baciocchi, R., Mazzotti, M., 2008. Precipitation in the Mg-carbonate system—effects of temperature and CO2 pressure. Chem. Eng. Sci. 63 (4), 1012–1028. https://doi.org/10.1016/j.ces.2007.09.052.
Hamilton, V.E., Christensen, P.R., 2005. Evidence for extensive, olivine-rich bedrock on Mars. Geology 33 (6), 433. https://doi.org/10.1130/G21258.1.
Hamilton, V.E., Christensen, P.R., Mcsween, H.Y., Bandfield, J.L., 2003. Searching for the source regions of Martian meteorites using MGS TES: integrating Martian meteorites

into the global distribution of igneous materials on Mars. Meteorit. Planet. Sci. 38 (6), 871–885. https://doi.org/10.1111/j.1945-5100.2003.tb00284.x.
Harner, P.L., Gilmore, M.S., 2015. Visible-near infrared spectra of hydrous carbonates, with implications for the detection of carbonates in hyperspectral data of Mars. Icarus 250, 204–214. https://doi.org/10.1016/j.icarus.2014.11.037.
Hays, L.E., Graham, H.V., Des Marais, D.J., Hausrath, E.M., Horgan, B., McCollom, T.M., Parenteau, M.N., Potter-McIntyre, S.L., Williams, A.J., Lynch, K.L., 2017. Biosignature preservation and detection in Mars analog environments. Astrobiology. https://doi.org/10.1089/ast.2016.1627 ast.2016.1627–39.
Hickson, T.A., Theissen, K.M., Lamb, M.A., Frahm, J., 2018. Lower Pahranagat Lake: modern analogue for extensive carbonate deposition in paleolakes of the Late Oligocene to Miocene Rainbow Gardens and Horse Spring Formations. J. Paleolimnol. 59 (1), 39–57.
Hoefen, T.M., Clark, R.N., Bandfield, J.L., Smith, M.D., Pearl, J.C., Christensen, P.R., 2003. Discovery of olivine in the Nili Fossae Region of Mars. Science 302 (5645), 627–630. https://doi.org/10.1126/science.1089647.
Horgan, B., Cloutis, E.A., Mann, P., Bell, J.F., 2014. Near-infrared spectra of ferrous mineral mixtures and methods for their identification in planetary surface spectra. Icarus 234, 132–154. https://doi.org/10.1016/j.icarus.2014.02.031.
Howard, A.D., Moore, J.M., Irwin, R.P., 2005. An intense terminal epoch of widespread fluvial activity on early Mars: 1. Valley network incision and associated deposits. J. Geophys. Res. 110 (E), E12S14. https://doi.org/10.1029/2005JE002459.
Hu, R., Kass, D.M., Ehlmann, B.L., Yung, Y.L., 2015. Tracing the fate of carbon and the atmospheric evolution of Mars. Nat. Commun. 6, 10003 https://doi.org/10.1038/ncomms10003.
Hunt, G.R., Salisbury, J.W., 1971. Visible and near infrared spectra of minerals and rocks. II. Carbonates. Mod. Geol. 2, 23–30.
Irwin, R.P., Craddock, R.A., Howard, A.D., Flemming, H.L., 2011. Topographic influences on development of Martian valley networks. J. Geophys. Res. 116 (E2), E02005 https://doi.org/10.1029/2010JE003620.
Kahn, R., 1985. The evolution of CO2 on Mars. Icarus 62 (2), 175–190. https://doi.org/10.1016/0019-1035(85)90116-2.
King, T.V.V., Ridley, W.I., 1987. Relation of the Spectroscopic Reflectance of Olivine to Mineral Chemistry and Some Remote Sensing Implications, 92(B11), pp. 11457–11469. https://doi.org/10.1029/JB092iB11p11457.
Knoll, A.H., 1996. Archean and Proterozoic paleontology. In: Jansonius, McGregor (Eds.), Palynology: Principles and Applications, 1. American Association of Stratigraphic Palynologists Foundation, pp. 51–80.
Koeppen, W.C., Hamilton, V.E., 2008. Global distribution, composition, and abundance of olivine on the surface of Mars from thermal infrared data. J. Geophys. Res. 113 (E), 5001. https://doi.org/10.1029/2007JE002984.
Königsberger, E., Königsberger, L.-C., Gamsjäger, H., 1999. Low-temperature thermodynamic model for the system Na2CO3-MgCO3-CaCO3-H2O. Geochim. Cosmochim. Acta 63 (1), 3105–3119. https://doi.org/10.1016/S0016-7037(99)00238-0.
Kremer, C.H., Mustard, J.F., Bramble, M.S., 2018. Origin and emplacement of the circum-Isidis olivine-rich unit. In: 49th Lunar and Planetary Science Conference, abstract #1545.
Kremer, C.H., Mustard, J.F., Bramble, M., 2019. A widespread olivine-rich ash deposit on Mars. Geology. https://doi.org/10.1130/G45563.1.
Langer, K., Florke, O., 1974. Near infrared absorption spectra of opals and the role of water in these SiO2-nH20 minerals. Fortschr. Mineral. 52 (1), 17–51.
Lopez-Gargia, P., Kazmierczak, J., Benzerara, K., Kempe, S., Guyot, F., Moreira, D., 2005. Bacterial diversity and carbonate precipitation in the giant microbialites from high alkaline Lake Van, Turkey. Extremophiles 9, 263–274.
Malin, M.C., Edgett, K.S., 2001. Mars Global Surveyor Mars Orbiter Camera: Interplanetary cruise through primary mission. Journal of Geophysical Research 106, 23429–23570. https://doi.org/10.1029/2000JE001455.
Mangold, N., et al., 2007. Mineralogy of the Nili Fossae region with OMEGA/Mars Express data: 2. Aqueous alteration of the crust. J. Geophys. Res. 112 (E) https://doi.org/10.1029/2006JE002835.
Mangold, N., et al., 2010. Mineralogy of recent volcanic plains in the Tharsis region, Mars, and implications for platy-ridged flow composition. Earth Planet. Sci. Lett. 294 (3–4), 440–450. https://doi.org/10.1016/j.epsl.2009.07.036.
Mangold, N., Adeli, S., Conway, S., Ansan, V., Langlais, B., 2012. A chronology of early Mars climatic evolution from impact crater degradation. Journal of Geophysical Research Planets 117 (E4). https://doi.org/10.1029/2011JE004005 n/a–n/a.
Mcewen, A.S., et al., 2007. Mars Reconnaissance Orbiter's High Resolution Imaging Science Experiment (HiRISE). J. Geophys. Res. 112 (E) https://doi.org/10.1029/2005JE002605.
Mclennan, S.M., 2003. Sedimentary silica on Mars. Geology 31 (4), 315. https://doi.org/10.1130/0091-7613(2003)031<0315:SSOM>2.0.CO;2.
Mcsween, H.Y., Labotka, T.C., Viviano-Beck, C.E., 2015. Metamorphism in the Martian crust. Meteorit. Planet. Sci. 50 (4), 590–603. https://doi.org/10.1111/maps.12330.
Michalski, J.R., Cuadros, J., Bishop, J.L., Darby Dyar, M., Dekov, V., Fiore, S., 2015. Constraints on the crystal-chemistry of Fe/Mg-rich smectitic clays on Mars and links to global alteration trends. Earth Planet. Sci. Lett. 427, 215–225. https://doi.org/10.1016/j.epsl.2015.06.020.
Morris, R.V., Ruff, S.W., Gellert, R., Ming, D.W., Arvidson, R.E., Clark, B.C., Golden, D.C., Siebach, K., Klingelhöfer, G., Schröder, C., 2010. Identification of carbonate-rich outcrops on Mars by the Spirit rover. Science 329 (5990), 421–424.
Müller, G., Irion, G., Förstner, U., 1972. Formation and diagenesis of inorganic Ca-Mg carbonates in the lacustrine environment. Die Naturwissenschaften 59 (4), 158–164. https://doi.org/10.1007/BF00637354.
Murchie, S., et al., 2007. Compact reconnaissance imaging spectrometer for Mars (CRISM) on Mars reconnaissance orbiter (MRO). J. Geophys. Res. 112 (E) https://doi.org/10.1029/2006JE002682.
Murchie, S.L., et al., 2009. Compact reconnaissance imaging spectrometer for Mars investigation and data set from the Mars reconnaissance orbiter's primary science phase. J. Geophys. Res. 114, E00D07. https://doi.org/10.1029/2009JE003344.
Murchie, S.L., et al., 2009. A synthesis of Martian aqueous mineralogy after 1 Mars year of observations from the Mars Reconnaissance Orbiter. J. Geophys. Res. 114 (5) https://doi.org/10.1029/2009JE003342.
Mustard, J.F., Poulet, F., Gendrin, A., Bibring, J.-P., Langevin, Y., Gondet, B., Mangold, N., Bellucci, G., Altieri, F., 2005. Olivine and pyroxene diversity in the crust of Mars. Science 307 (5), 1594–1597. https://doi.org/10.1126/science.1109098.
Mustard, J., Poulet, F., Head, J., Mangold, N., Bibring, J., Pelkey, S., Fassett, C., Langevin, Y., Neukum, G., 2007. Mineralogy of the Nili Fossae region with OMEGA/Mars Express data: 1. Ancient impact melt in the Isidis Basin and implications for the transition from the Noachian to Hesperian. J. Geophys. Res. 112 (E8), E08S03. https://doi.org/10.1029/2006JE002834.
Mustard, J.F., Ehlmann, B.L., Murchie, S.L., Poulet, F., Mangold, N., Head, J.W., Bibring, J.-P., Roach, L.H., 2009. Composition, morphology, and stratigraphy of Noachian Crust around the Isidis basin. J. Geophys. Res. 114 (7), E00D12. https://doi.org/10.1029/2009JE003349.
Narbonne G.M. and Arbuckle S.M. (1989) Lower Cambrian algal-archeocyathan reef mounds from the Wernecke Mountains, Yukon Territory. In Reefs, Canada and Adjacent Area (Geldsetzer, James & Tebbutt, eds) Canadian Society of Petroleum Geologists Memoir 13, 156–160.
Noffke, N., Gerdes, G., Klenke, T., Krumbein, W.E., 2001. Microbially induced sedimentary structures: a new category within the classification of primary sedimentary structures. J. Sediment. Res. 71, 649–656. https://doi.org/10.1306/2DC4095D-0E47-11D7-8643000102C1865D.
Pacton, M., Wacey, D., Corinaldesi, C., Tangherlini, M., Kilburn, M.R., Gorin, G.E., Danovaro, R., Vasconcelos, C., 2014. Viruses as new agents of organomineralization in the geological record. Nat. Commun. 5, 4298. https://doi.org/10.1038/ncomms5298.
Pacton, M., Sorrel, P., Bevillard, B., et al., 2015. Sedimentary facies analyses from nano- to milimeter scale exploring past microbial activity in a high-latitude lake (Lake Son Kul, Central Asia). Geol. Mag. 152 (5), 902–922.
Paul, D., Kumbhare, S.V., Mhatre, S.S., Chowdhury, S.P., Shetty, S.A., Marathe, N.P., Bhute, S., Shouche, Y.S., 2016. Exploration of microbial diversity and community structure of Lonar Lake: the only hypersaline meteorite crater lake within basalt rock. Frontiers Microbiology 6, 1553. https://doi.org/10.3389/fmicb.2015.01553.
Pentecost, A., 2005. Travertine. Springer.
Pieters, C.M., 1983. Strength of mineral absorption features in the transmitted component of near-infrared reflected light - first results from RELAB. J. Geophys. Res. 88, 9534–9544. https://doi.org/10.1029/JB088iB11p09534.
Pollack, J.B., Kasting, J.F., Richardson, S.M., Poliakoff, K., 1987. The case for a wet, warm climate on early Mars. Icarus 71 (2), 203–224. https://doi.org/10.1016/0019-1035(87)90147-3.
Potter-McIntyre, S.L., Williams, J., Phillips-Lander, C., O'Connell, L., 2017. Taphonomy of microbial biosignatures in spring deposits: a comparison of modern, Quaternary, and Jurassic examples. Astrobiology 17 (3), 216–230. https://doi.org/10.1089/ast.2016.1495.
Poulet, F., et al., 2009. Quantitative compositional analysis of martian mafic regions using the MEx/OMEGA reflectance data. 2. Petrological implications. Icarus 201 (1), 84–101. https://doi.org/10.1016/j.icarus.2008.12.042.
Poulet, F., Carter, J., Bishop, J.L., Loizeau, D., Murchie, S.M., 2014. Mineral abundances at the final four curiosity study sites and implications for their formation. Icarus 231 (C), 65–76. https://doi.org/10.1016/j.icarus.2013.11.023.
Power, I.M., Wilson, S.A., Thom, J.M., Dipple, G.M., Gabites, J.E., Southam, G., 2009. The hydromagnesite playas of Atlin, British Columbia, Canada: A biogeochemical model for CO2 sequestration. Chem. Geol. 260 (3–4), 286–300. https://doi.org/10.1016/j.chemgeo.2009.01.012.
Power, I.M., Wilson, S.A., Harrison, A.L., Dipple, G.M., McCutcheon, J., Southam, G., Kenward, P.A., 2014. A depositional model for hydromagnesite–magnesite playas near Atlin, British Columbia, Canada. In: Ariztegui, D. (Ed.), Sedimentology, 61(6), pp. 1701–1733. https://doi.org/10.1111/sed.12124.
Ramirez, R.M., Craddock, R.A., 2018. The geological and climatological case for a warmer and wetter early Mars. Nat. Geosci. 11 (4), 230. https://doi.org/10.1038/s41561-018-0093-9.
Renaut, R.W., 1993. Morphology, distribution, and preservation potential of microbial mats in the hydromagnesite-magnesite playas of the Cariboo Plateau, British Columbia, Canada. Hydrobiologia 267 (1-3), 75–98.
Renaut, R.W., Stead, D., 1990. Recent magnesite-hydromagnesite sedimentation in playa basins of the Cariboo Plateau, British Columbia. Geological Fieldwork 1991–1, 279–288.
Rice, M.S., Cloutis, E.A., Bell, J.F., Bish, D.L., Horgan, B.H., Mertzman, S.A., Craig, M.A., Renaut, R.W., Gautason, B., Mountain, B., 2013. Reflectance spectra diversity of silica-rich materials: sensitivity to environment and implications for detections on Mars. Icarus 223 (1), 499–533. https://doi.org/10.1016/j.icarus.2012.09.021.
Riding, R., 2000. Microbial carbonates: the geological record of calcified bacterial–algal mats and biofilms. Sedimentology 47, 179–214. https://doi.org/10.1046/j.1365-3091.2000.00003.x.
Rogers, A.D., Warner, N.H., Golombek, M.P., Head, J.W., Cowart, J.C., 2018. A really extensive surface bedrock exposures on Mars: many are clastic rocks, not lavas. Geophys. Res. Lett. 45 (4), 1767–1777. https://doi.org/10.1002/2018GL077030.

Rosen, M.R., Arehart, G.B., Lico, M.S., 2004. Exceptionally fast growth rate of <100-yr-old tufa, Big Soda Lake, Nevada: implications for using tufa as a paleoclimate proxy. Geology 32 (5), 409–412.
Ruff, S.W., 2017. Investigating the floor of Paleolake Jezero by way of Gusev Crater. In: Fourth International Conference on Early Mars (#3076).
Ruff, S.W., Niles, P.B., Alfano, F., Clarke, A.B., 2014. Evidence for a Noachian-aged ephemeral lake in Gusev crater, Mars. Geology 42 (4), 359–362. https://doi.org/10.1130/G35508.1.
Russell, M.J., Ingham, J.K., Zedef, V., Maktav, D., Sunar, F., Hall, A.J., Fallick, A.E., 1999. Search for signs of ancient life on Mars: expectations from hydromagnesite microbialites, Salda Lake, Turkey. Jour. of the Geological Society 156, 869–888.
Rutledge, A.M., Horgan, B.H.N., Havig, J.R., Rampe, E.B., Scudder, N.A., Hamilton, T.L., 2018. Silica dissolution and precipitation in glaciated volcanic environments and implications for Mars. Geophys. Res. Lett. https://doi.org/10.1029/2018GL078105.
Salvatore, M.R., Goudge, T.A., Bramble, M.S., Edwards, C.S., Bandfield, J.L., Amador, E. S., Mustard, J.F., Christensen, P.R., 2018. Bulk mineralogy of the NE Syrtis and Jezero crater regions of Mars derived through thermal infrared spectral analyses. Icarus 301, 76–96. https://doi.org/10.1016/j.icarus.2017.09.019.
Schon, S.C., Head, J.W., Fassett, C.I., 2012. An overfilled lacustrine system and progradational delta in Jezero crater, Mars: implications for Noachian climate. Planetary and Space Science 67 (1), 28–45. https://doi.org/10.1016/j.pss.2012.02.003.
Seelos, K., Buczkowski, D., Seelos, F., Murchie, S., CRISM Science Operations Center, 2012. MTRDR data analysis walk-through. In: CRISM 2012 Data Users' Workshop.
Seelos, F.P., Viviano-Beck, C.E., Morgan, M.F., Romeo, G., Aiello, J.J., Murchie, S.L., 2016. CRISM Hyperspectral Targeted Observation PDS Product Sets — TERs and MTRDRs, 47th Lunar and Planetary Science Conference (#1783).
Shahrzad, S., Kinch, K.M., Goudge, T.A., Fassett, C.I., Needham, D.H., Quantin Nataf, C., Knudsen, C.P., 2019. Crater Statistics on the Dark-Toned, Mafic Floor Unit in Jezero Crater, Mars. Geophys. Res. Lett. 46 (5), 2408–2416. https://doi.org/10.1029/2018GL081402.
Shearman, D.J., McGugan, A., Stein, C., et al., 1989. Ikaite, precursor of the thinolites in the Quaternary tufas and tufa mounds of the Lahontan and Mono Lake basins, western US. Geol. Soc. Am. Bull. 101, 913–917.
Siebach, K.L., Grotzinger, J.P., 2014. Volumetric estimates of ancient water on Mount Sharp based on boxwork deposits, Gale Crater, Mars. Journal of Geophysical Research Planets 119 (1), 189–198. https://doi.org/10.1002/2013JE004508.
Spotl, C., Burns, S.J., 1994. Magnesite diagenesis in redbeds: a case study from the Permian of the Northern Calcareous Alps (Tyrol, Austria). Sedimentology 41 (3), 543–565. https://doi.org/10.1111/j.1365-3091.1994.tb02010.x.
Stoddart, D.R., Cann, J.R., 1965. Nature and origin of beach rock. J. Sediment. Petrol. 35 (1), 243–247. https://doi.org/10.1306/74D7122B-2B21-11D7-8648000102C1865D.
Summons, R.E., Hallmann, C., 2014. Organic geochemical signatures of early life on Earth. In: Treatise on Geochemistry, 2nd Ed. Elsevier, pp. 33–46.
Summons, R., Amend, J., Bish, D., Buick, R., Cody, G., Des Marais, D., Dromart, G., Eigenbrode, J., Knoll, A., Sumner, D., 2011. Preservation of martian organic and environmental records. Astrobiology 11, 1, 1–47. https://doi.org/10.1089/ast.2010.0571.
Sun, V.Z., Milliken, R.E., 2018. Distinct Geologic Settings of Opal-A and More Crystalline Hydrated Silica on Mars, pp. 1–29. https://doi.org/10.1029/2018GL078494.
Sun, V.Z., Stack, K.M., 2019. Understanding the continuity of regional units in the Mars 2020 Jezero and Northeast Syrtis Regions: implications for the origin of the Mafic unit(s). In: 50th Lunar and Planetary Science Conference (abstract #2271).
Thompson, J., Ferris, F., 1990. Cyanobacterial precipitation of gypsum, calcite, and magnesite from natural alkaline lake water. Geology 18 (10), 995–998.
Thompson, J.B., Ferris, F.G., Smith, D.A., 1990. Geomicrobiology and sedimentology of the mixolimnion and chemocline in Fayetteville Green Lake, New York. Palaios 5, 52–75.
Tornabene, L.L., Moersch, J.E., McSween Jr., H.Y., Hamilton, V.E., Piatek, J.L., Christensen, P.R., 2008. Surface and crater-exposed lithologic units of the Isidis Basin as mapped by coanalysis of THEMIS and TES derived data products. J. Geophys. Res. 113 (E10), E12S09–30. https://doi.org/10.1029/2007JE002988.
Tucker, M.E., 1991. Carbonate diagenesis. Wiley-Blackwell (320 p).
Vance, R.E., Mathewes, R.W., Clague, J.J., 1992. 7000 year record of lake-level change on the northern Great Plains: A high-resolution proxy of past climate. Geology 20 (10), 879–882.
Viviano, C.E., Moersch, J.E., Mcsween, H.Y., 2013. Implications for early hydrothermal environments on Mars through the spectral evidence for carbonation and chloritization reactions in the Nili Fossae region. Journal of Geophysical Research Planets 118 (9), 1858–1872. https://doi.org/10.1002/jgre.20141.
Viviano-Beck, C.E., et al., 2014. Revised CRISM spectral parameters and summary products based on the currently detected mineral diversity on Mars. Journal of Geophysical Research Planets 119 (6), 1403–1431. https://doi.org/10.1002/2014JE004627.
Walter, M.R., Golubic, S., Preiss, W.V., 1973. Recent stromatolites from hydromagnesite and aragonite depositing lakes near the Coorong Lagoon. South Australia, J Sediment Petrol 43 (4), 1021–1030.
Webb, G.E., Kamber, B.S., 2010. Trace element geochemistry as a tool for interpreting microbialites. In: Golding, S.D., Glikson, M. (Eds.), Earliest Life on Earth: Habitats, Environments and Methods of Detection. Springer Netherlands, Dordrecht, pp. 127–170.
Werner, S.C., 2008. The early martian evolution—constraints from basin formation ages. Icarus 195 (1), 45–60. https://doi.org/10.1016/j.icarus.2007.12.008.
Wilhelm, M.B., Hewson, I., 2012. Characterization of thrombolitic bioherm cyanobacterial assemblages in a meromictic Marl Lake (Fayetteville Green Lake, New York). Geomicrobiol J. 29 (8), 727–732.
Willcox, A., Buisman, I., Sparks, R.S.J., Brown, R.J., Manya, S., Schumacher, J.C., Tuffen, H., 2015. Petrology, geochemistry and low-temperature alteration of lavas and pyroclastic rocks of the kimberlitic Igwisi Hills volcanoes, Tanzania. Chem. Geol. 405 (C), 82–101. https://doi.org/10.1016/j.chemgeo.2015.04.012.
Williford, K.H., et al., 2018. Chapter 11 - The NASA Mars 2020 Rover Mission and the Search for Extraterrestrial Life. In: From Habitability to Life on Mars, pp. 275–308. https://doi.org/10.1016/B978-0-12-809935-3.00010-4.
Wilson, S.A., Dipple, G.M., Power, I.M., Thom, J.M., Anderson, R.G., Raudsepp, M., Gabites, J.E., Southam, G., 2009. Carbon dioxide fixation within mine wastes of ultramafic-hosted ore deposits: Examples from the Clinton Creek and Cassiar Chrysotile deposits, Canada. Econ. Geol. 104 (1), 95–112. https://doi.org/10.2113/gsecongeo.104.1.95.
Wilson, S.A., Dipple, G.M., Power, I.M., Barker, S.L.L., Fallon, S.J., Southam, G., 2011. Subarctic Weathering of Mineral Wastes Provides a Sink for Atmospheric CO_2. Environ. Sci. Technol. 45 (18), 7727–7736. https://doi.org/10.1021/es202112y.
Wray, J.J., et al., 2011. Columbus crater and other possible groundwater-fed paleolakes of Terra Sirenum, Mars. J. Geophys. Res. 116 (E), E01001. https://doi.org/10.1029/2010JE003694.
Wray, J.J., Murchie, S.L., Bishop, J.L., Ehlmann, B.L., Milliken, R.E., Wilhelm, M.B., Seelos, K.D., Chojnacki, M., 2016. Orbital evidence for more widespread carbonate-bearing rocks on Mars. Journal of Geophysical Research Planets 121 (4), 652–677. https://doi.org/10.1002/2015JE004972.
Zedef, V., Russell, M.J., Fallick, A.E., Hall, A.J., 2000. Genesis of vein stockwork and sedimentary magnesite and hydromagnesite deposits in the ultramafic terranes of southwestern Turkey: A stable isotope study. Econ. Geol. 95 (2), 429–445. https://doi.org/10.2113/gsecongeo.95.2.429.
Zhu, T., Dittrich, M., 2016. Carbonate precipitation through microbial activities in natural environment, and their potential in biotechnology: a review. Front. Bioeng. Biotechnol. 4, 447-21. https://doi.org/10.3389/fbioe.2016.00004.